University of Tennessee, Knoxville

TRACE: Tennessee Research and Creative Exchange

Doctoral Dissertations

Graduate School

8-2019

Computational study on biomass fast pyrolysis: Hydrodynamic effects on the performance of a laboratory-scale fluidized bed reactor

Emilio Ramirez
University of Tennessee, eramire2@vols.utk.edu

Follow this and additional works at: https://trace.tennessee.edu/utk_graddiss

Recommended Citation

Ramirez, Emilio, "Computational study on biomass fast pyrolysis: Hydrodynamic effects on the performance of a laboratory-scale fluidized bed reactor. " PhD diss., University of Tennessee, 2019.
https://trace.tennessee.edu/utk_graddiss/5937

This Dissertation is brought to you for free and open access by the Graduate School at TRACE: Tennessee Research and Creative Exchange. It has been accepted for inclusion in Doctoral Dissertations by an authorized administrator of TRACE: Tennessee Research and Creative Exchange. For more information, please contact trace@utk.edu.

To the Graduate Council:

I am submitting herewith a dissertation written by Emilio Ramirez entitled "Computational study on biomass fast pyrolysis: Hydrodynamic effects on the performance of a laboratory-scale fluidized bed reactor." I have examined the final electronic copy of this dissertation for form and content and recommend that it be accepted in partial fulfillment of the requirements for the degree of Doctor of Philosophy, with a major in Energy Science and Engineering.

C. Stuart Daw, Major Professor

We have read this dissertation and recommend its acceptance:

Charles Finney, Nourredine Abdoulmoumine, David J. Keffer

Accepted for the Council:

Dixie L. Thompson

Vice Provost and Dean of the Graduate School

(Original signatures are on file with official student records.)

COMPUTATIONAL STUDY ON BIOMASS FAST PYROLYSIS: HYDRODYNAMIC EFFECTS ON THE PERFORMANCE OF A LABORATORY-SCALE FLUIDIZED BED REACTOR

A Dissertation Presented for the
Doctor of Philosophy
Degree
The University of Tennessee, Knoxville

Emilio Ramirez
August 2019

Copyright © 2019 by Emilio Ramirez
All rights reserved.

DEDICATION

This body of work is dedicated to my son, E. Mobius Ramirez.

When my simulations were going to shit and I felt like a complete failure,
You always found a way to reach me,
You reminded me of the important things in life,
Sometimes a smile,
A hug,
A kiss,
A question,
To be grateful,
To be humble.

Below, the picture that brought me back

ACKNOWLEDGEMENTS

Research Committee:
C. Stuart Daw
Charles E. A. Finney
David Keffer
Nourredine Abdoulmoumine

Mentors:
Lee Riedinger
James E. Parks II
John Turner
Sreekanth Pannala
Tingwen Li
Thomas D. Foust
William A.Rogers
Jack Halow

Other key people:
Kristin Smith
Katherine Gaston
Kristiina Iisa
Peter Ciesielski
Brennan Pecha
Rick French
Danny Carpenter
Braden Peterson
Jessica Olstadt
Justin Weber
Dirk VanEssendelft
Maggie Connatser
Samuel A Lewis Sr
Gavin M Wiggins

Bredesen Center for Interdisciplinary Research and Graduate Education
Consortium for Computational Physics and Chemistry: A research collaboration of national laboratories for the U.S. DOE Bioenergy Technologies Office
Fuels, Engines, and Emissions Research group at Oak Ridge National Laboratory
Biomass convErsion And Modeling (BEAM) team
NREL Thermal and Catalytic Process Development Unit

Friends and family were important in completing this work.
You know who you are.

ABSTRACT

Fluidized bed reactors are utilized in a wide range of chemical industries, including petroleum refining, pharmaceutical and commodity chemicals production, and biomass conversion to fuels and higher-value chemicals. Such reactors are useful where multiple fluids (gases or liquids) and particulate solids are brought together in intimate contact to promote heat and mass transfer and chemical reactions. Recently fluidized-bed research includes computational simulations that provide new insights into the dominant physics and chemistry processes that control reactor performance.

Computational simulations were utilized to understand how bubbling-bed hydrodynamics and fast-pyrolysis chemistry interact to control biomass pyrolysis reactor performance. The scope of this work is limited to bubbling bed conditions, designed and operated for lab scale studies of biomass fast pyrolysis, in a bed of inert Geldart Group B sand. Biomass particulates are injected near the bottom of the reactor and rapidly heated to release volatile compounds. The devolatilized biomass particles (char) and released volatile gases transit through the bed (at time scales depending on the hydrodynamic mixing state) and elutriate from the top of the reactor.

The bubbling-bed hydrodynamics were simulated with MFiX, an open- source software package based on the two-fluid (continuum) approach for representing the bubbling bed multiphase flows. Processes of interest included the transport of biomass char and released volatile gases, and how these change with fluidizing gas flow, low-intensity bubbling, to slugging, to high-intensity turbulence. A key observation is that fast-pyrolysis tar yield can be increased by reducing the residence time in the freeboard by shortening the freeboard length or by adding secondary air.

Also, of interest was how these transport processes are expected to affect the selectivity of product species exiting the top of the reactor.

One promising concept for monitoring hydrodynamics in bubbling bed reactors are high-speed pressure measurements to quantify key mixing and transport properties. Computational simulations were utilized to identify quantitative statistical features in high-speed pressure measurements in the upper section of the bed, below the static bed height, to use as process monitoring tools. Other promising directions were identified for future experimental and computational studies.

TABLE OF CONTENTS

LIST OF TABLES

LIST OF FIGURES

CHAPTER 0 INTRODUCTION

Introduction and Background

Biomass fast pyrolysis

A thermochemical route for liquid fuels

Fast pyrolysis is a thermochemical route available to develop liquid fuels [1, 2] and value-added chemicals from biomass [3-5]. Fast pyrolysis is carried out by rapidly heating biomass particles under low-oxygen conditions, typically at 300–600°C. During this stage, biomass is converted to char, ash, non-condensable gases, and vapors (tars). Vapors must be further processed through catalytic upgrading and/or separation techniques to isolate specific chemical compounds for liquid fuels or value-added chemicals [3]. However, good control of the reactor chemistry yield and composition is necessary to efficiently process vapors. Furthermore, different biomass feedstock types, sizes, and shapes can yield drastically different chemistry [6-8]. The studies contained in this document focus on woody-biomass fast pyrolysis.

Biomass fast-pyrolysis chemistry

Biomass fast-pyrolysis chemistry is complex, and kinetics are simplified using mass-based approaches, as opposed to molar concentrations, that can be utilized in simulations, Fig. 0-1(a). These kinetic approaches utilize first-order Arrhenius rates and one- or two- step conversions from wood to tar, char, and gas [9]. Some research groups [10] also start their kinetic scheme with lignin, cellulose, and hemicellulose instead of wood, Fig. 0-1(b). A more involved kinetic scheme utilizes lignin, cellulose, and hemicellulose and breaks these compounds down with a first-order, multistep approach to many chemical compounds [11]. Furthermore, these kinetic schemes are usually created in plug-flow, entrained-flow [12], or other bench-scale reactors which do not have the same hydrodynamics as fluidized beds. Each kinetic scheme is packaged with assumptions that have advantages and disadvantages which must be carefully considered when simulating bubbling fluidized beds [13].

Bubbling-bed reactor

Bubbling beds are widely utilized in industrial thermochemical processes as well as bench-scale studies due to their versatility for efficiently contacting gas and solids, and they have been identified as one of the most promising candidate reactor types for biomass fast pyrolysis [14]. For this reason, this work focuses on developing a better understanding of how bubbling fluidized-bed reactors can be used for production of "infrastructure ready" liquid fuels from woody-biomass fast pyrolysis. Some of the major features of these reactors are highlighted in Fig. 0-2.

Fluidization

Fluidized beds

A simple description of a bubbling fluidized bed is a vertical pipe with a perforated-plate distributor (other types are available) at the bottom which is used to evenly distribute a fluidizing gas into the pipe. Inside the pipe, immediately above the distributor a bed of particles resides, typically sand or catalyst. Fluidizing gas is pushed through the distributor into the bed of particles. Inside the bed of particles, the gas–particle, particle–particle, gas–wall, and particle–wall interactions are very complex [16]. When the drag force overcomes the gravitational force of the particles, the bed of sand is lifted, and gas moves through the sand interstices. At higher fluidizing gas flow, the excess gas can no longer move through the interstices, and gas bubbles form inside the bed of sand. As fluidizing gas flow is increased, the bubbling fluidized bed goes through various fluidization regimes, such as fixed, bubbling, slugging, and turbulent, shown in Fig. 0-3.

Slugging is the fluidizing state where bubble sizes reach ~60% of the reactor diameter. As fluidizing gas flow continues to increase past the slugging regime, in the turbulent regime the bubbling bed elutriates solid particles past the freeboard region and out the top of the reactor. Reactors designed to operate at turbulent conditions or higher flow recirculate the solids back into the bed and are classified as circulating fluidized beds [17]. This study focuses on the fluidization regimes from bubbling-to-slugging operation.

Bubbling-to-slugging fluidization

The transition from bubbling to slugging, as shown from experimental data in Fig. 0-4, is complex and changes with the reactor static bed height (height of the sand bed un-fluidized), height-to-diameter ratio (H/D), particle size, particle density, temperature, and pressure. Smaller bench-scale fluidized-bed reactors tend to reach slugging conditions. The regime diagram from Shaul et al. [19] integrates the Geldart classification system [20] and helps interpret the effects of operating parameters in terms of dimensionless numbers such as Reynolds and Archimedes particle numbers. While maintaining particle Archimedes number constant, the H/D is increased, and the slugging transition occurs at lower fluidized gas flow and smaller particle Reynolds number. Particle size and reactor temperature have the largest impact on particle Archimedes number, reflected in bubbling intensity. However, the Archimedes number only describes single particle size, whereas bubbling beds are composed of particle size distributions (PSDs) [21] with various properties. For example, if the PSD has a positive skewness toward a smaller particle size, this causes a decrease in bubble size and shorter fluidization-gas residence time in the bed [22-24]. However, if larger particles are added to the bed, so PSD is negatively skewed toward the larger particle size, and there is no noticeable effect on bubbles [22]. These are important considerations because as fuel particles of varying size enter the reactor, over time these can have negative effects on fluidization quality. Bed particle size can also change, due to attrition, fragmentation, or addition of heavy bottom ash particles, causing changes in bubbling, residence time, mass, heat transfer, and ultimately chemistry. These are some of the challenges with accurately predicting effects of hydrodynamics in a bubbling bed.

Bubbles in fluidized beds

Bubbling–bed hydrodynamics are complex and are governed by bubble dynamics that affect mixing, heat transfer, and particle/gas/vapor residence time. Bubbles behave differently in gas–solid systems than gas–liquid systems due to a bubble boundary defined by a cloud of solid–gas emulsion, Fig. 0-5. The boundary region between bubbles and the surrounding dense phase is a complex zone that can vary depending on the bubble size and velocity, but for practical purposes, it is frequently assumed that the bubble edge can be approximately demarcated by the region where the void fraction exceeds 0.7 [25]. Rowe et al. [26] showed there is a circulating region inside the bubble and the emulsion as the gas bubble travels upward. Gas enters the bubble through the bubble wake, and some gas recirculates around the bubble while most exits at the top of the bubble, along the bubble front. Alternatively, solids approaching the bubble front move around the bubble as the bubble rises, and in the drift region, solids are pulled into the bubble. In the wake region, there is a low-pressure region that recirculates solids. Some solids enter the bubble and get recirculated back into the emulsion. In contrast, at slugging conditions, the large ogive (bullet shaped) bubbles rise upward slower due to wall effects. Although the gas flow is increased, the large bubbles rise slower than the gases flowing through them [27]. This results in inefficient solid-gas contacting and gas bypassing through the large ogive bubbles [28, 29]. Thus, bubble size, speed, and frequency affect mixing, heat transfer, and gas/vapor residence time. This should affect reactive chemistry based on bubbling-regime dynamics. For this reason, a quantitative approach to determine the various fluidization regimes — bubbling, bubbling to slugging, and slugging — is needed.

The bubbling-to-slugging transition

Qualitative vs quantitative approaches

Although there is extensive research on the bubbling-bed regime transition, there is a need to have a better understanding of the transition from bubbling to slugging. Part of the problem is that there are different definitions for slugging fluidization. Based on visual observations, slugging commences when bubble sizes reach ~60% of the reactor diameter. However, there is no widely accepted method to quantitatively determine the transition from bubbling to slugging. Established methods to determine the transitions from fixed to bubbling fluidization and slugging to turbulent fluidization utilize pressure measurements taken near the bottom of the reactor bed. While these pressure measurement locations can detect these transitions, this approach/location does not appear to capture the transition from bubbling to slugging [27]. As noted in the fluidization introduction, bubble size, speed, and frequency affect hydrodynamics, which directly impact mixing, heat transfer, chemistry, and residence time [30]. This requires developing a method to quantitatively determine the transition from bubbling to slugging to measure the fluidization regime.

Problem Statement

Fluidized bubbling beds are designed for continuous operation of thermochemical processes, where fuel (biomass and/or coal) particles are continuously conveyed into the reactor.

Bubbling–bed hydrodynamics can change over time and drift from optimal reactor conditions. Fig. 0-6 shows how fluidization gas flow affects chemistry yield and composition in biomass fast–pyrolysis experiments [31]. However, the exact hydrodynamic effects have not been directly related to chemistry. Fluidized-bed fast pyrolysis differs from using other reactor types, in that bubble dynamics also affect mixing, elutriation, residence time, yield and composition. Effects in bubbles versus the particle/gas emulsion can have a detrimental effect. Although slugging is expected to negatively affect gas and solids contacting because it increases the effective level of gas bypassing, the quantitative details of how gas–solids contacting is affected by the bubbling-to-slugging transition and the impact on conversion for biomass fast pyrolysis are not clear.

Available regime maps do not explicitly account for particle size distributions, which also affect bubble size, mixing, heat transfer, and residence time. Depending on production needs, fluidization can drift from optimal operating conditions, resulting in expensive production losses. Operating the reactor at significantly lower flow to prevent slugging or the slugging transition can result in non-optimal yields, which is not economically attractive. In continuously operated fluidized-bed reactors, fluidization quality changes slowly over time due to the large mass of particles composing the bed materials, which may not be directly obvious to operators. Therefore, detecting hydrodynamic fluidization quality in real time is important to operate the reactor at optimal conditions near critical bubbling conditions.

A diagnostic method to reliably quantify bubbling hydrodynamics is needed so bench to industrial scale fluidized-bed reactors can be optimized for their specific process. Such a diagnostic tool should be easy to implement into a control system infrastructure and be easy to interpret regime transition by fluidized-bed operators. These challenges are not exclusive to bubbling-bed operations, they are also important to circulating fluidized beds. During startup, circulating fluidized beds can go through bubbling and slugging before reaching turbulent and circulating fluidized bed conditions. Similarly, during shutdowns and at reduced load, circulating fluidized bed can also reach slugging and bubbling conditions. Operations should be able to determine fluidization conditions to avoid operating in a critical condition and to maximize fast pyrolysis yields.

Implications

This research utilizes a specific approach for modeling the hydrodynamics of bubbling fluidized bed reactors of Geldart Group B particles and is expected to lead to the following advances:

- An improved understanding of the basic physics involved in the transition from bubbling to slugging;
- A more quantitative understanding of how bubbling and slugging hydrodynamics can affect pyrolysis yield;
- Identification of the optimal hydrodynamic state in bubbling-bed reactors for maximizing the yield of bio-oils from biomass fast pyrolysis;
- Identification of on-line pressure-based monitoring approaches that can be used to improve bench and industrial scale fluidized-bed pyrolysis reactor performance.
- Identification of potential approaches for improving the performance of bubbling fluidized bed reactors in general (i.e., not just for biomass pyrolysis).

Research Outline

This dissertation is organized around three sequential objectives of activity, which are summarized below. A key component of each objective is the identification and testing of guiding hypotheses concerning the physics of slugging, the impact of slugging on fast pyrolysis yield, and possible ways to monitor the approach to slugging using pressure measurements suitable for practical reactor systems.

Objective 1- Improved understanding of the physics of slugging in fluidized beds of Geldart Group B particles

Description

Use CFD simulations of the bubbling-to-slugging transition to numerically investigate the basic physics of the associated hydrodynamics and identify key associated spatiotemporal features that might be measured.

Guiding hypotheses

1. The transition to slugging in a bubbling bed of Geldart Group B particles occurs over a range of fluidizing gas flow rather than abruptly at a single critical value of gas flow.
2. The transition to slugging in a bubbling bed of Geldart Group B particles is also correlated with distinctive and reproducible changes in the spatiotemporal characteristics of bubbles, including the distribution of bubble sizes and frequencies.
3. The transition to slugging in a bubbling bed of Geldart Group B particles is correlated with distinctive and reproducible changes in the spatiotemporal characteristics of pressure fluctuations at the bed wall.

Approach

- Based on a detailed review of the literature covering previous experimental measurements and computational simulation related to the bubbling-to-slugging transition in Group B beds, design a set of numerical experiments using the two-fluid version of MFiX (to be defined below) for simulating a reference lab-scale fluidized bed operating under stationary conditions for a range of gas flows between minimum fluidization and the point of maximum slugging at 4–5 times minimum fluidization.
- Analyze 2D and 3D MFiX simulation results to determine what is needed to achieve reproducible results exhibiting convergent spatiotemporal statistics and computational grid independence.
- Generate and analyze simulated bubble and pressure measurements at multiple locations in the bed to identify the key spatiotemporal features as a function of gas flow.
- Perform sensitivity analyses of the previous results to assumptions used for the analyses and simulation parameters. Compare the above results to the predictions of slugging correlations in the literature and previously published experimental measurements.

Objective 2- Relate slugging to bio-oil yield for biomass fast pyrolysis in bubbling beds

Description

Use CFD simulations to relate bubble characteristics and the transition from bubbling to slugging to changes in the yield/selectivity of biomass fast pyrolysis.

Guiding hypotheses

1. The expected yield of condensable bio-oil from a bubbling bed pyrolysis reactor is reduced by the onset of slugging, due to gas bypassing, poor gas–solids contacting, and excessive biomass elutriation.
2. The maximum yield of condensable bio-oil from a bubbling bed pyrolysis reactor occurs just before the transition to fully developed slugging begins (i.e., when the gas flow is increased to a point where large bubbles just begin to form near the surface of the bed and due to very rapid bubble coalescence near the distributor).
3. There is an optimal height in the bed, associated with residence time, where maximum oil yield can be achieved, that relates reactor geometry, operating conditions, and residence time.
4. The hydrodynamics and reactions can be separated to efficiently simulate the reactor

Approach

- Add an experimentally validated reduced-order kinetic model for wood pyrolysis to the 3D fluidized bed simulations from Objective 1.
- Evaluate the results from the above simulations (reduced-order kinetic model) to compare how the oil yields in each case are affected by changing the fluidizing gas flow from near minimum fluidization up to the maximum slugging condition at a fixed biomass feed rate.
- Perform sensitivity analyses of the previous results to assumptions used for the analyses and simulation parameters. Compare the above results to experimental measurements from collaborators at the National Renewable Energy Laboratory (NREL) and/or previously published experimental data in the literature.
- Compare results with a hybrid low-order model that uses the MFiX residence time distributions.

Objective 3- Identify how to use pressure fluctuations to monitor and control bio-oil yield from bubbling-bed biomass pyrolysis reactors

Description

Use computational fluid dynamics (CFD) simulations to identify a specific approach for how to use pressure fluctuations to monitor and control bio-oil yield from bubbling bed biomass pyrolysis reactors.

Guiding hypotheses

1. The optimal location for measuring pressure fluctuations at the bed wall is near the top of the expanded bed.
2. Pressure fluctuations that reflect bubble speeds and/or coalescence events are the best characteristics with which to monitor the transition toward slugging.
3. It is possible to measure and process on-line pressure signals fast enough to detect significant shifts toward or away from optimal yield conditions over periods of a minute or less.

Approach

- Utilize 3D biomass fast pyrolysis bubbling fluidized bed simulations at a range of flows, from bubbling to slugging, using the CFD package MFiX.
- Analyze pressure at multiple heights using other time series analysis approaches: frequency domain, time frequency domain, or state space domain.
- Use trends from objective 2 to identify optimal fluidization condition needed to maximize oil yield.

Combine the results from objective 1 and 2 to identify a reasonable pressure measurement scheme for using real-time, non-intrusive, high-speed pressure diagnostics measurements to maintain the optimal oil yield.

Dissertation structure

This dissertation is organized into 5 chapters, which are briefly summarized below. A literature review is also outlined in each chapter.

Introduction provides an overall introduction and background that explains the motivation, the state of previous related research, and the objectives. General information about the MFiX CFD platform used for the simulations is also provided.

Chapter 1 reviews the descriptions, guiding hypotheses, and computational approach used in Objective 1. Objective 1 simulation results concerning the new information learned about the physics of the bubbling-to-slugging transition are discussed in detail and summarized, along with more general conclusions about their significance. This work was published in an article titled: "Computational study of the bubbling-to-slugging transition in a laboratory-scale fluidized bed." in Chemical Engineering Journal 308 (2017) 544–556. https://doi.org/10.1016/j.cej.2016.08.113.

Chapter 2 reviews the descriptions, guiding hypotheses, and computational approach used for Objective 2, which discusses results concerning the new information learned about the bubbling-to-slugging transition effects on oil yield from fast pyrolysis of wood. This work will be submitted in an article titled: "Computational study on biomass fast pyrolysis: Hydrodynamic effects on the performance of a laboratory-scale fluidized bed reactor." to Chemical Engineering Journal.

Chapter 3 reviews the descriptions, guiding hypotheses, and computational approach used for Objective 3, which discusses simulation results concerning the new information learned about how the bubbling-to-slugging transition could potentially be monitored in real time using pressure fluctuations for controlling oil yield from fast pyrolysis of wood. Conclusions about the significance for thermochemical biomass conversion technology is also discussed. A manuscript similar in organization to the Objective 1 and Objective 2 publication will be submitted to a prominent chemical reaction engineering journal.

The conclusion gives an overall summary of the results and conclusions from all 3 objectives of this study, as well as recommendations for future simulations and experiments associated with biomass pyrolysis. This chapter also provides potential applications to more general chemical conversion processes.

Appendix: Figures

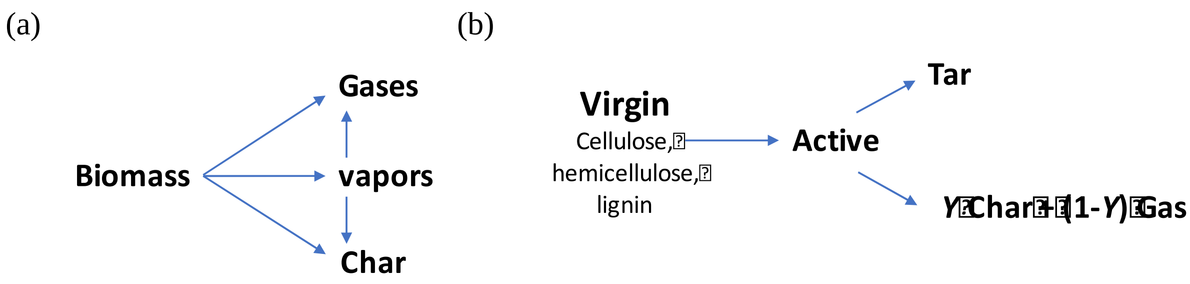

Fig. 0-1 Biomass fast pyrolysis kinetic schemes. (a) Di Blasi, 2008 [9]. (b) Miller and Bellan, 1998 [10].

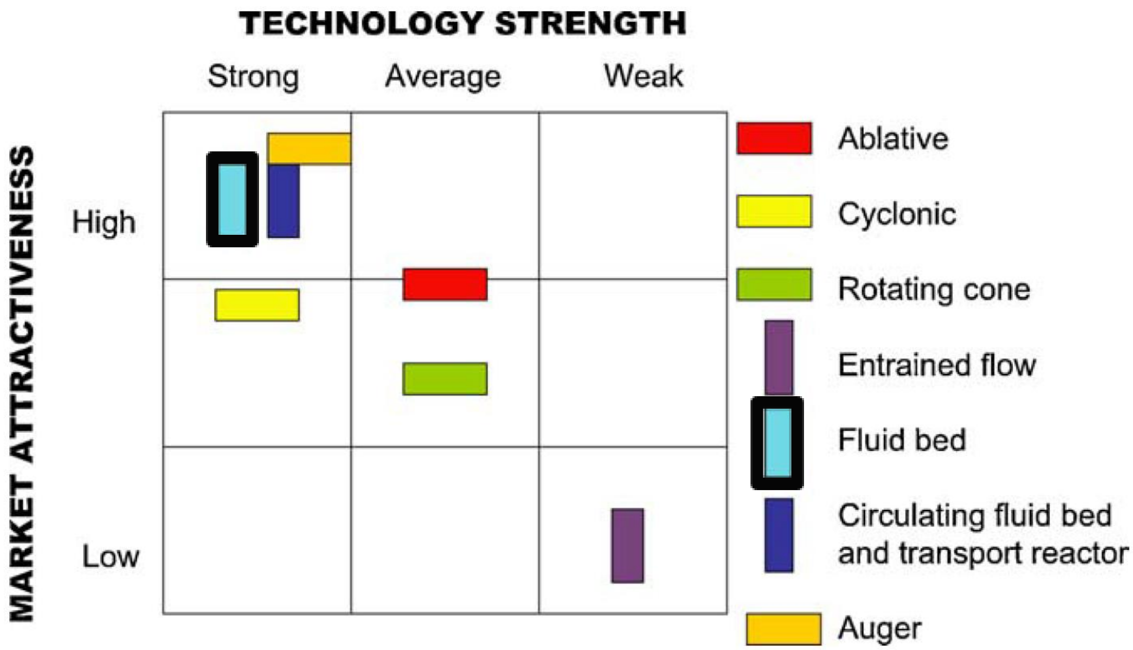

Fig. 0-2 Commercial potential of various fast pyrolysis technologies [15].

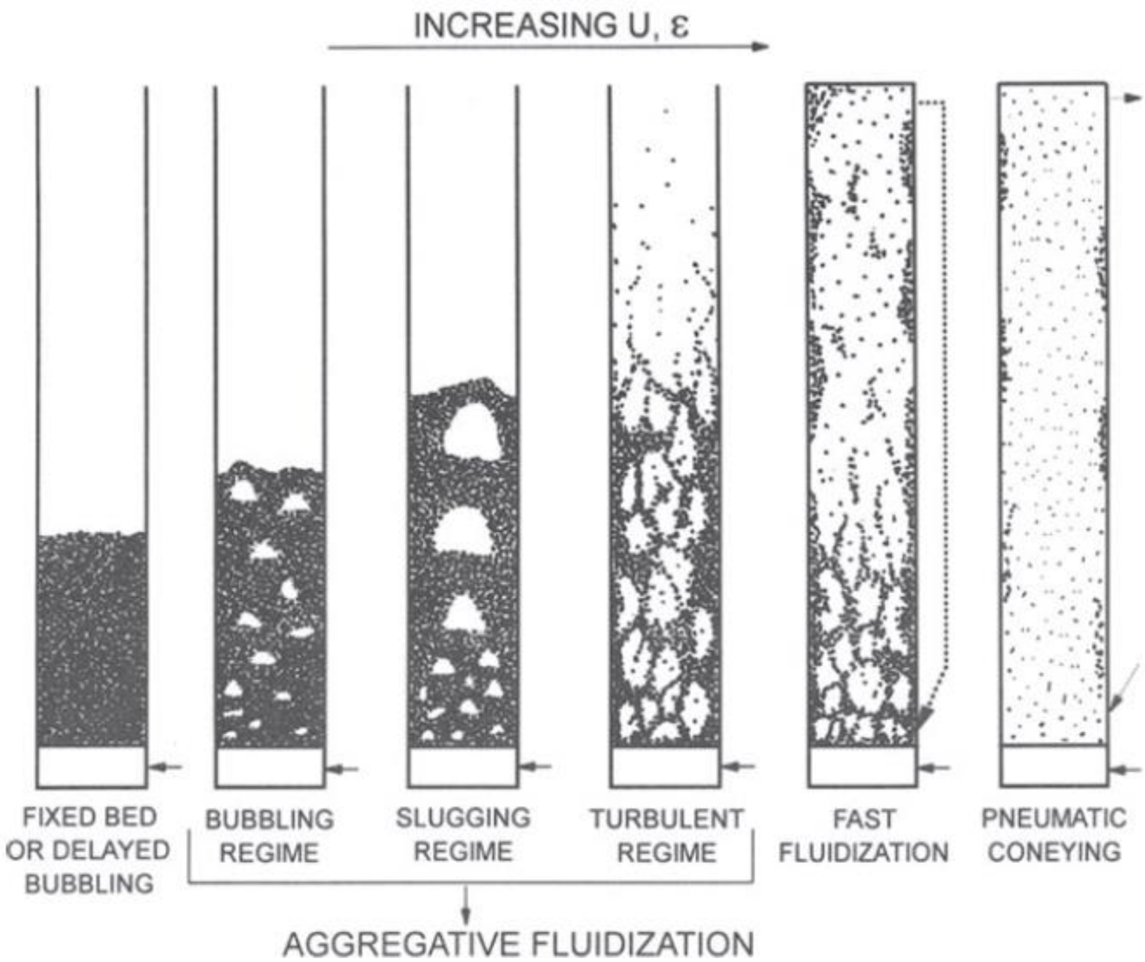

Fig. 0-3 Fluidization regimes in gas–solid fluidized beds [18].

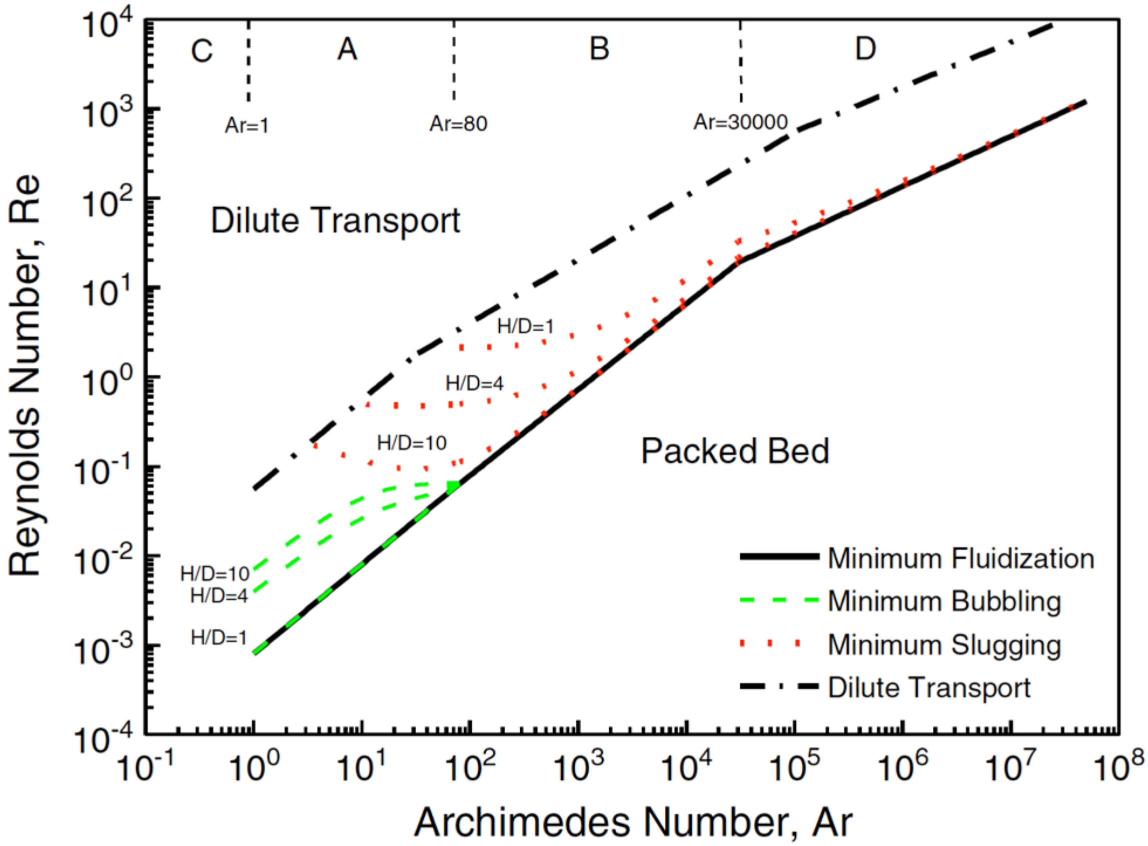

Fig. 0-4 Bubbling bed flow regime diagram [19].

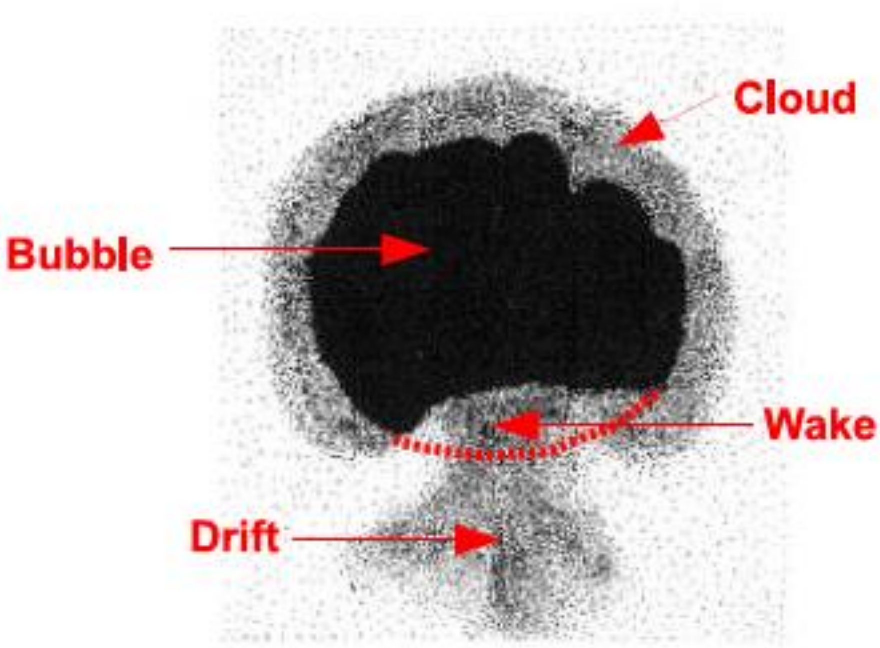

Fig. 0-5 Bubble image in a gas–solid bubbling bed [26].

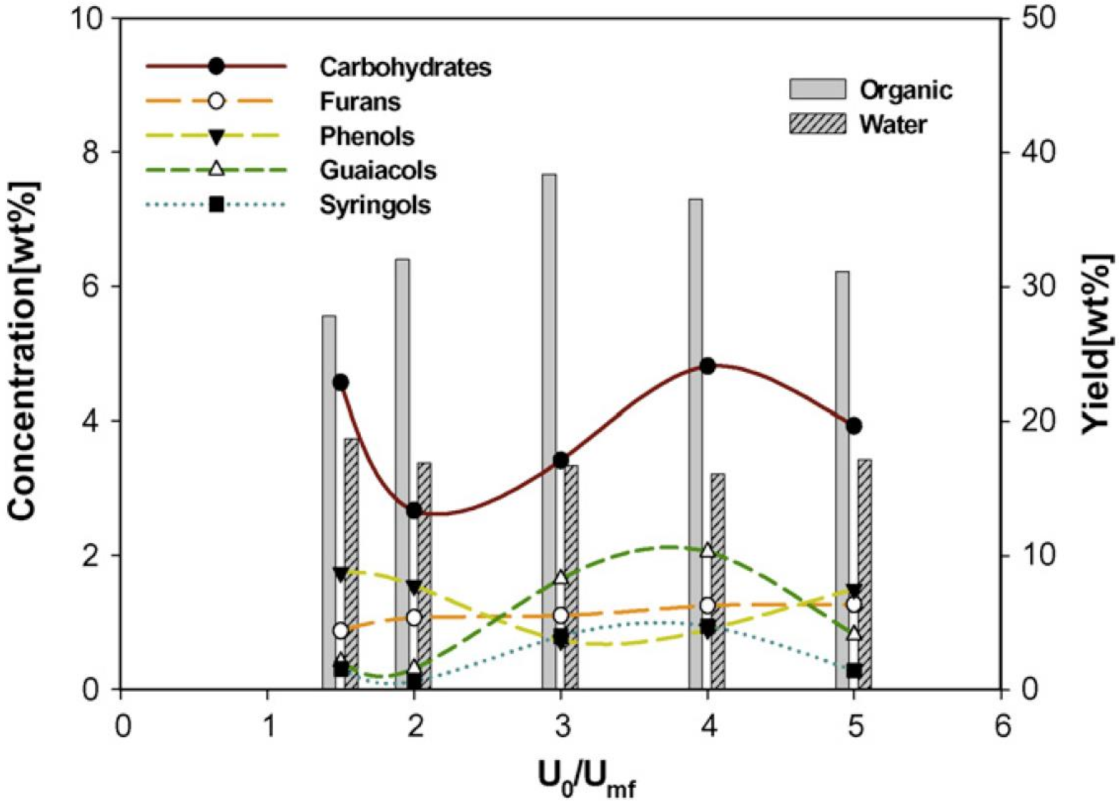

Fig. 0-6 Bubbling-bed fluidized gas flow effects on biomass fast pyrolysis [31].

CHAPTER 1 : CHARACTERIZING HYDRODYNAMICS OF THE BUBBLING-TO-SLUGGING TRANSITION IN A LABORATORY-SCALE FLUIDIZED BED

A version of this chapter was originally published by Emilio Ramirez et al.:

Ramirez, E., Finney, C. E. A., Pannala, S., Daw, C. S., Halow, J., Xiong, Q. "Computational Study of the Bubbling-to-Slugging Transition in a Laboratory-Scale Fluidized Bed." *Chemical Engineering Journal* 308 (2017/01/15/2017): 544-56. https://doi.org/10.1016/j.cej.2016.08.113

The work in this chapter was analyzed and written by Emilio Ramirez. Guidance was provided by Sreekanth Pannala, Stuart Daw, and Charles Finney. Emilio utilized the University of Tennessee writing center to rewrite successive iterations of the chapter. At the final stage before submitting to the Journal, Stuart Daw reviewed the paper and made recommendations. Charles also reviewed and made recommendations and formatting changes. The journal peer reviewers made recommendations to the paper. Emilio submitted the paper and ensured all requirements were fulfilled.

As mentioned in the introduction, bubbling-to-slugging fluidization is not well understood. In order to describe effects of hydrodynamics on chemistry processes, the bubbling-to-slugging transition must be characterized. In this chapter, simulations are used to non-intrusively probe the physics of a fluidized bed as it transitions from bubbling to slugging. Having acquired an understanding of the bubbling-to-slugging transition, the chemistry at bubbling, bubbling-to-slugging, slugging, and turbulent fluidization can be investigated through simulations. This chapter contains vital bubbling and slugging hydrodynamic information for the reacting flow simulations in later chapters. The guiding hypotheses for this work include: (1) the transition from bubbling to slugging in a bubbling bed of Geldart Group B particles occurs over a range of fluidizing gas flow rather than abruptly at a single critical value of gas flow; (2) The transition to slugging in a bubbling bed of Geldart Group B particles is also correlated with distinctive and reproducible changes in the spatiotemporal characteristics of bubbles, including the distribution of bubble sizes and frequencies; (3) The transition to slugging in a bubbling bed of Geldart Group B particles is correlated with distinctive and reproducible changes in the spatiotemporal characteristics of pressure fluctuations at the bed wall. This chapter shows these hypotheses are correct and guidance is given on how to characterize the fluidization regimes with non-intrusive pressure measurements.

Abstract

We report results from a computational study of the transition from bubbling to slugging in a laboratory-scale fluidized-bed reactor with Geldart Group B glass particles. For simulating the three-dimensional fluidized-bed hydrodynamics, we employ MFiX [Multiphase Flow with interphase eXchange], a widely studied multi-phase flow simulation tool, that uses a two-fluid Eulerian–Eulerian approximation of the particle and gas dynamics over a range of gas flows. We also utilize a previously published algorithm to generate bubble statistics that can be correlated with pressure fluctuations to reveal previously unreported details about the stages through which the hydrodynamics progress during the bubbling-to-slugging transition. We expect this new information will lead to improved approaches for on-line reactor diagnostics, as well as new approaches for validating the results of computational fluidized-bed simulations with experimental measurements.

Introduction and Background

Gas–solid fluidized-bed reactors are widely used in the chemical industry, including biomass conversion [15, 31-33], petroleum refining [34], and pharmaceutical [35, 36] and commodity chemicals production [37]. For this reason, there is widespread interest in establishing a comprehensive understanding of the gas–solid hydrodynamics to optimize processes in which fluidized-bed reactors are key components. Three of the most important hydrodynamic states or flow regimes in fluidized-bed reactors are referred to as freely bubbling, slugging, and turbulent fluidization. Each regime has distinct physical characteristics that produce widely different levels of heat and mass transfer between the gas and solid phases [31, 38]. Thus, it is important to distinguish how the fluidized-bed design and operating conditions correlate with fluidization state. Where possible, identifying on-line process measurements monitoring the fluidization state can be especially useful. This study focuses on understanding how to use pressure measurements to distinguish between free bubbling and slugging.

The free-bubbling state is typically the first condition encountered as the gas flow is increased above the minimum fluidization state [39] in beds of solids within the Group B category of the Geldart's classification scheme [20]. In this regime, pockets of gas (bubbles) form near the bottom of the bed and rise upward until they reach the surface, at which point they erupt. The appearance of the fluidized bed in this case is typically described as similar to that of a boiling liquid. The solids and gas motion associated with the rising bubbles [40] leads to enhanced heat and mass transfer, which is one of the primary advantages for carrying out reactions between fluids and solids in bubbling fluidized beds. Many descriptions of this flow condition are available in literature with comparisons between liquid-gas and solids-gas systems [41-43].

As the gas bubbles rise in a fluidized bed, they typically grow larger due to coalescence and decreased pressure. When the gas flow is sufficiently high and/or the bed sufficiently deep, slugging occurs. Slugging has long been recognized as an area of concern because it is characterized by the formation of large gas bubbles that produce intense oscillations of the bed solids. Criteria have been proposed for the conditions necessary for slugging to develop, such as the following: (1) the static bed height must exceed a critical height; (2) the superficial gas velocity must exceed a minimum (slugging) velocity; and (3) bubbles must be able to grow to a size that approaches the diameter of the fluidized-bed vessel [44, 45]. Typically, many observers report that slugging evolves from the freely bubbling fluidization state as superficial gas velocity is increased, but it is often unclear in the literature just where (or if) there is a clear point of demarcation between free bubbling and slugging. Minimum slugging correlations [46-48] developed from experiments also result in very different values for inlet velocities. Furthermore, some studies [49] have even mistaken the peak in standard deviation as the slugging transition.

Early investigators [46-48, 50-53] developed minimum slugging correlations based on experimental observations. Although these relations are useful for understanding general trends, they relied heavily on subjective visual observations and qualitative features. More recent studies [27, 54-62] have utilized direct quantitative measurements of pressure and void fraction to monitor the spatiotemporal behavior of bubbles. Fan et al. [27], for example, reported a decrease in bubble rise velocity associated with slugging based on cross correlation of pressure measurements in the upper portion of the bed. Similarly, Lee et al. [57] and Saxena and Rao [63] investigated the slugging transition by analyzing pressure measurements from the upper half of a laboratory fluidized bed. [25, 64-67], on the other hand, used electrical capacitance tomography (ECT) to image changes in bubbles associated with the slugging transition. In all these experiments, however, the complex nature of the free bubbling to slugging transition has not been found to be amenable to a clear and consistent physical model.

Computational fluid dynamics (CFD) has a long history of application for dynamic simulation of fluidized beds. Ideally, it should be possible to incorporate sufficient details of the physics of granular and multi-phase flows to replicate all of the salient hydrodynamic features of slugging fluidized bed reactors. The process of capturing all of the critical aspects of the physics at multiple scales remains extremely challenging however, and there are many opportunities for additional improvements. Examples of the challenges and complexities involved in CFD simulations of slugging fluidized beds are highlighted in recently published work such as that by Ichiki et al. [68] , Pain et al. [69, 70], Zhang and Yu [71], Reuge et al. [40, 72], Goldschmidt et al. [73], Loha et al. [74, 75], Fede et al. [76], Xie et al. [77], Li et al. [78], and Bakshi et al. [79, 80]. We emphasize here that our goal is not to attempt to develop and improved any specific model of fluidized bed physics but rather to pursue a better understanding of the basic quantitative trends underlying bubble dynamic behavior as it is predicted by such simulations. We specifically target the dynamics of bubbles and the onset of slugging, because these are known to be critical features that are central in determining the performance of practical bubbling bed reactors. Ultimately, we also are concerned with identifying how bubble patterns can be used to experimentally test the validity of the computational simulations and as a practical monitoring tool (i.e., which bubble measurements should be most useful for validation and on-line diagnostics).

The primary objective of this study is to improve understanding of the transition between free bubbling and slugging by probing the physical details of the process revealed in computational simulations of a laboratory-scale bubbling fluidized bed. We hypothesize that computational studies of this type, as long as they are done with proper care, can provide information that is not directly available from experimental measurements. With this additional information, it should be possible to develop methods based on high speed pressure measurements to detect the approach of slugging in both laboratory and industrial reactors before it becomes problematic. This information can be useful in improving the physical models on which computational simulations are based.

Technical Approach

Fluidized bed simulation conditions

To reflect a lab-scale reactor of current relevance, we assumed the geometry of an experimental laboratory reactor used for biomass processing research at the National Renewable Energy Laboratory (NREL). A schematic of the reactor is shown in Fig. 1-1. The inner diameter D_r and height of the reactor H_r are 0.0508 and 1.27 m, respectively. However, for simulation purposes, the computational domain was reduced to a height of 0.4 m. Operating conditions were chosen to match baseline experiments at NREL and are listed in Table 1-1. Initially, glass particles with diameter d_s of 2.5×10^{-4} m and density ρ_s of 2484 kg/m^3 were set at a static bed height of H_o = 0.2032 m, with an initial void fraction of 0.4. The glass particle-particle properties were defined with a coefficient of restitution of 0.8 [40] and angle of repose at 30°.The particle-wall collision specularity coefficient was set to 0.6, however when normalized slip velocity goes to zero, it is calculated internally using a relation developed by Li et al. [78, 81]. The reactor outlet is open to pressure at 255 kPa. Each simulation was initiated by uniformly adding nitrogen gas through the reactor bottom with a mass flow inlet based on superficial gas velocity U, as a multiple of the minimum fluidization gas velocity U_{mf}. The minimum fluidization velocity was calculated at 0.03 m/s, and the Syamlal-O'Brien drag-model [82] parameters (see Section 2.2) were assigned based on the calculated U/U_{mf} and operating conditions. U/U_{mf} was calculated using the Richardson equation [39] and values in Table 1 together with nitrogen density using the ideal gas form and viscosity using the NASA polynomial for transport properties.

Simulations were conducted with all operating parameters held constant and only inlet velocity, U, was varied from 1.25 to 2.75 U/U_{mf} to identify the onset of the bubbling-to-slugging transition and fully developed slugging. The shown herein are for a single static bed depth, and the transition flow and location should be expected to change with bed height, diameter, and particle characteristics. However, the general utility of this methodology should be expected to hold.

Computational methods

We employed computational fluid dynamics (CFD) [83] to simulate the hydrodynamics in the bubbling bed reactor described above over a range of fluidization velocities. Numerous fluidized-bed researchers have found CFD to be a useful complement to experimental measurements [78, 79, 84, 85]. One of the benefits of CFD is that it can provide spatiotemporal details about pressures, velocities, and concentrations that are either impossible or extremely difficult to obtain experimentally. CFD has also been employed in numerous studies of gas–solid fluidized beds [84, 86], but very limited number of CFD studies have addressed the bubbling-to-slugging transition [45, 87, 88].

The specific CFD implementation used in this study employed the Eulerian–Eulerian computational Two-Fluid Model (TFM) [89, 90], which approximates the flowing phases as interpenetrating continua. This is in contrast to numerical simulations that resolve discrete particles or molecules [88, 91-93]. While the TFM approach does not resolve individual particles, it has been demonstrated to reproduce major hydrodynamic features, including bubbles [40, 77, 79]. Detailed information on the TFM formulation can be found in Gidaspow [89].

To carry out our simulations, we utilized MFiX (Multiphase Flow with Interphase eXchanges), which is an open-source CFD software developed primarily at the National Energy Technology Laboratory [94]. The gas phase was simulated as incompressible, and stress tensors for the gas and solid phases were related to shear stress using Newton's law. To model solids transport properties, such as solids pressure and viscosity, the kinetic theory of granular flow [94] together with the Schaeffer frictional stress tensor formulation [95] and the sigmoidal blending stress function [77, 86, 96] were employed to relate the computed solids temperature with solids transport properties. Furthermore, the gas–solid momentum transfer used the Syamlal-O'Brien correlation [82] for the drag model. The discretization scheme utilized a finite-volume approach with a staggered 3D grid [97]. Scalar values, pressure and void fraction, were stored in the cell center, while velocities were computed on the cell surfaces. Additionally, second-order discretization was utilized using the superbee approach which improved convergence and accuracy of the simulation. A modified SIMPLE approach [97] is also used and improves speed and stability through variable time stepping, solid volume fraction correction, and solids-pressure evaluation. The no-slip condition was applied to the gas phase on the side walls, while the Jackson and Johnson partial-slip wall boundary condition [98] was applied to the solid phase.

To characterize the spatiotemporal dynamics generated by MFiX, we tracked detailed variations in void fraction and pressure as time series at each computational grid point (no reactions or heat or mass transport were included). As explained below, these raw time series were then further processed to produce simulated (virtual) measurements of the bubble patterns and local pressure fluctuations. We then analyzed and compared these time series at each axial location in the bed to understand their correlation with the bubbling and slugging states.

A general concern for multiphase flow CFD simulations is establishing a computational grid size that is sufficiently refined so spatiotemporal dynamics no longer depend on grid resolution (i.e., grid independence). We initially used a 2D fluidized bed simulation to study the impact of the mesh cell size in the x and y-directions on the statistical convergence of the simulated time series. Fig. 1-2 illustrates the effect of mesh cell aspect ratio (AR), $AR=\Delta y/\Delta x$, on the simulated pressure time series, standard deviation, skewness, and kurtosis. These results show mean pressure profiles are not sensitive to cell aspect ratio. However, the higher-order moments are sensitive to cell aspect ratio, which capture higher dimensional dynamics associated with bubbles and mixing. The 40-second 2D simulation with $AR=1$ at 5 U/U_{mf} was further refined to show grid independence from 15×120 cells to 30×240 cells which resulted in run times of 16.5 and 122 hours, respectively.

To account for higher dimensional dynamics [77], a 3D fluidized bed was simulated at 2.75 U/U_{mf} with a fine cylindrical mesh where $\Delta r = \Delta y$, resulting in a uniform mesh with 15 cells in the radial direction and 240 cells in the axial direction, and with 6 azimuthal cells. Skewness and kurtosis did not change as the number of cells in the azimuthal direction was changed to 6, 12, and 24. Based on these results, we selected 6 cells in the azimuthal direction for continued simulations.

Statistical methods

To quantify spatiotemporal dynamic transitions, we determined the statistical properties of pressure and void fraction time series at different axial positions in the bed. We specified normalized axial locations as H/H_o by specifying 10 equally spaced locations H_i up to the static bed height, H_o. We typically examined the bubble statistics at the horizontal planes at 0.1 up to 1.0 H/H_o. We then generated time series by interpolating the pressure and void fraction measurements from the nearest grid points at each simulation time step (0.01 s). For pressure, all the grid point values in a plane were then averaged together to create a single average pressure time series for each bed axial location. Experimental groups [99, 100] have found pressure measurements are influenced by a volumetric region close to the pressure port, and the analysis method used here captures dynamics in a defined volumetric region composed of cells near the probe measurement point.

To assist in understanding the physics involved, we also processed the void fraction time series at each grid point with MS3DATA, a special algorithm recently developed by Bakshi et al [79], to resolve bubble sizes and numbers in fluidized beds. MS3DATA is a code developed in MATLAB and identifies bubbles in a five-step process [80]: data collection, bubble detection, conflict resolution, bubble properties and Lagrangian velocimetry. Initially the code collects void fraction data and bubble boundary resolution. It is followed by applying the user specified void-fraction threshold criteria and bubble linking, to define regions of contiguous subthreshold void fraction. The code then performs bubble conflict resolution by assigning unique bubble numbers to every grid cell. Bubble properties such as location, size, span, and shape are then assigned. The code can also track bubbles across successive time frames, but this analysis was not performed in this investigation.

For consistency, only cells with void fraction > 0.7 [25, 66, 79, 101] were considered as representing bubbles, and we found results did not change significantly by selecting a slightly different cut-off value. Bubble-counting domains were defined as axial locations up to the halfway points of adjacent axial planes (e.g., the volume between 0.85 and 0.95 H/H_o for counting at 0.9 H/H_o). Bubbles whose centroids resided within each axial domain were used by MS3DATA to calculate bubble size and number. Within each axial domain, bubble diameter d_b was evaluated using the linked bubble volume V_b according to $d_b = \sqrt[3]{6V_b/\pi}$. More details of the bubble-statistics algorithm in MS3DATA can be found in Bakshi et al. [102]. Initial tests showed pressure and bubble statistics became statistically stationary after 7 seconds of physical time. Therefore, although the simulations were sampled for 40 seconds at 100 Hz, the first 10 seconds were discarded, resulting in time series ranging from 10 to 40 sec for pressure and bubble statistics.

Numerous statistical descriptions, some of which are based on concepts from nonlinear and complex systems theory, have been proposed for characterizing time-series measurements from fluidized beds [43, 54, 57, 99, 103-109]. For this study we elected to concentrate on more traditional statistical measures to simplify the analysis and development of relationships between the pressure and bubble patterns. These statistics included histograms of the time-series values as well as quantitative characterizations utilizing the mean, standard deviation, skewness, and kurtosis. We also utilized the autocorrelation and cross-correlation functions [110] to evaluate relationships between different measurements at different points in time.

In some cases, the time series were normalized by their mean to highlight certain features. These cases are described in the Results and Discussion section. We also utilized the method proposed by Scott [111] to select the best bin sizes for constructing frequency histograms.

Results and Discussion

The visual appearance of the bubbles generated by MFiX was observed graphically in terms of void fraction iso-surfaces using Paraview [112] as illustrated in the following section below. To systematically quantify the simulated bubble patterns, we evaluated bubble statistics derived from the MFiX void fraction output using MS3DATA. We then evaluated the pressure time series features at each level to determine how they relate to the observed bubble behavior.

Bubble characteristics at low gas flows (free bubbling)

Fig. 1-3 (a-e) illustrate typical bubble characteristics we observed in low gas flow simulations. Fig. 1-3(a) shows the predicted time-average profiles for bubble size and concentration at a gas flow corresponding to U = 1.25 U/U_{mf} as determined from the MFiX output with MS3DATA [102]. Fig. 1-3(b) illustrates an example instantaneous snapshot of bubbles predicted for this same condition from the MFiX output with Paraview. Fig. 1-3(c-e) reveals characteristic bubble size growth as the bubbles move from lower to higher levels. This is consistent with the expected effects of bubble-to-bubble coalescence and reduced pressure [28, 113]. However, MS3DATA results indicate the number of bubbles increase with height until reaching the splash (eruption) zone [28]. We conjecture that this growth in numbers might be explained as the result of bubble splitting and/or the increase in gas flow above U_{mf} due to the reduced pressure. Bakshi et al. [80] published work which utilized MS3DATA on larger-diameter fluidized beds (15, 30, 50 and 70 cm). In these studies, they observed a larger number of bubbles (bubble count/frame) in the bottom relative to the top of the bed. This was also the trend we saw for reasonable assumptions about the void fraction cutoff limit at high gas flows. However, we emphasize that direct comparisons between the reactors simulated by Bakshi et al. and the reactor in this study are likely to be misleading because of the different reactor sizes and particle properties. In particular, the larger diameters of the Bakshi et al. reactors (making it possible to generate larger bubbles with reduced wall drag) and their larger particles (putting them on the Geldart Group B/D boundary) would be expected to significantly influence the bubble behaviors.

Although the simulated bubbles described above appear to reflect the expected trend in bubble size, it is not clear to us that the predicted bubble shapes are consistent with direct visual observations reported by experimental studies. In particular, it appears that the simulated bubble shapes are less regular and somewhat flattened compared to images from experimental ECT and x-ray observations [26, 114, 115] at similar fluidization states. Additionally, we did not expect the number of bubbles to increase with height as much as indicated by the MS3DATA results. Instead, this particular trend may provide a good way to test the soundness of bubbling bed simulations. If experiments can confirm that the predicted bubble number trends are indeed wrong for these conditions, it may reveal an inherent shortcoming in the two-fluid approximation that needs to be resolved in future studies. Based on other investigations [40, 74, 75, 79, 116] it might be possible to address this shortcoming by tuning one or more MFiX parameters based on experimental measurements [40, 58, 62, 73, 80]. On the other hand, it may be that the two-fluid simulations are revealing a feature of bubbling beds that has not been previously recognized.

Bubble characteristics at high gas flows (fully developed slugging)

At much higher gas flows (e.g., $U = 2.75\ U/U_{mf}$) the simulated time-average bubble profiles change dramatically as depicted in Fig. 1-4(a), where the average bubble concentration reaches a maximum much lower in the bed and then drops precipitously with height. On the other hand, the average bubble size near the top of the bed grows until it approaches 60% of the bed diameter. At H/Ho ~ 0.5 the bubble size and bubble concentration curves exhibit significant changes in slope, which we conjecture may be the result of bubble coalescence events similar to those observed in experiments by [28, 62]. It is important to note that mean bubble number per frame reflects the average volumetric bubble number concentration in an axial plane. When viewed this way, our results show that at high gas flows, the region of the bed below 0.4 *H/Ho* exhibited a decreased bubble count per frame as the void fraction cutoff value was decreased from 0.7 to 0.55. We also note, however, that in the lower region of the bed, the simulated bubbles at high gas flow had less distinct boundaries, making it more difficult to discriminate between separate bubbles (and thus accurately count bubbles) when the cutoff void fraction used to recognize bubbles is decreased to 0.55 or below. As long as cutoff values of 0.7 and 0.6 were specified, the general axial trend in bubble frequency did not change much.

In Fig. 1-4(b) we see that the largest simulated bubbles in the upper part of the bed begin to assume ogive (bullet-like) shapes, which nearly fill the bed cross section, fully developed slugging bubbles. We conjecture that as these bubbles grow larger, the increased wall drag should slow their rise velocity, allowing smaller trailing bubbles to catch up and coalesce with them, making them larger still. This suggests that the bubbling-to-slugging transition is inherently a type of avalanching or critical transition process [54].

Bubble pattern differences are also evident in the time-average histograms of bubble size. Near the bottom of the bed Fig. 1-4(c)) the bubble-size histogram has a positive tail that grows more pronounced with height and transitions to a bimodal shape near the top of the bed Fig. 1-4(d) and (e)). We conjecture that this bimodality results from repeated coalescence events between some but not all of the rising bubbles, reflecting a global bifurcation process consistent with the observations of visualization experiments [25, 50, 66]. Similar bifurcation phenomena have been observed in bubble columns of highly viscous fluids during bubble coalescence [108, 117], implying that this might be an example of a more general bubble phenomenon [118]. Although liquid-gas and solid-gas bubbles are governed by different physics [41], it seems plausible that there could be similarities in their regime transitions [41-43].

Bubble patterns at intermediate gas flows (between free bubbling and fully developed slugging)

For gas flows between the high and low limits, the simulated bubbles exhibited intermediate emerging characteristics as depicted in the example time sequence in Fig. 1-5. Under these conditions, we observed repeated instances of smaller bubbles merging together to form larger bubbles. While these larger bubbles initially accelerated relative to the small bubbles (note the larger travel distance of bubble cluster A compared with bubble cluster B), the acceleration became retarded when the bubbles grew sufficiently that their edges approached the wall. These interactive alterations of bubble size and speed appeared to be the essential processes behind the emergence of slugging in the MFiX simulations.

Fig. 1-6((a) and (b)) illustrate the trends in the vertical time-average bubble size and concentration profiles extracted with MS3DATA[102] from the MFiX output over the entire flow range between 1.25 and 2.50 U/U_{mf}. From these, it can be seen that the average bubble diameters are always largest near the top of the bed for all gas flows, although the difference in bubble size between the top and bottom increases with increasing flow. The biggest increase in this difference appears to happen for flows just above 1.75 U/U_{mf}. On the other hand, the trend in bubble concentration (Fig. 1-6(b)) appears to undergo an even more distinct transition when the gas flow exceeds 1.5 U/U_{mf}. Above 1.5 U/U_{mf} the bubble concentration in the lower bed begins to exceed that in the upper bed. The upper bed also reaches a maximum bubble concentration. Careful observations of the detailed bubble sequences generated by MFiX indicate that this is the gas flow condition in which the intermediate emerging bubble characteristics from Fig. 1-5 begin to appear near the top of the bed. Thus, this is the beginning of the bubbling-to-slugging transition. Similarly, at 2 U/U_{mf}, bubble concentration first reaches a minimum near the top of the bed, indicating large, ogive bubbles first begin to emerge near the top of the bed. Bubble concentration at higher gas flows appears to converge to this same minimum bubble concentration near the top of the bed, indicating the end of the bubbling-to-slugging transition and the beginning of the fully developed slugging regime.

Additional perspectives on the intermediate-flow bubble patterns are revealed in the time-average bubble-size histograms in Fig. 1-7. In this figure, two demarcation lines are drawn: the first (marked in orange) indicates the approximate vertical locations and gas flows where significant bimodal features and ogive bubbles begin to appear, and the second (marked in green) indicates where bimodality and ogive bubble shapes become dominant features. We suggest that these lines outline a region of gas flow and bed height, within which, the free bubbling to slugging transition occurs. Bubble size histograms (Fig. 1-7) and bubble concentration (Fig. 1-6(b)) illustrate the bubbling-to-slugging transition occurs between 1.5 to 2 U/U_{mf}, also corresponding to the bubble histograms at the top of the bed.

Trends in predicted pressure fluctuations

As might be expected, the two-fluid MFiX simulations predict a complex but significant relationship between the bubbling transition patterns and pressure variations. As described above, the observed bubble behavior varied significantly with axial position, and this was mirrored by corresponding changes in the relationship with pressure. Some major features of this relationship and how it varied with position are summarized below.

Pressure fluctuations at low gas flow (freely bubbling)

Fig. 1-8(a-h) depict key characteristics of the pressure-fluctuation profiles predicted by the simulation at low gas flow (free bubbling at U = 1.25 U/U_{mf}). As expected, the mean pressure values at each level dropped monotonically in moving from the bottom to the top of the bed (Fig. 1-8(a)). Consistent with the previously described bubble growth trends with height, the standard deviation of the pressure fluctuations also grew with height (Fig. 1-8(a)). Similarly, skewness (S_p) and kurtosis (K_p) variations with height (Fig. 1-8(b)) were also consistent with changes in the pressure-fluctuation distributions with height (Fig. 1-8(f-h)) and reflect major shifts in the bubble-size distributions. We conjecture that these changes in distribution are associated with changes in the bubble shape and coalescences described above and expect that these statistics should contain useful diagnostic information [99].

Pressure fluctuations at high gas flow (fully developed slugging)

At high gas flow (U = 2.75 U/U_{mf}) the predicted pressure-fluctuation time series and statistical profiles exhibit significant changes as illustrated in Fig. 1-9(a-h).

As in the low-flow condition, sharp positive and negative spikes were visible in the pressure time series, resulting in large changes in standard deviation, skewness, and kurtosis values related to the histograms with height. We speculate that these spikes reflect the influence of local, low-amplitude wake and drift bubble passage effects as suggested by Rudisuli [28], as well as bubble coalescence events and the downward propagation of global pressure waves originating from bubble eruption, bed expansion, and contraction [28]. We also suspect that the bimodality in the pressure fluctuations near the top of the bed may be correlated with the bimodal bubble-size distributions described above. Other investigators [99] have proposed that these changes in the skewness and kurtosis of pressure fluctuations might be used as a bubble diagnostic [119] that is not as easily observable [120] in the mean and standard deviation. Also, the standard deviation of pressure decreases at higher H/H_o due to the lower hydrostatic pressure and bubble-eruption events at the bed surface, which equalize pressure with the freeboard.

Pressure fluctuations at intermediate gas flows (between free bubbling and fully developed slugging)

As with the bubble patterns, pressure fluctuations at intermediate gas flows exhibited characteristics between those observed at the low and high flow limits in this study. An example of these intermediate characteristics is depicted in Fig. 1-10(a-h).

The significant changes occurring in the pressure fluctuations between the low and high gas flow, indicate that pressure histogram statistics might serve as useful diagnostics for the freely bubbling to slugging transition as illustrated in Fig. 1-11 for skewness and Fig. 1-12 for kurtosis. This appears to be especially true for measurements from the upper region of the bed.

The relative importance of the skewness and kurtosis changes in these simulated pressure fluctuations appears to be consistent with the experimental observations of Lee et al. [57], who noted that a minimum in skewness in the upper bed ($0.65 < H/H_o < 1.0$ [121]) appeared to correlate with the bubbling-to-slugging transition. Based on our simulation results, the peak of S_p at the lower part of the bed ($H/H_o < 0.7$) might also be a characteristic indicator of the onset of the transition to slugging. Lee et al. [57] also found that an increase in K_p for pressure fluctuations in the upper section of the bed correlated with the bubbling-to-slugging transition. This appeared to be consistent with our simulations, as shown in Fig. 1-12(a).

Data from Fig. 1-12(a) were re-plotted (Fig. 1-12(b)) to illustrate trends in K_p which relate to the fully developed slugging bubbles observed in section 3.1.3. At 2 U/U_{mf} near the top of the bed, K_p first becomes negative, which appears to indicate the beginning of fully developed slugging. As gas flow increased, the K_p curves shifted to lower locations in the bed, as similarly predicted by the bubble statistics. Furthermore, to supplement this observation, the inflection point in standard deviation occurs at 2 U/U_{mf}. This observation is consistent with experimental observations by Daw et al. [54] where the "maximum stable slugging" conditions occurred where there was an inflection point in the standard deviation curve.

Time scale information in the pressure fluctuations

Besides exhibiting changes in statistical distribution with gas flow, the simulated pressure fluctuations also exhibited changes in time scale that correspond to shifts in bubble behavior. This is illustrated by changes in the pressure time series autocorrelation function, as depicted in Fig. 1-13. As the simulated gas flow increased, the autocorrelation became more periodic (especially at higher levels in the bed), revealing the impact of a few, large bubbles. The time scales of the largest oscillations at high flow were typically 0.3–0.5 s, corresponding to the frequency range associated with the large ogive bubbles in the upper bed. This implies that time-scale variations, such as observed in nonlinear-dynamics [43, 54, 55, 105, 109], as well as statistical distribution variations in the pressure fluctuations, such as those presented here, should be useful diagnostic tools for monitoring the bubbling-to-slugging transition. As noted above however, interpretation of these diagnostics will depend greatly on where (H/H_o) the pressure measurements are made.

Cross-correlations between bubble patterns and pressure variations

Cross-correlation provides another method for quantitatively confirming the predicted physical connection between the void fraction (bubble behavior) and pressure fluctuations. Example results for the two-fluid MFiX simulations are depicted in Fig. 1-14, where the cross-correlation of void fraction with respect to pressure from bubbling to fully developed slugging at 0.9 is compared with the void fraction and pressure differential time series. As can be seen, the cross-correlation between these time series begins rising rapidly with gas flow and always reaches a maximum just below the static bed height. In the future, we expect that cross-correlations such as this can provide a useful way to compare computational simulations with experimental measurements in order to validate and/or refine computational fluidization models.

Comparison of the predicted trends with previous correlations

As discussed earlier, an important motivation for studies of this type is the apparent inconsistency of slugging predictions from correlations in literature. Fig. 1-15 below illustrates this for the present case by comparing the predictions of slugging correlations proposed by Stewart and Davidson [48], Baeyens and Geldart [46], Broadhurst and Becker [47] and Shaul et al. [122] with the gas flows predicted by MFiX for the initial onset of the bubbling-to-slugging transition and complete transition to slugging, fully developed slugging. As can be seen there is considerable variation among the predictions from these correlations about the gas flow at which slugging should occur. Some of this variation may be due to differences in the criteria used by the authors to define slugging, and this should not be surprising given the complex nature of the bubbling-to-slugging transition revealed in this study. Assuming that the trends in the present MFiX simulations can be experimentally validated, it might be more useful to develop correlations that predict the flows at both the beginning and end of the slugging transition process. This is clearly an area where development of an improved understanding of the physics underlying slugging and a more precise terminology related to its occurrence would be helpful.

Conclusions and Recommendations

Results from the three-dimensional computational simulations of a laboratory-scale fluidized bed indicate that the transition from bubbling-to-slugging is a complex process that occurs over a range of gas flows rather than abruptly at a single flow. The transition process appears to involve a cascade of bubble coalescences that produce size and speed changes which begin near the bed surface and then progress downward toward the distributor as gas flow increases. The state of maximum slugging intensity appears to be reached when the most intense coalescence point approaches the bottom of the bed. The general dynamical trend predicted by our simulations appears to be consistent with the trends observed in other experimental studies of bubble behavior in viscous liquids and bubbling fluidized beds equipped with bubble imaging capabilities.

Detailed analyses of the simulated bubble patterns and high-speed pressure fluctuations indicate that both amplitude and time-scale statistics derived from the pressure fluctuations can be a useful diagnostic for tracking bubble behavior and the transition from free bubbling to maximum intensity slugging (fully developed slugging). The most useful pressure amplitude statistics include the kurtosis and skewness of pressure fluctuation histograms. Time-lagged autocorrelations in the pressure time series appear to correlate with bubble sizes and speeds. However, the pressure features most useful for diagnosing bubble behavior depend strongly on the vertical location in the bed where the pressure measurements are made. Based on the analyses described here, the optimum location for pressure measurements to monitor bubble behavior related to the slugging transition appears to be near the top of the bed, below the static bed height.

There are several remaining areas that should be investigated concerning the future work on bubbling-to-slugging transition in beds of Geldart Group B solids:

- Direct comparisons between computational simulations and high-speed experimental void fraction and pressure measurements [99, 100] are needed to validate/improve existing CFD models.
- Computational simulations of the bubbling-to-slugging transition with other CFD approaches such as the Eulerian–Lagrangian Discrete Element Method (DEM) are needed to resolve questions about the best approach for capturing the fundamental physics.
- More detailed studies of the detailed relationship between bubble and pressure dynamics are needed to allow pressure signals to be a useful indicator of bubble patterns.
- Further analyses are needed to understand how spatial voidage and pressure measurement locations can affect the dynamic information available for generating useful diagnostics.
- Computational simulations and corresponding experimental measurements are needed to determine how significant the bubbling-to-slugging transition is likely to be in altering chemical conversion and the efficiency of heat and mass transfer.

Appendix: Figures and Tables

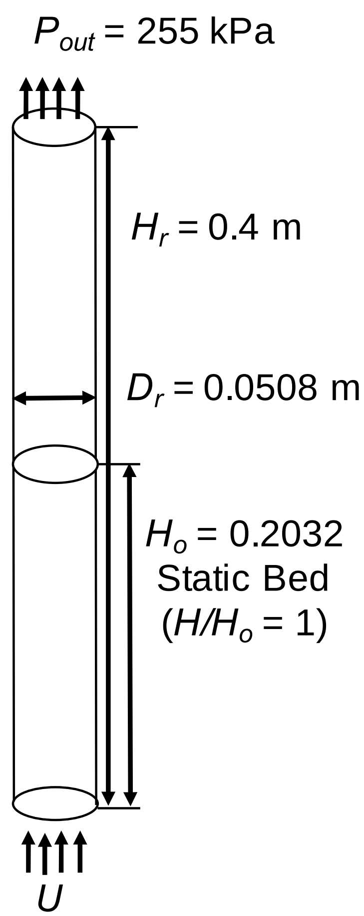

Fig. 1-1 Schematic diagram of the simulated bubbling bed

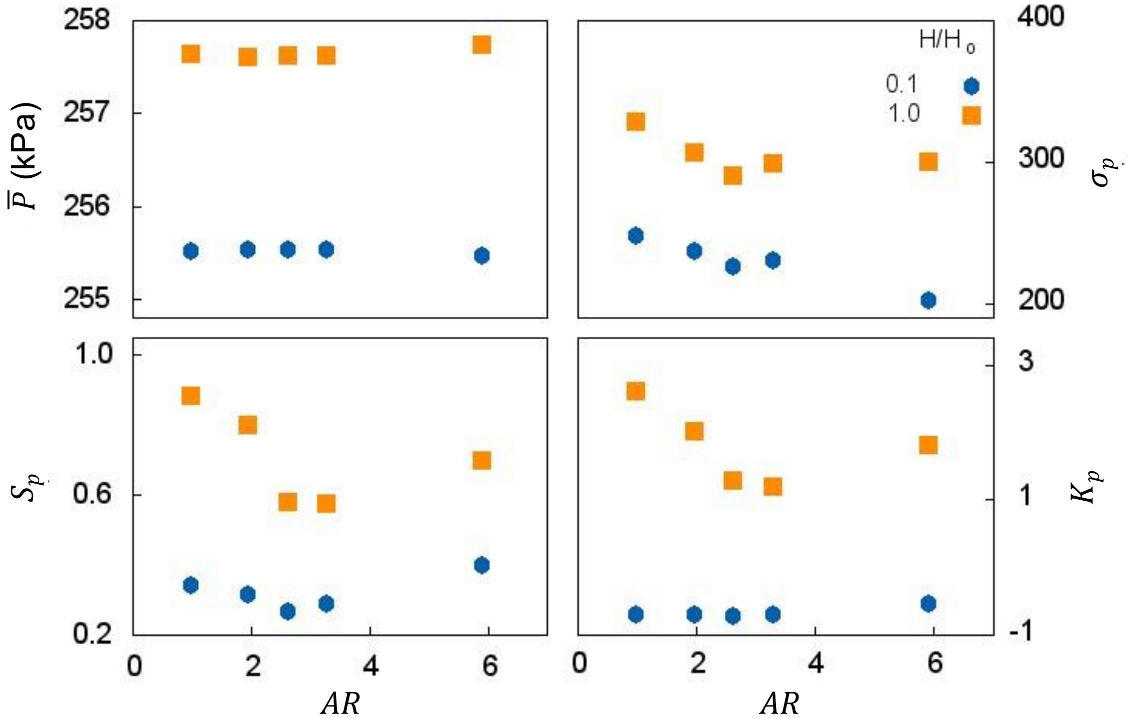

Fig. 1-2 Pressure statistics convergence at different computational grid aspect ratios, *AR*=*Δy*/*Δx*.

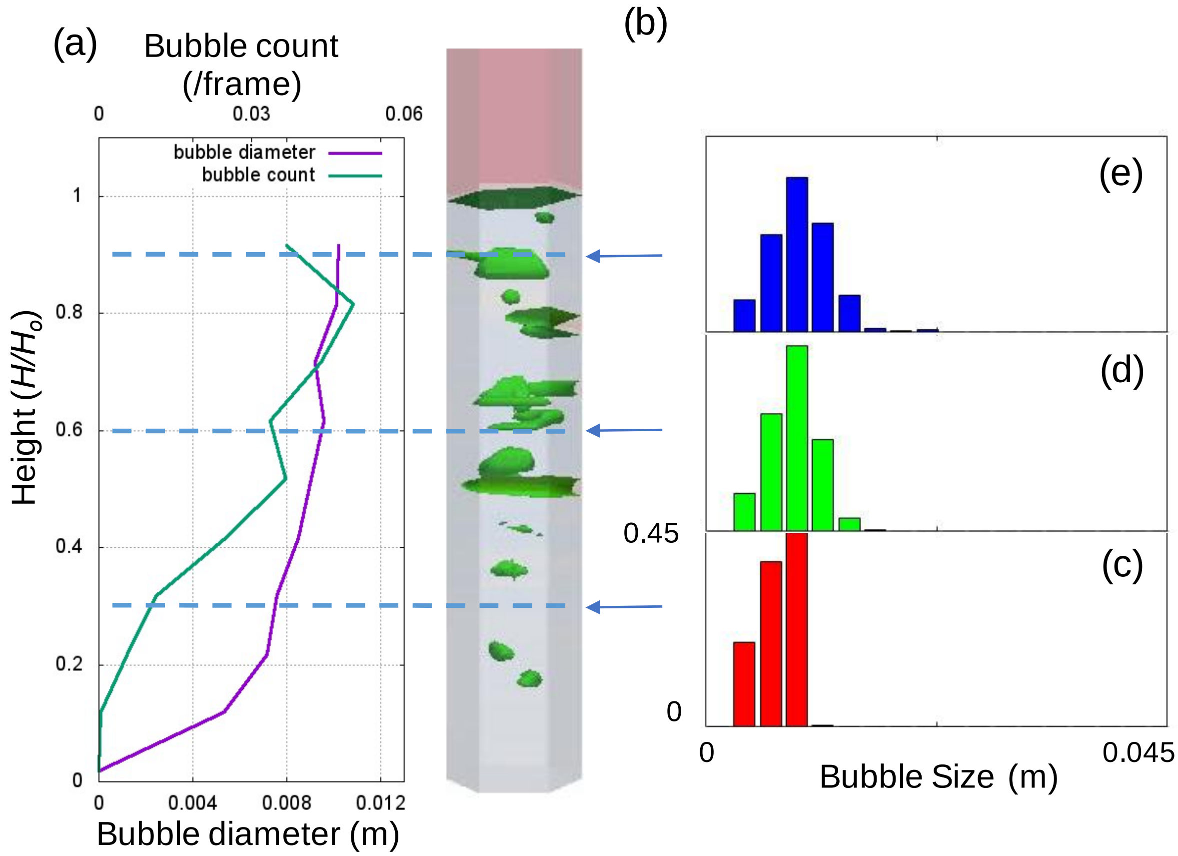

Fig. 1-3 (a) Time-average vertical profiles of the simulated bubble size and bubble count (concentration) per frame under low gas flow conditions (U=1.25 U/U_{mf}); (b) instantaneous snapshot of bubble iso-surfaces; (c-e) bubble size histograms at H/H_o = 0.3, 0.6, and 0.9, respectively.

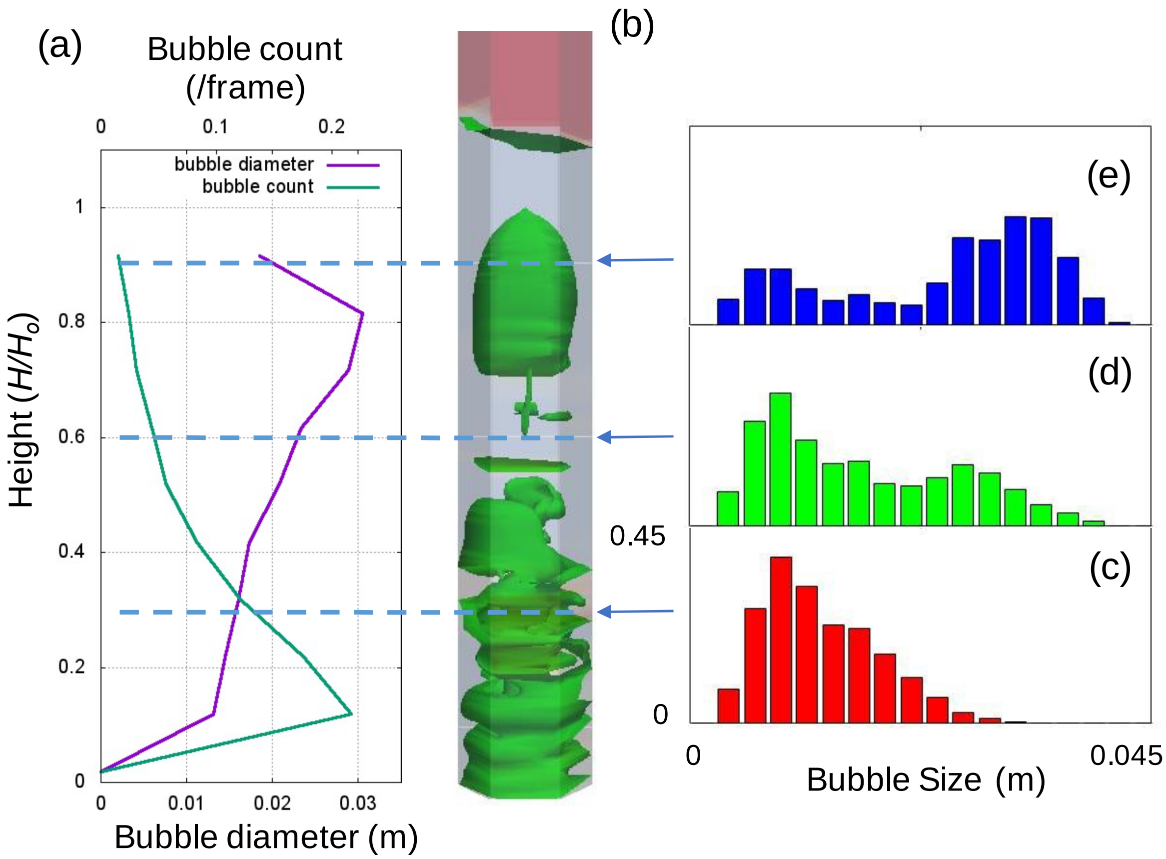

Fig. 1-4 (a) Time-average vertical profiles of the simulated bubble size and bubble count (concentration) per frame under high gas flow (U = 2.75 U/U_{mf}); (b) instantaneous snapshot of bubble iso-surfaces; (c-e) bubble size histograms at H/H_o = 0.3 (c), 0.6 (d), and 0.9 (e).

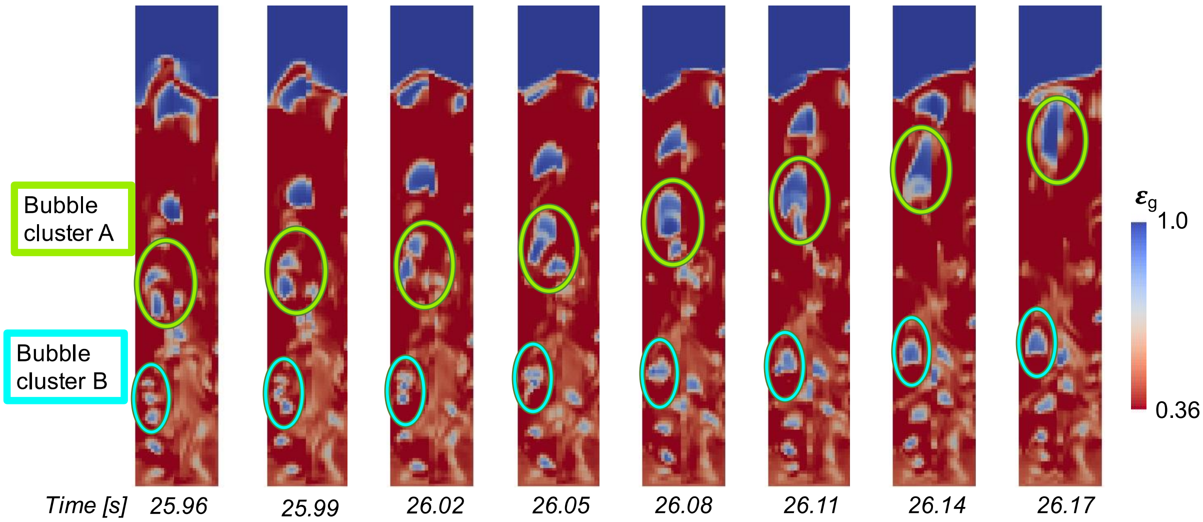

Fig. 1-5 Bubble shape evolution at 0.03 s time steps at intermediate gas flow (U = 1.75 U/U_{mf}). The highlighted regions compare two different bubble size clusters at different locations.

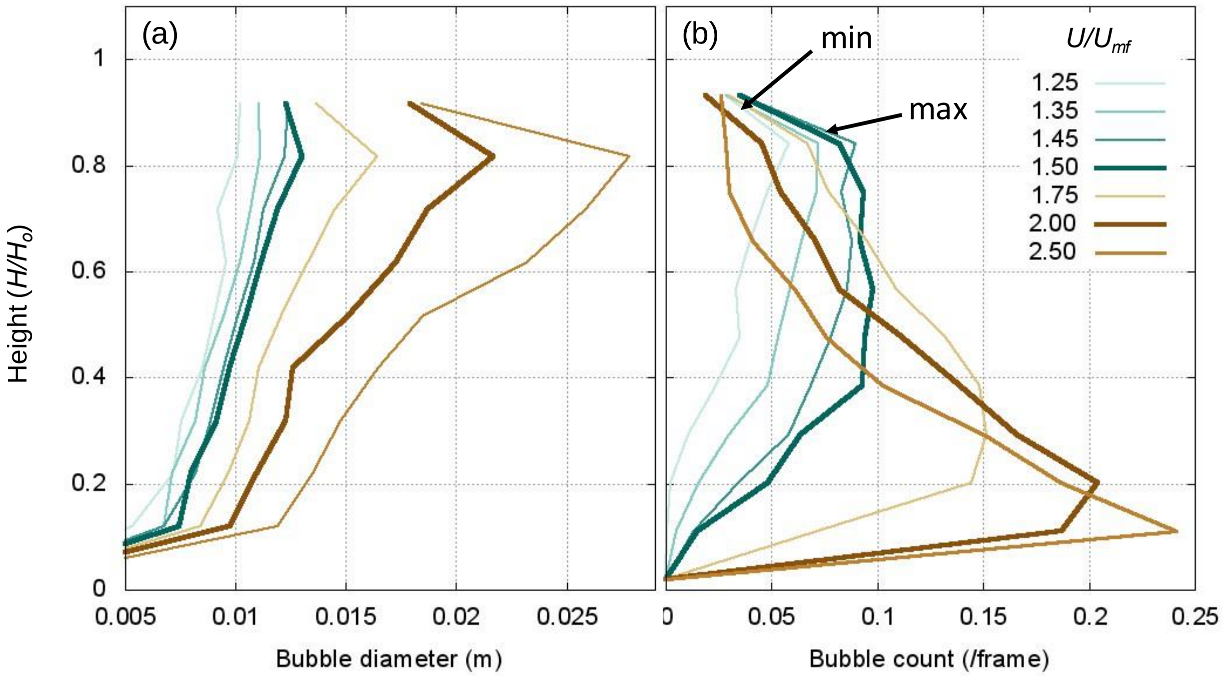

Fig. 1-6 Predicted time-average bubble diameter (a) and bubble count (concentration) per frame (b) profiles in the bed for a range of gas flows.

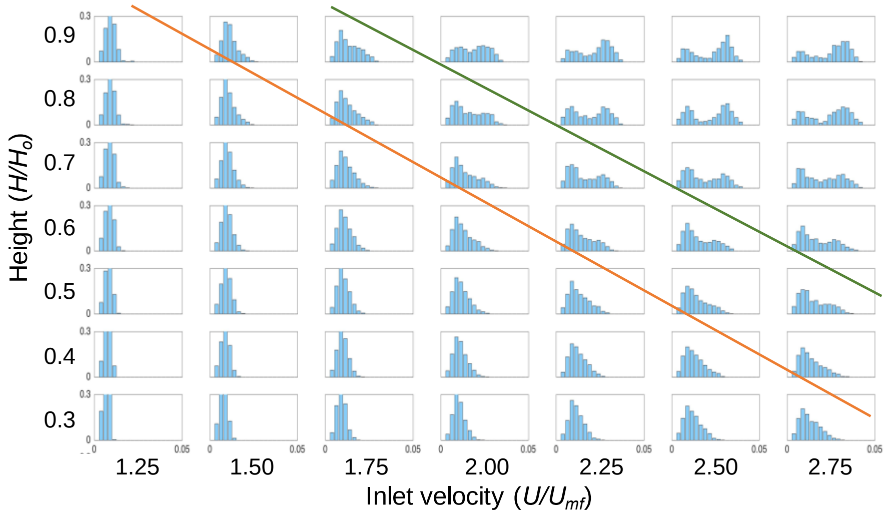

Fig. 1-7 Bubble-size histograms at different H/H_o and U/U_{mf}.

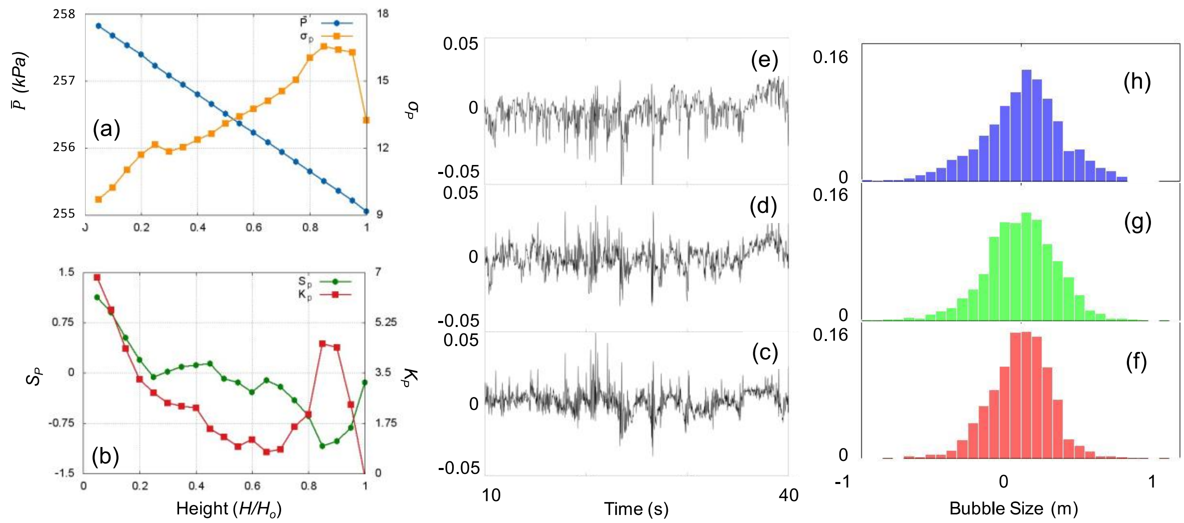

Fig. 1-8 Pressure fluctuation patterns at 1.25 U/U_{mf}: (a) time-average pressure ($\overline{P}$) and standard deviation (σ_p); (b) skewness (S_p) and kurtosis (K_p); normalized pressure time series and pressure probability distributions at H/H_o = 0.3 (c,f), 0.6 (d,g), 0.9 (e,h).

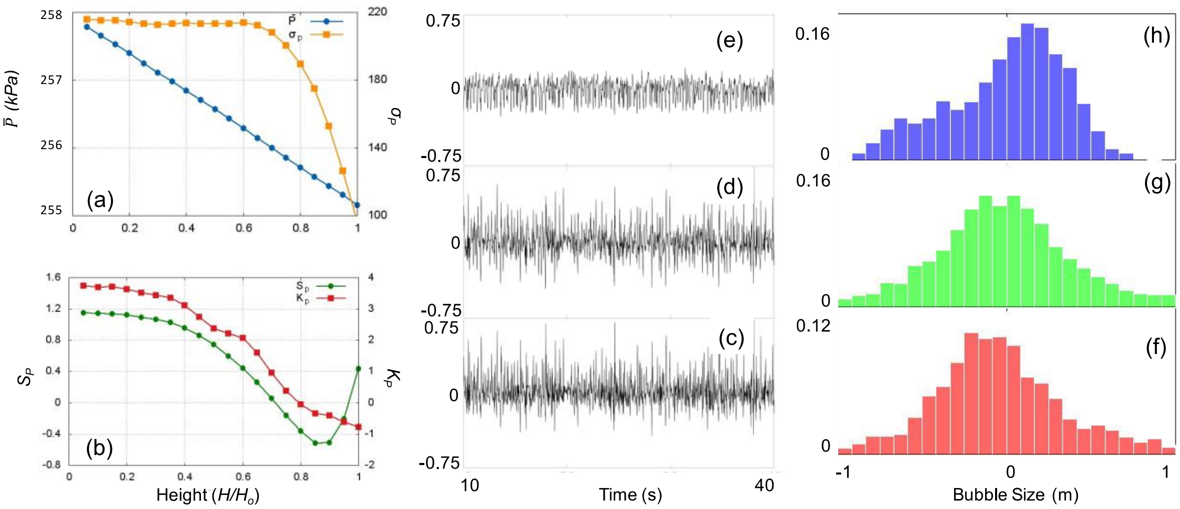

Fig. 1-9 Pressure fluctuation patterns at 2.75 U/U_{mf}: (a) time-average pressure ($\overline{P}$) and standard deviation (σ_p); (b) skewness (S_p) and kurtosis (K_p); normalized pressure time series and pressure probability distributions at H/H_o = 0.3 (c,f), 0.6 (d,g), 0.9 (e,h).

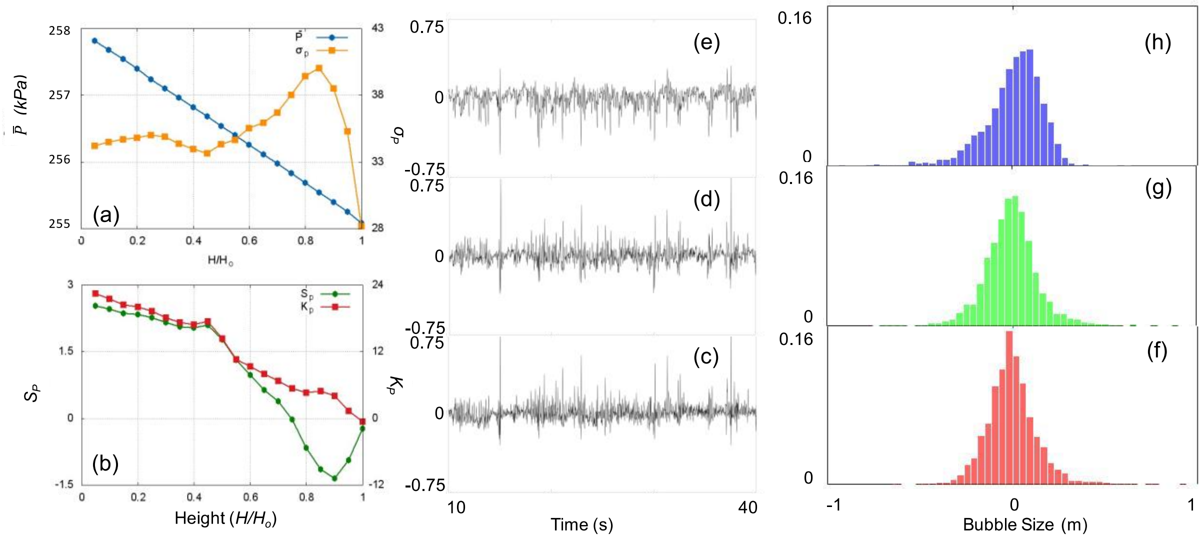

Fig. 1-10 Pressure fluctuation patterns at 1.5 U/U_{mf}: (a) time-average pressure ($\overline{P}$) and standard deviation (σ_p); (b) skewness (S_p) and kurtosis (K_p); normalized pressure time series and pressure probability distributions at H/H_o = 0.3 (c,f), 0.6 (d,g), and 0.9 (e,h).

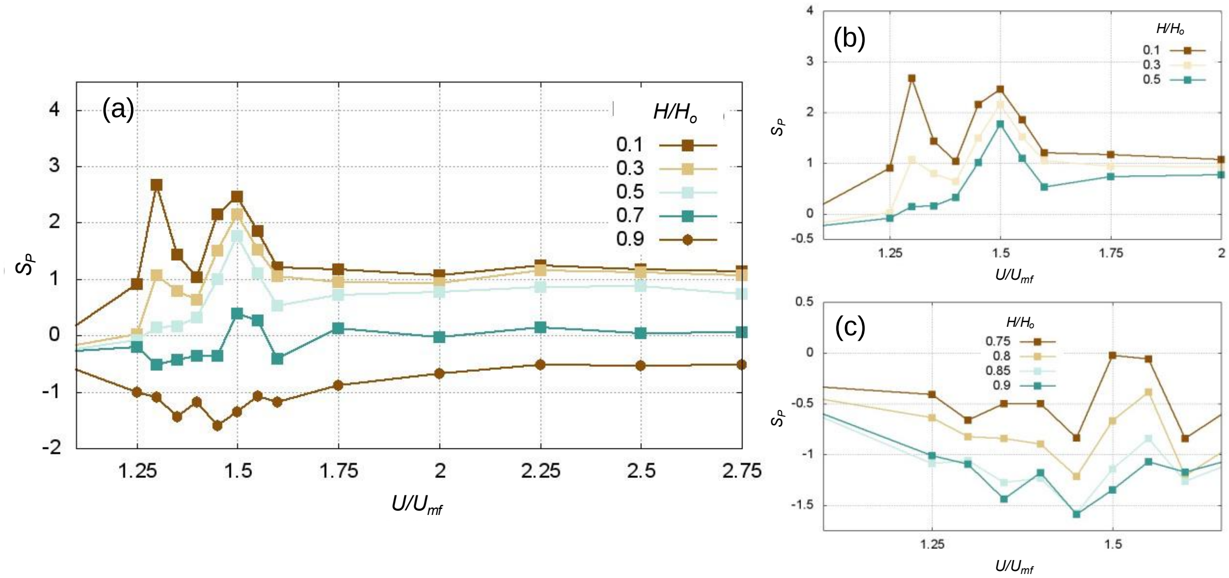

Fig. 1-11 Variations of skewness (S_p) in the predicted pressure fluctuations with respect to gas flow at different bed heights (a); S_p with respect to U at H/H_o < 0.7 (b); and S_p with respect to U at 0.7 < H/H_o < 1.0 (c).

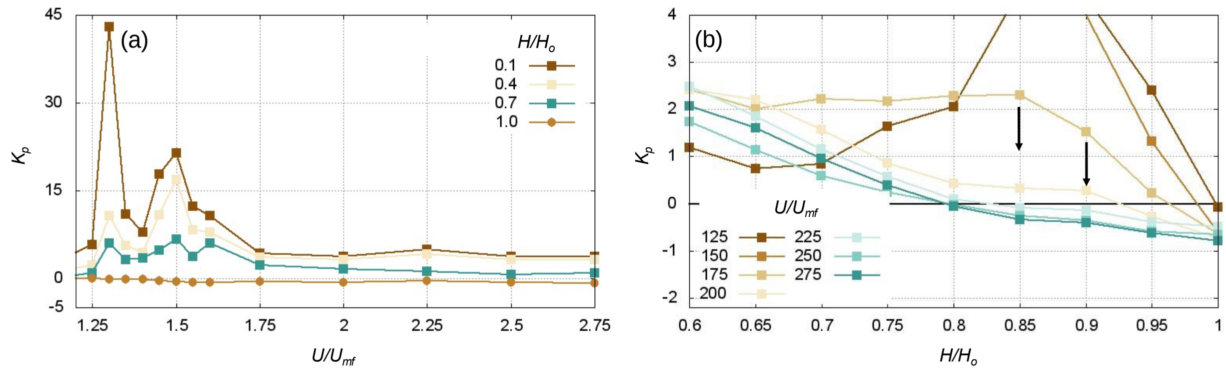

Fig. 1-12 Variations of kurtosis (K_p) in the predicted pressure fluctuations with respect to gas flow at different bed heights (a); K_p with respect to bed height at various gas flows (b).

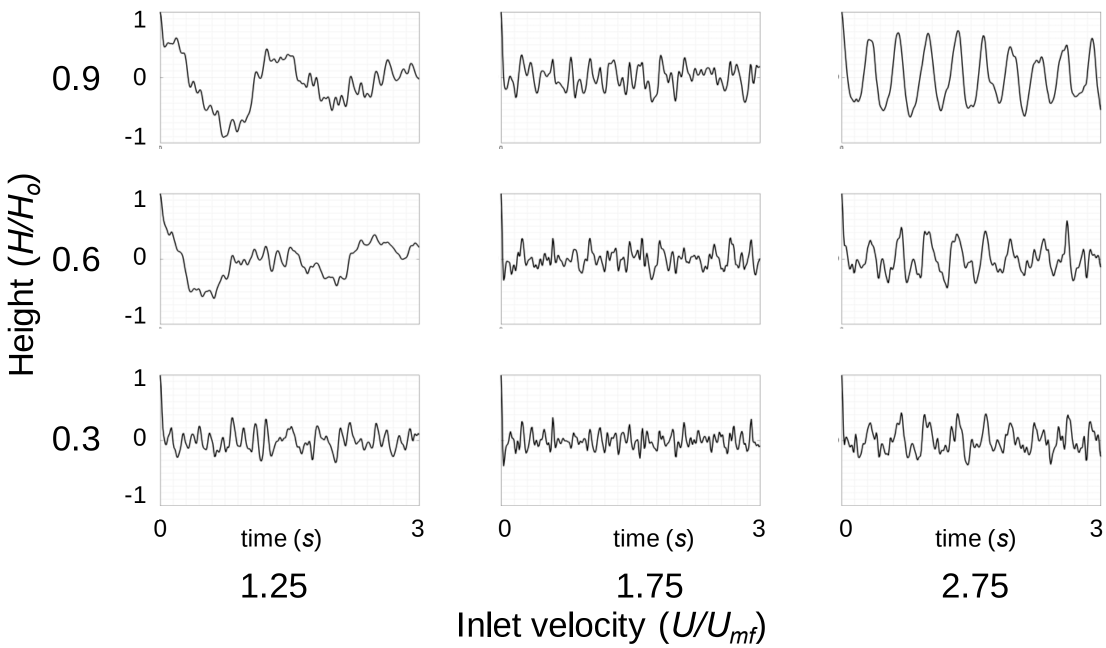

Fig. 1-13 Example autocorrelation functions for the simulated pressure fluctuations at 3 vertical locations for low, intermediate, and high gas flows.

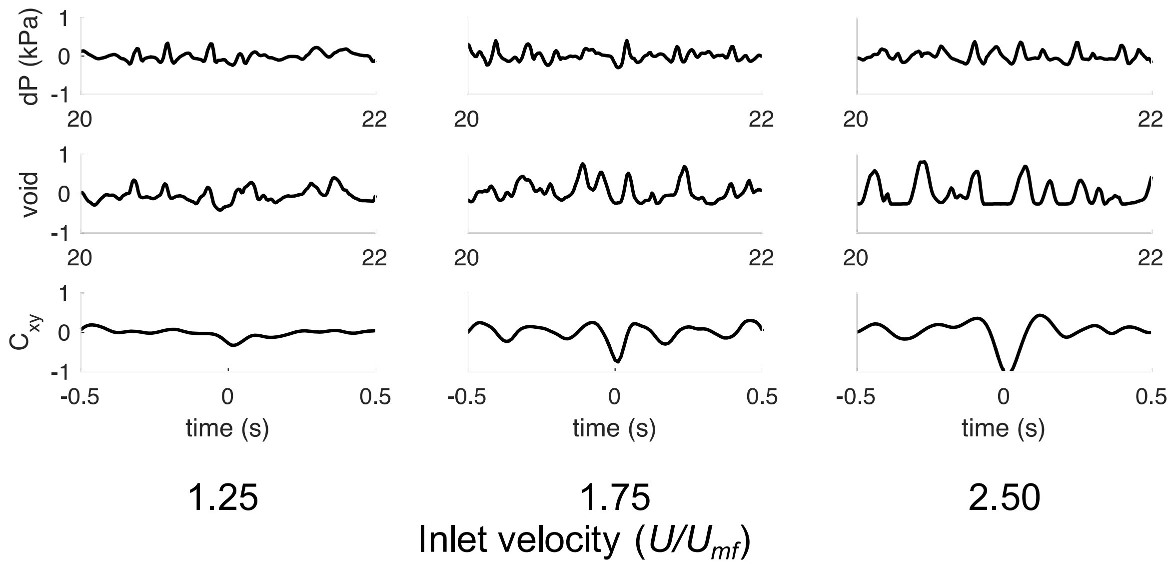

Fig. 1-14 Maximum absolute magnitude of the cross-correlation between pressure and void fraction time series with respect to *H* at different *U*.

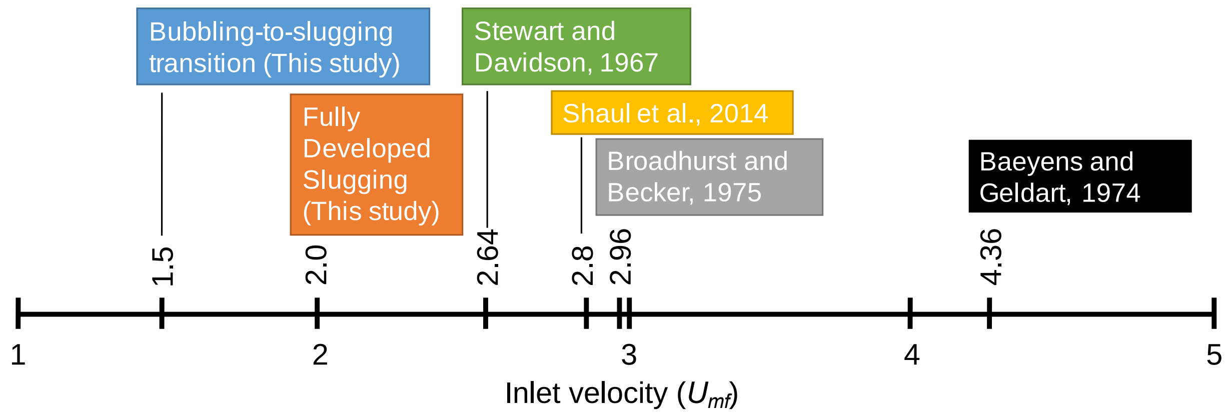

Fig. 1-15 Comparison between this study and slugging correlations

Table 1-1 Operating conditions

Definition	**Units**	**Experiment**
Particle diameter	m	2.5×10^{-4}
Particle density	kg/m^3	2484
Bulk density	kg/m^3	1552
Temperature	K	773
Pressure	kPa	289
Fluidizing N_2 (range)	kg/s	$8.46 - 18.6\times10^{-5}$

CHAPTER 2 : HYDRODYNAMIC EFFECTS ON THE PERFORMANCE OF A LABORATORY-SCALE FLUIDIZED-BED BIOMASS FAST-PYROLYSIS REACTOR

A version of this chapter will be originally published by Emilio Ramirez et al.:

Ramirez, E., Li, T., Shahnam, M., & Daw, C. S. (In Preparation). "Computational study on biomass fast pyrolysis: Hydrodynamic effects on the performance of a laboratory-scale fluidized bed reactor."

The work in this chapter was analyzed and written by Emilio Ramirez. Guidance was provided by Tingwen Li, Mehrdad Shahnam, and Stuart Daw. Tingwen Li reviewed and ensured the simulation would satisfy hydrodynamic aspects. Tingwen, Mehrdad, and Sreekanth Pannala ensured the simulation reaction setup was consistent and robust. Stuart provided guidance on the CFD/MATLAB model. Stuart also reviewed the introduction and abstract. Emilio will be submitting the paper and will ensure all journal requirements are fulfilled.

In this chapter biomass pyrolysis chemistry at bubbling, bubbling-to-slugging, slugging, and turbulent fluidization regimes were investigated. Work on the bubbling-to-slugging transition from the previous chapter was utilized to characterize bubbling hydrodynamics and relate biomass particle mixing, elutriation, segregation, and chemistry. This work uses CFD simulations to acquire an understanding of the dynamics inside a biomass pyrolysis bubbling-bed reactor. The guiding hypothesis for this work include: (1) the hydrodynamics and chemical reactions can be separated to efficiently simulate the biomass fast-pyrolysis reactor; (2) The maximum yield of condensable bio-oil from a bubbling-bed pyrolysis reactor occurs just before the transition to fully developed slugging begins (i.e., when the gas flow is increased to a point where large bubbles just begin to form near the surface of the bed and due to very rapid bubble coalescence near the distributor). This work showed the guiding hypotheses were correct. The MFiX hydrodynamic and reacting case and the hybrid MFiX/MATLAB case had similar yield to the experiment.

Furthermore, biomass fast-pyrolysis bubbling-bed reactors that reach fully developed slugging, which depend on particle properties and bed height, achieved maximum yield at turbulent fluidization conditions, which require high superficial gas flow.

Abstract

Fast pyrolysis is a leading candidate process for converting biomass to liquid fuels and chemicals. During fast pyrolysis in bubbling- or circulating-bed reactors, biomass particles are rapidly heated through contacting with hot gases and solids, and their constituent components decompose into volatile and gaseous vapors, ash, and char. The product vapors include fuel-compatible and/or high-value chemical components, whose relative yields are highly dependent on the mixing processes and residence times in the reactor. Understanding and predicting these mixing processes and residence times and their dependence on reactor operation and biomass characteristics is critical for applying lab-reactor measurements to the prediction of industrial scale process performance.

In this study, a bubbling-bed fast pyrolysis reactor is simulated in 3D to explore the expected effects of fluidizing gas flow on the yield of condensable oils (tars) from wood pyrolysis. The specific concern is how the predicted tar yields vary as the fluidizing gas flow is increased from just above minimum fluidization to the bubbling-to-slugging transition, with all the other operating variables held constant. To account for detailed hydrodynamic effects, the reactor is simulated with MFiX, which is an open-source software package supported by the U.S. Department of Energy (DOE) that utilizes a continuum (two-fluid) strategy for modeling fluidized-bed reactors. In a previous related study [123], MFiX was also used to reveal how bubble dynamics

would be expected to change with fluidizing gas flow and how these changes might be observed with pressure measurements,.

To assess the validity and relevance of the predicted trends, the simulation results are compared with experimental yield measurements from a lab-scale bubbling-bed biomass pyrolysis reactor. Based on these results, it is possible to identify important implications and recommendations for future numerical simulations and experiments.

Introduction and Background

Fast pyrolysis

Pyrolysis involves the thermal decomposition of solid biomass molecules (typically classed as cellulose, hemi-cellulose, or lignin) when they are heated in the absence of oxygen [124]. The term 'fast pyrolysis' is typically applied to very rapid heating processes that raise biomass particle temperatures at rates of hundreds or even thousands of °C/s [125]. Such rapid heating conditions occur frequently during combustion, but they are also implemented in thermochemical conversion processes specifically to produce decomposition products with intrinsic value as fuel or chemical precursors [126].

Numerous lab-scale studies of bubbling-bed pyrolysis have demonstrated that biomass fast pyrolysis at reactor temperatures around 500 °C produces the maximum yield of condensable liquids ('tars') [127]. In these reactors, the primary bed material is usually sand or some similar inert particles of Geldart Group B that are fluidized with a hot inert gas such as nitrogen. Ground biomass particles are continually fed in through the reactor wall into the fluidized mixture of hot sand and gas, thereby releasing pyrolysis tars and light gases along with residual solid char and ash [128]. Incompletely devolatilized biomass and char particles are typically only removed from lab-scale reactors via elutriation, while the primary bed particles are too large and/or heavy to elutriate. Understanding and reproducing the performance of lab-scale reactors at pilot and industrial scales is quite challenging because of the complexities of mixing, transport, and reaction processes occurring between the gas and particles. These complexities are enhanced even further by strong nonlinear interactions between the transport and reaction processes that are difficult or impossible to quantify from experimental measurements alone. Thus, computational modeling has become an essential tool for interpreting and extrapolating the information generated by lab-scale experiments [129, 130].

Fluidized-bed hydrodynamics

The rates of biomass particle heating and extent of the pyrolysis reactions depend strongly on the fluidization state of the sand as well as the biomass particle shape and size distribution and characteristic residence time in the bed. Of course, these factors are directly related to the efficiency of gas–solids mixing and are thus dependent on the fluidization gas flow and bubbling intensity. Bubbles govern solids and gas circulation rates [61, 80, 123], bubble size directly affects gas–solids heat and mass transfer [131], and gas velocities in the bed and freeboard directly affect the rate of particle elutriation [132]. The residence time of released pyrolysis vapors also determines the degree with which homogeneous gas-phase reactions can be completed [133]. Thus, understanding the scaling relationships among all these factors in bubbling beds is essential for understanding how lab-scale pyrolysis results should be extrapolated to larger process reactors.

Focus of this work

The focus of the present work is to utilize a widely available fluidized-bed computational simulation tool (MFiX) to understand how the hydrodynamics in lab-scale bubbling-bed pyrolyzers would be expected to impact the yield of condensable liquids (tars) as the fluidization gas flow is increased between low-level fluidization and incipient slugging. Thus, the essential physical factors to be addressed will need to account for the dominant interactions between bubbling-bed hydrodynamics and biomass pyrolysis chemistry under lab-reactor conditions. Based on preliminary high-level arguments, it is hypothesized that there may be an optimal fluidization state in the bubbling-to-slugging transition (BTST) where the yield of woody biomass tars is maximized. It is expected that the simulation results developed here will enable acceptance or rejection of this hypothesis.

Technical Approach

Fluidized-bed simulation conditions

This work utilized the geometry of an experimental laboratory-scale reactor used for biomass-processing research at the National Renewable Energy Laboratory (NREL). A schematic of the reactor is shown in Fig. 2-1. The inner diameter D_r and height H_r of the reactor are 0.0508 and 0.4335 m, respectively. Operating conditions were chosen to match baseline experiments at NREL and are listed in Table 2-1 [128, 134]. Initially, quartz sand particles with Sauter mean diameter d_s of 5.0×10^{-4} m and density ρ_s of 2500 kg/m^3 were set at an expanded bed height H_o of 0.1475 m, with an initial void fraction of 0.59. The sand particle–particle properties were defined with a coefficient of restitution of 0.9 [40, 135-137] and angle of repose at 55° [138].The particle–wall collision specularity coefficient was set to 0.6; however, when normalized slip velocity goes to zero, it is calculated internally using a relation developed by Li et al. [78, 81]. Reacting pine biomass spherical particles, with char-like properties, of Sauter mean diameter d_{sm} of 2.78×10^{-4} m and density ρ_s of 80 kg/m^3 [Table 2-1] were uniformly inserted through a point source, 0.01016 m high from the bottom, at 0.0001181 kg/s. Particle size distribution information can be found in [139]. The reactor outlet is open to pressure at 133 kPa. Each simulation was initiated by uniformly adding pre-heated nitrogen gas at 773 K through the reactor bottom with a mass flow inlet based on superficial gas velocity, U, as a multiple of the minimum fluidization gas velocity, U_{mf}. The minimum fluidization velocity was measured at 0.0263 m/s at STP and corrected to 0.056 m/s to account for 'hot' reactor operating conditions, and the Syamlal-O'Brien drag-model [82] parameters were assigned based on the corrected U_{mf}.

Simulations were conducted with all operating parameters held constant, and only inlet velocity was varied between 1.3 – 8 U/U_{mf}. These inlet fluidization velocities allowed us to identify effects on pyrolysis chemistry from various fluidization regimes, namely bubbling, bubbling-to-slugging transition, fully developed slugging [123] and turbulent. Results shown herein are for a single static bed depth and residence time, mixing, and reaction effects should be expected to change with bed height, bed diameter, and particle properties.

Reaction kinetics

Biomass fast-pyrolysis experiments were simulated in the reactor utilizing first-order irreversible Arrhenius equations with the lumped kinetic approach of Liden et al [133]. Chemical-kinetic parameters used in the model can be obtained from [133]. This kinetic scheme converts biomass to tar, char, and gas during the first reaction step. A secondary competing reaction occurs which converts the tar to gas. This makes tar (oil) yield a function of particle and tar residence time. To achieve maximum yield, biomass particles must stay in the reactor long enough to fully de-volatize the biomass to gas, tar, and char. However, if tar resides in the reactor too long, further decomposition from tar to gas occurs. Optimal residence time in the reactor appears to be dependent on reactor geometry and hydrodynamics.

Hydrodynamics and residence time

Gas–particle mixing

Biomass particles inserted into the bed of sand are quickly swept away throughout the bed at different rates. Fluidizing inlet air flow directly affects the bubbling intensity, bubble size, and frequency along the axial height [123], resulting in different biomass/char particle mixing regimes [140, 141]. However, it is difficult or impossible to experimentally measure, in real time, the internal char/biomass particle movement and concentration relative to gas bubbles and sand/gas emulsion without disturbing the solids flow [142]. Particle mixing in our models were verified by simulating the Park and Choi [141] experiment. Park and Choi determined mixing based on the concentration of char (char volume fraction) at 5 axial volumes in the bed, which gives an indication of particle movement. Simulation results showed the layer of char at the top of the bed becomes less concentrated with increased gas mass flow resulting in better char/sand mixing, Fig. 2-2. Bubbles appear to be the main mixing mechanism and as fluidizing gas mass flow increased, more bubbles developed and resulted in better char/sand mixing. Mixing directly affects biomass dispersion and devolatization depth throughout the reactor and facilitates better distribution of gas/tar throughout the bed. Furthermore, biomass conversion to tar deeper in the bed results in increased tar/gas residence time and more contact with hot inert particles, which causes secondary tar cracking to gas.

Particle elutriation

Particle elutriation, the process by which a particle is removed from the reactor, depends on sand and biomass particle properties, freeboard/bubbling bed length, and fluidizing gas properties and mass flow. At the surface of the bubbling bed, gas drag effects on biomass particles become larger, causing particles to be lifted away from the bed into the freeboard. Splash effects, from bubbles rupturing at the bed surface, also facilitate particle upward movement away from the surface of the bed. As biomass particles become entrained in the fluidizing gas and exit at different rates, they create a characteristic particle residence time distribution.

To ensure the model captures the elutriation physics, the Berruti experiment [132] was simulated, and the residence time distributions curves compared. Experiment details can be found in Berruti 1988. Fig. 2-3 shows the general trend of the RTD curve was captured with the MFiX simulation and the corresponding model parameters were applied to the rest of the simulations.

PFR and CSTR limits

Bubbling fluidized beds are considered well mixed, but the bubbling bed contents are highly heterogeneous [143] and can be modeled as a series of continuous stirred tank reactors (CSTRs) [144]. However, as the number of CSTR stages are increased, the exit age distribution (RTD) from the model changes from representing a bubbling fluidized bed to plug flow characteristic, with a pulse injection (single residence time) [144]. The CSTR assumes steady state and perfectly mixed behavior, but since fluidized beds have non-ideal mixing, macromixing, and back mixing information, an RTD can be acquired from a multizone model. Experiments or simulations of the reactor are still required to capture the residence time of tracer gas/particles.

Fig. 2-4 shows tar yield data from the low-order model for the PFR and CSTR. Due to back mixing in the CSTR, best performance can be achieved from the plug flow reactor model. The PFR and the single CSTR achieve higher yield at t=0.2 with t_s/t_g=5 and t=0.4 at t_s/t_g=5, respectively. As we increase the CSTR stages, we approach PFR conditions and can achieve higher yield. The RTD data of the CSTR causes a distribution of gas/particle residence times which ultimately results in non-optimal yield. Depending on the ratio of the solid/gas residence time, distinctly different yields are acquired. Yields from the Liden kinetic scheme will fall somewhere between single CSTR and PFR yields.

CFD simulation

Major assumptions and constraints

Computational fluid dynamics (CFD) [83] is employed to simulate the biomass fast pyrolysis process in the bubbling-bed reactor described above over a range of fluidization velocities. Numerous fluidized-bed researchers have found CFD to be a useful complement to experimental measurements [78, 79, 84, 85]. One benefit of CFD is that it provides spatiotemporal details about pressures, velocities, flows, and concentrations that are either impossible or extremely difficult to obtain experimentally. CFD has also been employed in numerous studies of gas–solid fluidized beds [84, 86], but very limited number of biomass fast pyrolysis CFD studies have addressed hydrodynamic effects [15, 31].

The specific CFD implementation used in this study employed the Eulerian–Eulerian computational Two-Fluid Model (TFM) [89, 90], which approximates the flowing phases as interpenetrating continua. The TFM is in contrast to numerical simulations that resolve discrete particles or molecules [88, 91-93]. While the TFM approach does not resolve individual particles, it has been demonstrated to reproduce major hydrodynamic features, including bubbles [40, 77, 79], residence time [145], and mixing [146, 147]. Detailed information on the TFM and reaction formulation can be found in Gidaspow [89] and [97].

To carry out our simulations, we utilized MFiX (Multiphase Flow with Interphase eXchanges), which is an open-source CFD software developed primarily at the National Energy Technology Laboratory [94]. The multi-species gas phase was simulated as compressible, and stress tensors for the gas and solid phases were related to shear stress using Newton's law. To model solids transport properties, such as solids pressure and viscosity, the kinetic theory of granular flow [94] together with the Schaeffer frictional stress tensor formulation [95] and the sigmoidal blending stress function [77, 86, 96] were employed to relate the computed solids temperature with solids transport properties. Furthermore, the gas–solid momentum transfer used the Syamlal-O'Brien correlation [82] for the drag model. The discretization scheme utilized a finite-volume approach with a staggered 3D grid [97]. Scalar values, pressure and void fraction, were stored in the cell center, while velocities were computed on the cell surfaces. Additionally, second-order discretization was utilized using the SMART approach together with the chi-scheme which improved convergence and accuracy of the simulation [148]. A modified SIMPLE approach [97] is also used and improves speed and stability through variable time stepping, solid volume fraction correction, and solids-pressure evaluation. The no-slip condition was applied to the gas and solid phase on the side walls, while the Jackson and Johnson partial-slip wall boundary condition [98] was applied to the solid phase.

To characterize the spatiotemporal dynamics generated by MFiX, we tracked detailed variations in pressure and gas and solid species mass as time series at each computational grid point. As explained below, these raw time series were then further processed to produce simulated (virtual) measurements of the local pressure fluctuations, pyrolysis yield, and residence time distribution for the gas/tar and biomass. We then analyzed and compared the pressure time series at upper axial location in the bed to determine the bubbling and slugging states [123]. The pyrolysis yield at the outlet was measured to determine conversion of gas, tar, and char coming out of the reactor. The gas and biomass tracer mass time series were then analyzed to acquire residence time distribution at the various fluidization states.

Simulation results assumed biomass devolatization time is on the order of 1 second [9], and char-like properties were used for the biomass to capture flow statistics, residence time, and mixing. Furthermore, our simulation does not account for attrition or fragmentation, and a single size was used for the sand phase and a different single size was used for the biomass/char/ash phase based on data from NREL [139]. The molecular weights were chosen based on the types of species in each phase. However, there is uncertainty in the molecular weights based on the heterogeneity of the biomass material, the material type, and how it was harvested.

Mesh and stationary issues

A general concern for multiphase flow CFD simulations is establishing a computational grid size that is sufficiently refined so spatiotemporal dynamics no longer depend on grid resolution (i.e., grid independence). Based on prior mesh resolution studies [123], the cylindrical mesh was chosen with 15 cells in the radial direction and 256 cells in the axial direction, and with 6 azimuthal cells.

Methods of analysis applied to simulation results

Mixing and residence time metrics

Biomass particle mixing metrics utilized by experimentalists [141] were used to evaluate mixing in our simulation. The char volume fraction along the axial direction was measured at 5 equal locations. MFiX char volume fraction data was placed on the same figure to compare results. The metric was then used to compare the pyrolysis bubbling bed reactor simulations at different operating conditions.

Residence time distribution (cumulative distribution) curves were acquired from the tracer mass exiting the reactor. Ten (10) tracer biomass particles were placed in the reactor at different times at the various superficial velocities, U/U_{mf}. Initially biomass particle flow into the reactor was 0.1181 g/s for 20 seconds of simulation time. Stationary state was reached after ~8 seconds and was run longer to eliminate any transient effects. At 20 seconds of simulation time, the char biomass particle flow was replaced with the first char biomass tracer flow for 0.1 second. At 20.1 seconds, the char biomass particle flow was reestablished, and first char tracer particle flow stopped. At 22 seconds of simulation time, the char biomass particle flow was replaced with the second char biomass tracer flow for 0.1 second. At 22.1 seconds, the char biomass particle flow was reestablished, and second char tracer particle flow stopped. This procedure continued for a total of 10 tracer particles. This allowed for a continuous flow without disturbing the bubbling bed hydrodynamics. The concentration of tracer particles, normalized with total tracer mass, exiting the reactor out the top was measured to create a cumulative distribution over time. Similarly, 10 tracer gases were injected near the distributor to acquire 10 RTDs of the gas. A mean RTD curve was calculated for the 10 tracer particle RTDs and 10 tracer gas RTDs. Furthermore, the standard deviation was calculated from the 10 mean residence times acquired from the 10 tracer RTD curves. The standard deviation value was then utilized to shift the mean RTD curve in the positive and negative direction to create RTD confidence intervals. The mean RTD curve and RTD confidence intervals for char and tar tracers at each U/U_{mf} were then applied to the hybrid low order Liden kinetics model.

An important consideration at lower flows is that with mean residence times 10–20 seconds, the 2-second injection intervals results in correlated samples, which are not statistically correct and result in a smaller dispersion (tighter confidence intervals). Independent samples are achievable with tracer injections separated in time by more than the particle residence time or with an ensemble of randomized initial conditions (a bootstrapping technique), which requires significant computing resources and time, and which will be treated in full later.

Hydrodynamic metrics

Hydrodynamics were evaluated using pressure statistics in the upper 75% location of the static bed, 0.75 H_o [123]. Pressure statistics from the CFD simulations were used to determine the mass flow at the bubbling to slugging transition, fully developed slugging [123], and turbulence regime.

Identification of characteristic zones in the reactor

The bubbling bed reactor is composed of 2 main sections, the bed and freeboard. Within the bed, there are 3 regions: bottom, upper, and splash zone. The bottom bed is where small bubbles form as gas enters through the distributor. These small bubbles coalescence together as they rise upward toward the upper bed zone. In the upper part, bubbles reach the maximum size before reaching the splash zone. In the splash zone, bubbles erupt, causing particles to be ejected upward.

After the splash zone, particles begin their descent through the freeboard, where the slip velocity between gas/particle determine how fast particles elutriate out of the bed. For analysis of our models, we focus on the two main sections, the bed and freeboard. In the hybrid low-order model two CSTRs were used to represent the bubbling bed, lower and upper sections, and one PFR represents the freeboard region. Three (two CSTRs and one PFR) parameters were used in the hybrid low-order model to replicate the char and tar RTD profiles extracted from the CFD simulation.

Sensitivity of results to major parameter values

To minimize error in the simulated RTD parametric tests were performed with particle size and density. Parameters were selected which were considered to have an effect on biomass particle residence time. Particle properties and reactor operating conditions were selected to test sensitivity of these changes on biomass particle RTD. Each test was conducted with the exact same setup except one parameter was changed in the simulation (*ceteris paribus*), for a total of 27 simulations using 36 processors each. Each case took ~115 hours (4.8 days) of computing time, which varied ± 1 day based on the parameter tested. The parameters of interest are as follows: mesh (or grid) resolution, biomass density, biomass size, particle–particle coefficient of restitution, particle–particle coefficient of friction, particle segregation slope coefficient, drag-model type, reactor fluidizing gas type (density and viscosity), reactor gas mass flow inlet rate, and reactor temperature. See Table 2-2 for the simulation matrix.

Fig. 2-5 shows how the corresponding box and whisker plot [149] was extracted from a single RTD curve (sometimes termed ‘F-curve’ [132]), which is composed of tracer data at stationary state. The mean (50%), standard deviation (68%), and 2 standard deviations (95%) were extracted directly from a single RTD curve, not calculated. The mean, standard deviation, and 2 standard deviations are shown in the box and whisker plot, in red, blue and green, respectively. A long tail in the RTD plot is represented in the box and whisker figure with large standard deviations (68% and 95%). RTD data were visually represented with box and whisker plots to clearly show differences.

As noted in the residence time metric, a statistical representation of the char and tar RTD is necessary which requires independent samples from the same reactor to create a mean RTD curve, not just one tracer RTD. Independent samples are achievable with sufficiently long simulations with decorrelated tracer injections or with ensembles of randomized initial conditions, which requires significant computing resources and time and which will be treated in full later.

Results and Discussion

Overall tar yield trends with BTST fluidization state

Three reactor simulation approaches were compared: MFiX hydrodynamics with pyrolysis chemistry (MFiX model), a MATLAB reactor model with pyrolysis chemistry (MATLAB model), and MFiX hydrodynamics coupled to a MATLAB pyrolysis chemistry model (MFiX/MATLAB hybrid model), Fig. 2-6. The MFiX model and the MFiX/MATLAB hybrid model gave good agreement with experimental results using a 10 cm static bed height. This reactor with a 10 cm high bed was further simulated from 2 – 7 U/U_{mf} and found it transitioned from bubbling to turbulent fluidization, bypassing the slugging regime due to the shallow 10 cm bed. The MFiX/MATLAB hybrid model was utilized in the rest of this work using a 20 cm static bed height.

The higher bed height allowed the reactor bed to operate in the bubbling, bubbling-to-slugging, fully developed slugging, and turbulent fluidization regimes.

Fluidizing gas mass flow was varied for the pyrolysis reactor with the 20 cm bed height while all other parameters remained unchanged. Fast pyrolysis reaction chemistry yields were measured at the exit of the reactor and normalized with total biomass mass flow. Fig. 2-7 shows resulting yields at various U/U_{mf} with confidence intervals represented by the lines. A description of how the confidence intervals were calculated is described in Methods of analysis applied to simulation results. In the bubbling regime, 1.3 – 2.0 U/U_{mf}, tar yield increased with fluidizing gas mass flow. When the reactor transitions from bubbling to slugging, 2.0 – 3.5 U/U_{mf}, the tar yield reached ~0.49 and then continued to increase. As fluidizing gas increased above 4 U/U_{mf}, the tar fraction increased, and the bed became more turbulent. Fluidization regimes affect tar fraction yield at the reactor exit and reactor operation must be considered in design of experiments. To help understand tar yield at the reactor exit further analysis was conducted on the char particles and vapors inside the reactor.

Hydrodynamic, mixing, and residence time trends with fluidization state

Here we focus on hydrodynamic effects on biomass particle mixing. Fig. 2-8 (a) – (d) shows the char layer in the upper part of the bed decreases with an increase in fluidizing gas inlet mass flow. Bubble size and frequency increase with fluidizing mass flow, resulting in better mixing and greater char volume fraction within the bed. Simulation videos showed char particles being moved in the bed by the wakes of the bubbles.

Fig. 2-8 (e) – (h) shows the flow of biomass particles in the pyrolysis reactor through an axial cross section of the bed, at bubbling, bubbling-to-slugging, fully developed slugging, and turbulent fluidization conditions. The flow dynamics and bubbling change with the different fluidization regime, which also has implications for the residence time distribution and error in RTD data. Each fluidization regime/transition is not well defined, but rather are normative terms, that are characterized with specific char/tar/gas residence time distribution and mixing dynamics that affect pyrolysis yield.

Fig. 2-9 shows a time-averaged reactor axial profile of char concentration. At bubbling fluidization, the char concentration appears to be uniform throughout the bed after the initial entry location. As U/U_{mf} increased from bubbling to turbulent fluidization (at 1.5 – 2.40 – 3.80 – 7.50 U/U_{mf}), the char concentration in the bottom half of the bed decreases, whereas in the upper half of the bed char concentration increases from bubbling to fully developed slugging, showing the large ogive, slugging bubbles, cause a longer hold up of char particles in the upper part of the bed. At the highest flow, turbulent fluidization, char concentration is almost the same as in the bottom half, indicating that the residence time of particles in the bed is decreased in the turbulent regime.

Fig. 2-10 shows char particle residence time decreases, and the residence time distribution becomes narrow with increasing fluidizing gas mass flow. However, the char particle residence time reaches a limit above 5.5 U/U_{mf}. At 6 U/U_{mf} the char RTD curve increases over the 5.0 and 5.5 U/U_{mf} curve. This is also the transition to turbulent fluidization, indicating effects of the fluidization regime.

Fig. 2-11 shows the RTD of tar tracer, which was placed at the bottom, near the distributor, of the reactor. As nitrogen gas mass flow increased, the tar RTD decreased. The RTD of tar was at least 5 times shorter than the RTD of char particles. Similarly, the tar RTD at 6 U/U_{mf} increased over 5.0 and 5.5 U/U_{mf}. Unlike the char RTD, the tar RTD did not appear to reach a limit; it continued to decrease, indicating one can decrease the residence time of tar in the reactor by going beyond turbulent fluidization. To ensure consistency, RTD sensitivities were tested in the following section.

Impact of parametric sensitivities

Initially a mesh resolutions study was conducted that tested the Syamlal-O'Brien and Gidaspow drag models. Fig. 2-12 shows RTD mean and standard deviations for the drag models at 3 different mesh resolutions: 6.6 d_p, 5.4 d_p, and 5.0 d_p (0.8, 1.0, and 1.2 relative to original mesh). Regardless of the drag model, results show there were minimal differences between the mesh resolutions, indicating the Syamlal-O'Brien or the Gidaspow drag law using the nominal case (1.0 mesh) can be used to model the 2FBR. For consistency in the simulation approach, the Syamlal-O'Brien drag model was used for the rest of this work.

Fig. 2-13 shows temperature effects on the biomass particle residence time. Gas viscosity and drag model were adjusted with change in temperature. Biomass RTD was tested from 723 K to 873 K. Fluctuations in temperature appear to cause random variations in the RTD, possibly caused by finite-sample effects from not integrating over a large-enough tracer population or long enough in time. Increasing the temperature to gasifier conditions (> 1100K) may show other trends but were beyond the scope of this pyrolysis study.

Fig. 2-14 shows effects of different fluidizing gas on RTD, at the same volumetric flow (L/min) and at the same mass flow (U/U_{mf}). Tests included increasing N_2 gas flow 1.5-fold (2×-flow) and using H_2 or steam (H_2O) as the fluidizing medium. Model assumptions include gas density and viscosity and drag change with temperature and gas type. Increasing N_2 fluidizing gas flow (N_2 gas ×2) causes the mean residence time and confidence interval to decrease as expected.

However, as gas flow continues to increase, particle RTD reaches a lower limit. Hydrogen and steam were also tested based on operating plans for the 2FBR. The steam (H_2O gas volume) and hydrogen (H_2 gas volume) cases used the same fluidizing gas volumetric flow rate as nitrogen (N_2 gas), flowing nitrogen at 12.8 LPM. Compared to nitrogen, steam (H_2O gas volume) slightly decreased the RTD. Alternatively, hydrogen gas (H_2 gas volume) caused a significant increase in the biomass particle RTD. At the same volumetric flow rate, the total hydrogen mass flow is one magnitude lower. However, hydrogen viscosity is ~½ of steam, which also affects particle residence time.

Reactor fluidizing gas is typically controlled using volumetric flow but can also be controlled using superficial gas velocity relative to the minimum fluidization velocity (U/U_{mf}). This ratio is often used to describe the intensity of the turbulence in bubbling beds, because it is related to the number and size of bubbles produced for flows above minimum fluidization [144]. Fig. 2-14 also shows RTD results for steam (H_2O gas mass) and hydrogen (H_2 gas mass) at the same U/U_{mf}. The 2FBR nitrogen fluidizing gas has a minimum fluidization velocity U_{mf} = 5.66 $cm \cdot s^{-1}$, whereas steam and hydrogen are 8.8 and 79.21 $cm \cdot s^{-1}$, respectively. Viscosity for steam and hydrogen at 773 K was also included, at 2.8×10^{-4} and 1.6×10^{-4} $g \cdot cm^{-1} \cdot s^{-1}$, respectively. At 4 U/U_{mf}, hydrogen fluidizing gas has 16 times higher velocity throughout the reactor than nitrogen fluidizing gas. This high velocity results in gas residence shorter than 1 second. However, steam (H_2O gas mass) at 4 U/U_{mf} has a similar RTD as nitrogen at double the flow (N_2 gas ×2). This shows that operating the reactor's inlet fluidizing gas using U/U_{mf} with a mixture of nitrogen, steam, and hydrogen can result in shorter residence times, so flows of gas mixtures must be adjusted accordingly. [Note: the reactor of interest has a shallow bed which appears to transition from bubbling to turbulent fluidizing regime, with no slugging.]

Fig. 2-15 shows how biomass particle collision properties affect RTD. The mean RTD decreased and confidence intervals increased with an increase in the coefficient of friction. In comparison, mean RTD and the confidence interval increased with the coefficient of restitution. Coefficient of restitution is a measure of how much energy is conserved during particle−particle contact interaction, that is, how elastically particles to bounce off each other. As particle−particle dampening (coefficient of restitution) increased, the RTD also increased. Another property is the segregation slope coefficient which is the ability for particles to segregate in mixtures (bubbling bed). As the segregation slope coefficient increased, the mean RTD and 68% confidence interval increased, however, the overall tail decreased. The heterogenous properties of biomass particles and the complex biomass−biomass and biomass−sand interactions in the bed of sand makes it difficult to determine experimental particle–particle contact properties. Results from this study can be used to calibrate future particle–particle contact properties in bubbling-bed models.

Fig. 2-16 shows effects of biomass particle density and size. As biomass particle density increased, mean residence time and confidence intervals increased, indicating lighter biomass particles, such as softwood, of the same size as pine or pelletized wood, will have a shorter time to fully de-volatize at the same fluidized-bed operating conditions. However, at the same reactor operating conditions, particle RTD reaches a minimum limit regardless of how small or how weightless the particle becomes. Biomass feed stock is not one particle size; it comes in a particle size distribution with bottom and top size. Larger particles will have a longer RTD than smaller particles. Particle size distribution and density (softwood, hardwood, pelletized wood) must be carefully selected for the reactor operation of interest.

Results from low-order approximations based on CFD information

The MFiX/MATLAB hybrid model represents sections in the reactor as continuous stirred tank reactors (CSTRs) which account for back mixing [144]. Tar vapor and char particle tracer RTDs are acquired from an MFiX hydrodynamic model. The MFiX RTDs are then fitted to three CSTR zones that capture the curvature of the characteristic RTD. Fig. 2-17 shows the RTD from MFiX overlaid with the RTD acquired from the low-order CSTR model using 3 stages. These 3 stages are then applied to the MATLAB pyrolysis chemistry model that uses the Liden kinetics.

The MFiX/MATLAB hybrid model showed tar yield varied not only due to increased fluidizing gas flow, but also due to fluidization regime. Fig. 2-7 showed the reactor with a 20 cm static bed height had a maximum yield of 71% at 8 U/U_{mf} (turbulent regime). In comparison the reactor operated with a 10 cm bed had the highest yield of 64% at 4 U/U_{mf} (bubbling regime), Fig. 2-18. Operating the reactor with a different bed height resulted in maximum tar yield at different U/U_{mf}. Furthermore, there does not appear to be a linear behavior between U/U_{mf}, tar yield, and bed height.

Fig. 2-18 shows tar yield decreases over the axial height of the reactor, represented by 3 CSTR stages. At each stage the amount of wood decreases, with the last stage generating the least amount of tar and cracking tar to non-condensable gasses. Furthermore, as shown in Fig. 2-7, tar and gas are inversely related. At 5 – 8 U/U_{mf}, char residence time appears to reach a limit, Fig. 2-10, but tar residence time continues to decrease, Fig. 2-11, with tar yield increasing, Fig. 2-7.

Based on these results, tar yield can be improved if residence time in the last stage is decreased by reducing the length and/or size of the freeboard region or reducing the temperature in the freeboard.

Confirmation of key CFD assumptions with low-order results (e.g. particle density assumption)

These modeling approaches, MFiX and MFiX/MATLAB hybrid model, made the following assumptions: constant biomass particle density, constant biomass particle size, and no moisture. Prior work from DiBlasi [150] showed the time required to completely convert wood particles to char is < 2 seconds, which has a minimal effect on the RTD. Effects of particle density and particle size on RTD were tested in previous sections. Moisture was neglected to acquire a fundamental understanding of hydrodynamics; furthermore, there is minimal experimental kinetic and hydrodynamic data to include moisture. Future simulation and experimental work should include these effects.

Conclusions and Recommendations

Predicted impact of the BTST on tar/oil yield

This work focused on hydrodynamic effects on pyrolysis yield from fluidized bed in various operating regimes. Model validation was performed with a 10 cm bed depth which did not reach slugging conditions. The reactor operated with a 10 cm bed achieved 64% yield at 4 U/U_{mf}, in the bubbling regime, which required minimal pumping energy. However, the 20 cm bed reactor, analyzed in this work, reached 71% yield at 8 U/U_{mf}, in the turbulent fluidization regime. Based on these results, biomass fast-pyrolysis reactors should be operated with a shallow bed that does not experience slugging conditions. This model utilized a lumped kinetic approach which provided tar yield, but not composition. At these different fluidization regimes, composition will be very different, and operation conditions must be carefully planned.

A fundamental understanding of hydrodynamic effects on pyrolysis yield is needed from experimental work. Information from experimental work that is necessary for simulation studies include inert sand, fresh biomass, and biomass char particle properties, quantity and particle size distribution, fluidizing gas flow and type (N_2, hydrogen, steam), reactor diameter and height, temperature, and pressure.

Summary of the present MFiX simulations

The MFiX simulations used in this work utilized reacting flow and non-reacting flow. The simulation setup used the two-fluid model which included gases (tar, gas, tar tracer, nitrogen) and solids (sand, char, char tracer). Most of the results focused on residence time of solids and gases, however, the reacting flow case has the ability to account for moisture effects in the simulations but was not enabled for this work. Assumptions were made about the biomass particle density and size to ensure we acquire results consistent with experimental work.

The CFD simulation software is complex and requires a learning curve that is specific to the application of interest. Some challenges with MFiX include the initial problem setup and parametric sweeps which are being improved by the GUI. Other challenges include getting the solution to converge efficiently to solution. This also required numerous trials to understand how to setup the simulation to efficiently run on the computing machine.

Final remarks

Results from the three-dimensional computational simulations of a laboratory-scale fluidized bed indicate that optimizing a fluidized-bed pyrolysis reactor is a complex process that depends on reactor geometry, particle and gas properties, and other reactor operating parameters. Pyrolysis oil yield appears to be related to the particle and tar residence time. The highest tar yield appears to be achieved in the turbulent regime when high fluidizing gas flow reduces the tar residence time in the bed and freeboard.

There are several remaining areas that should be investigated concerning optimizing a reactor for biomass pyrolysis processing in beds of Geldart Group B solids:

- Direct comparisons between computational simulations and high-speed experimental void fraction and pressure measurements [99, 100] at a range of fluidizing gas mass flows are needed to validate/improve existing CFD models.
- Experimental pyrolysis yield measurements at various axial heights of the pyrolysis reactor.
- Direct comparisons between computational simulations and high-speed non-intrusive experimental tracer particle measurements [140].

Appendix: Figures and Tables

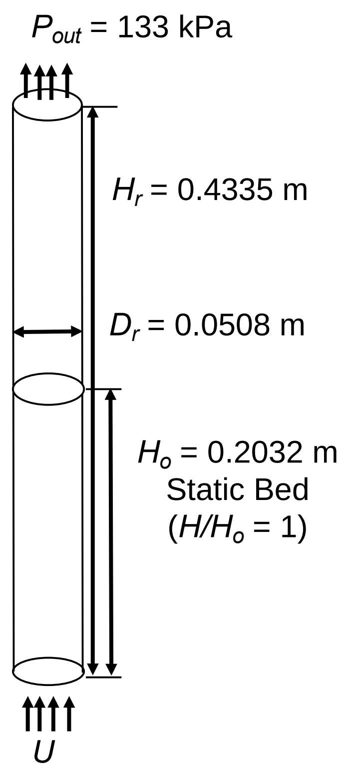

Fig. 2-1 Bench-scale fast pyrolysis reactor at NREL, known as the 2FBR pyrolysis reactor, for thermochemical conversion of woody biomass particles.

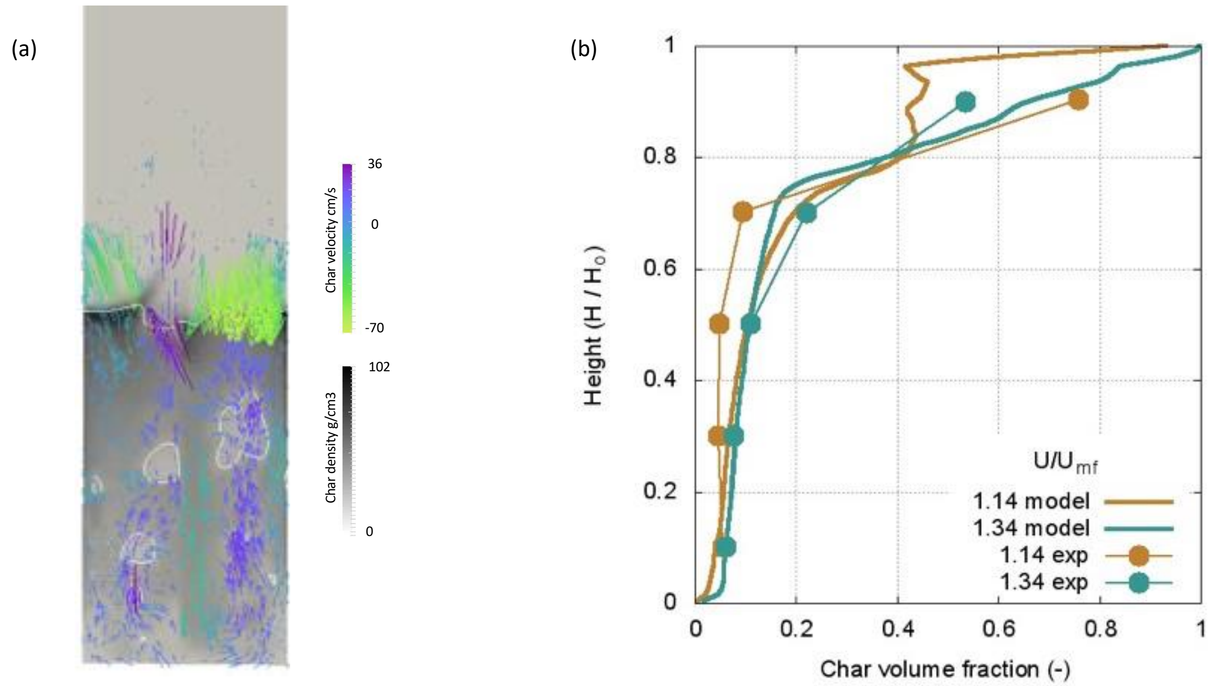

Fig. 2-2 (a) Axial slice of 3D bubbling bed simulation at 1.34 U/U_{mf}. (b) Comparison of simulation and experiment char mixing (Park and Choi 2013).

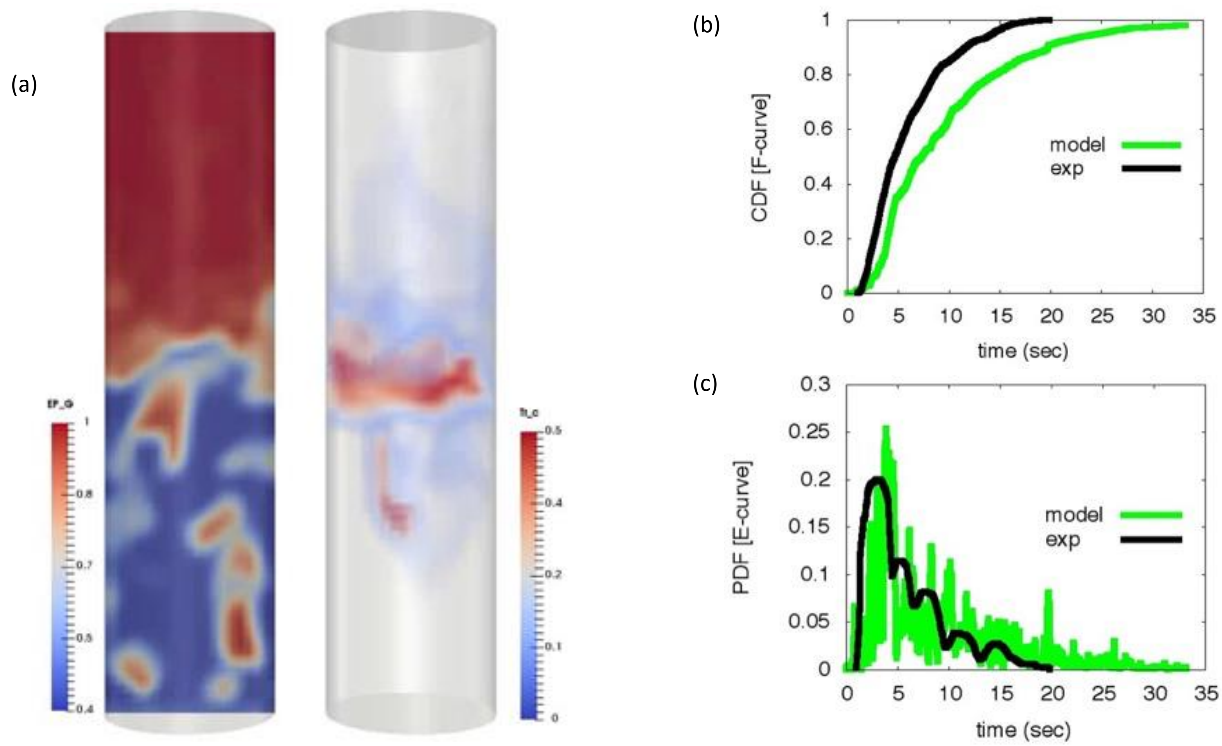

Fig. 2-3 (a) Axial slice of 3D bubbling bed simulation residence time distribution (RTD) study. (b) and (c) Comparison of simulation and experiment RTD (Berruti 1988).

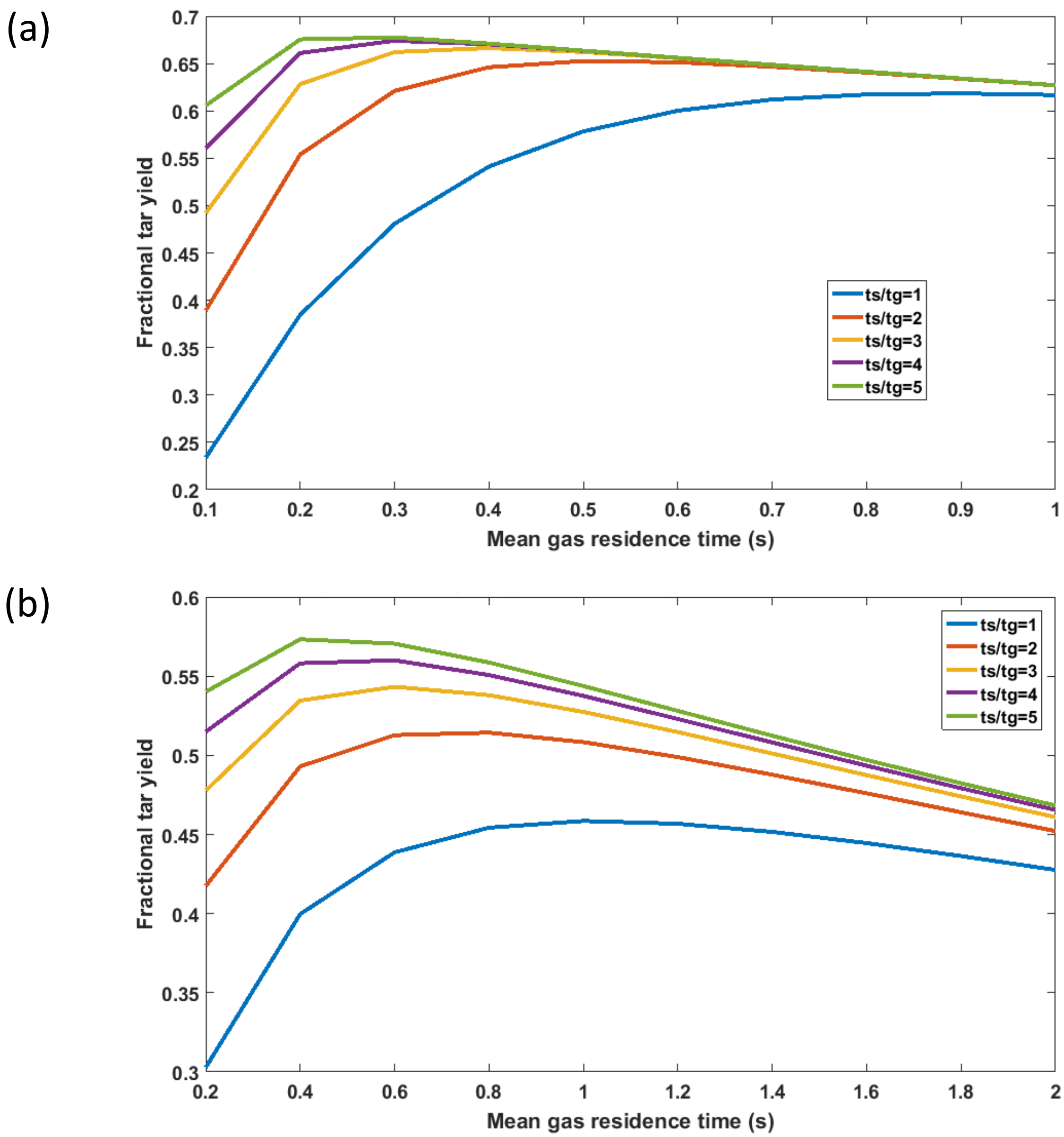

Fig. 2-4 (a) Liden plug flow reactor tar yield predictions versus gas and solids residence time. (b) Single continuous stirred tank reactor (CSTR) tar yield predictions versus gas and solids residence time.

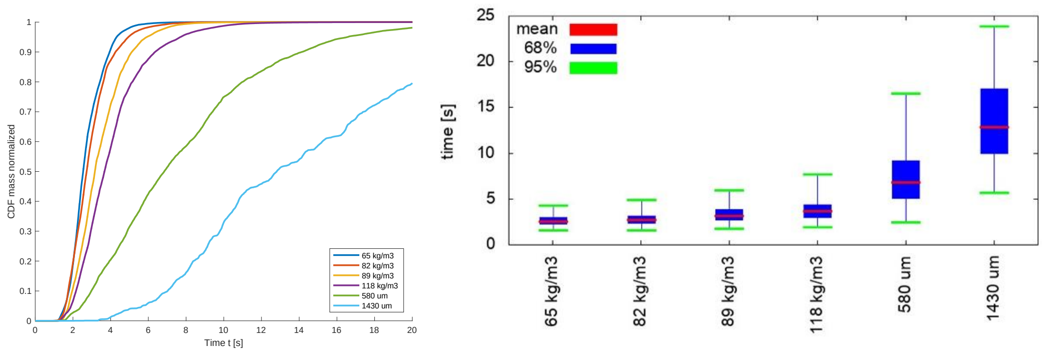

Fig. 2-5 Box and whisker plot extracted from the biomass RTD curve (F-curve).

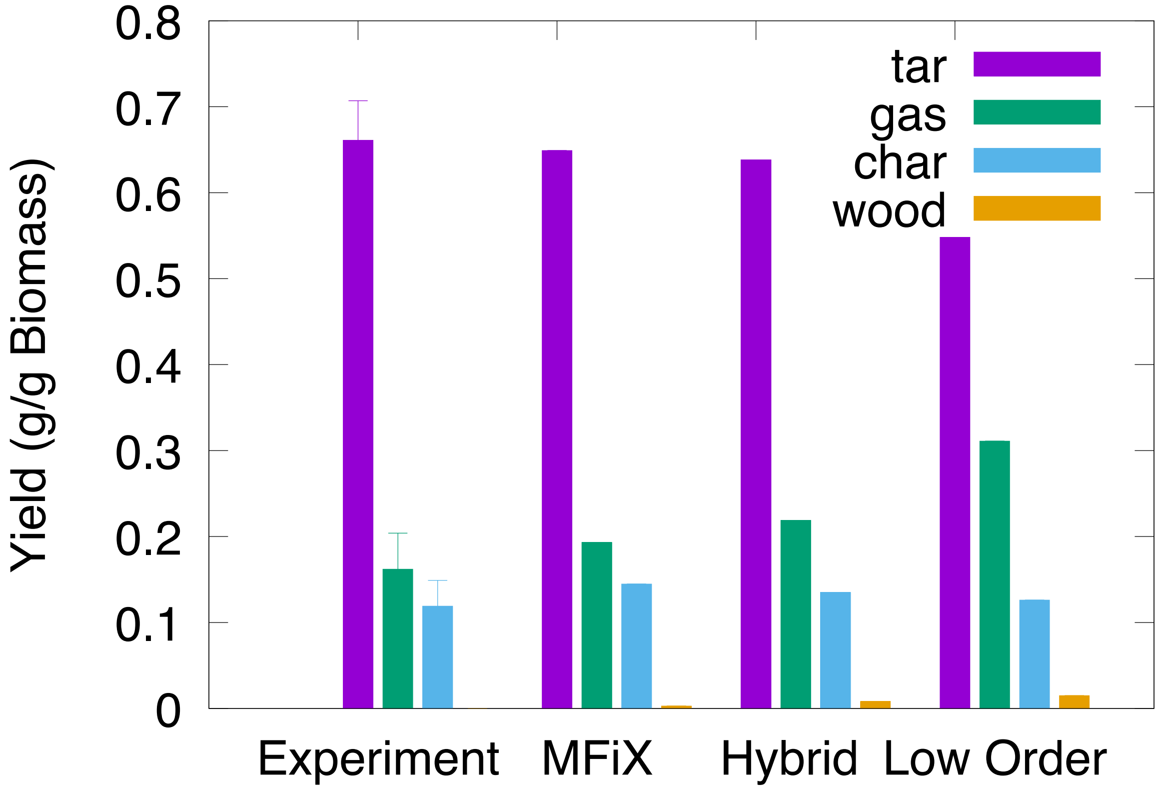

Fig. 2-6 Biomass fast pyrolysis yields from a bubbling bed experiment [128, 134], 3D CFD model (MFiX), hybrid low-order model together with a 3D CFD model (Hybrid), and a low order reactor model. The Liden kinetics [133] were used in the three modeling approaches.

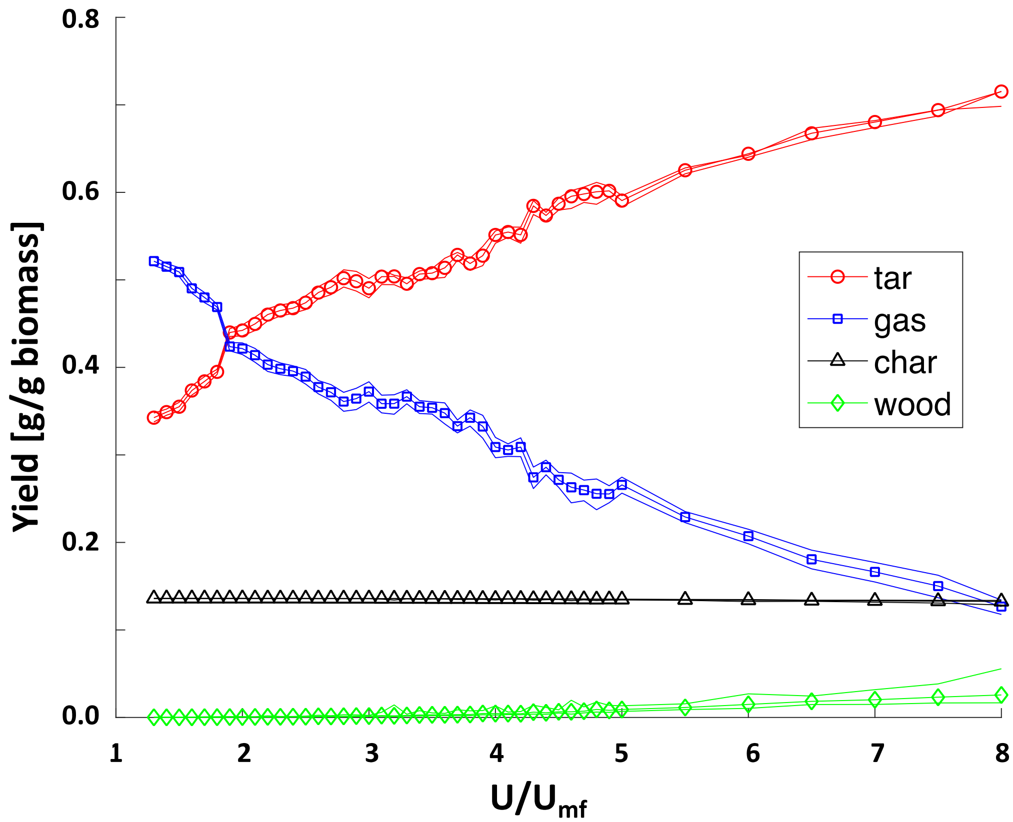

Fig. 2-7 Pyrolysis yield (Liden) in 20 cm fluidized bed (bubbling, slugging, turbulent) at various superficial velocities, *U/U_{mf}*. Line bands represent ±1σ confidence intervals.

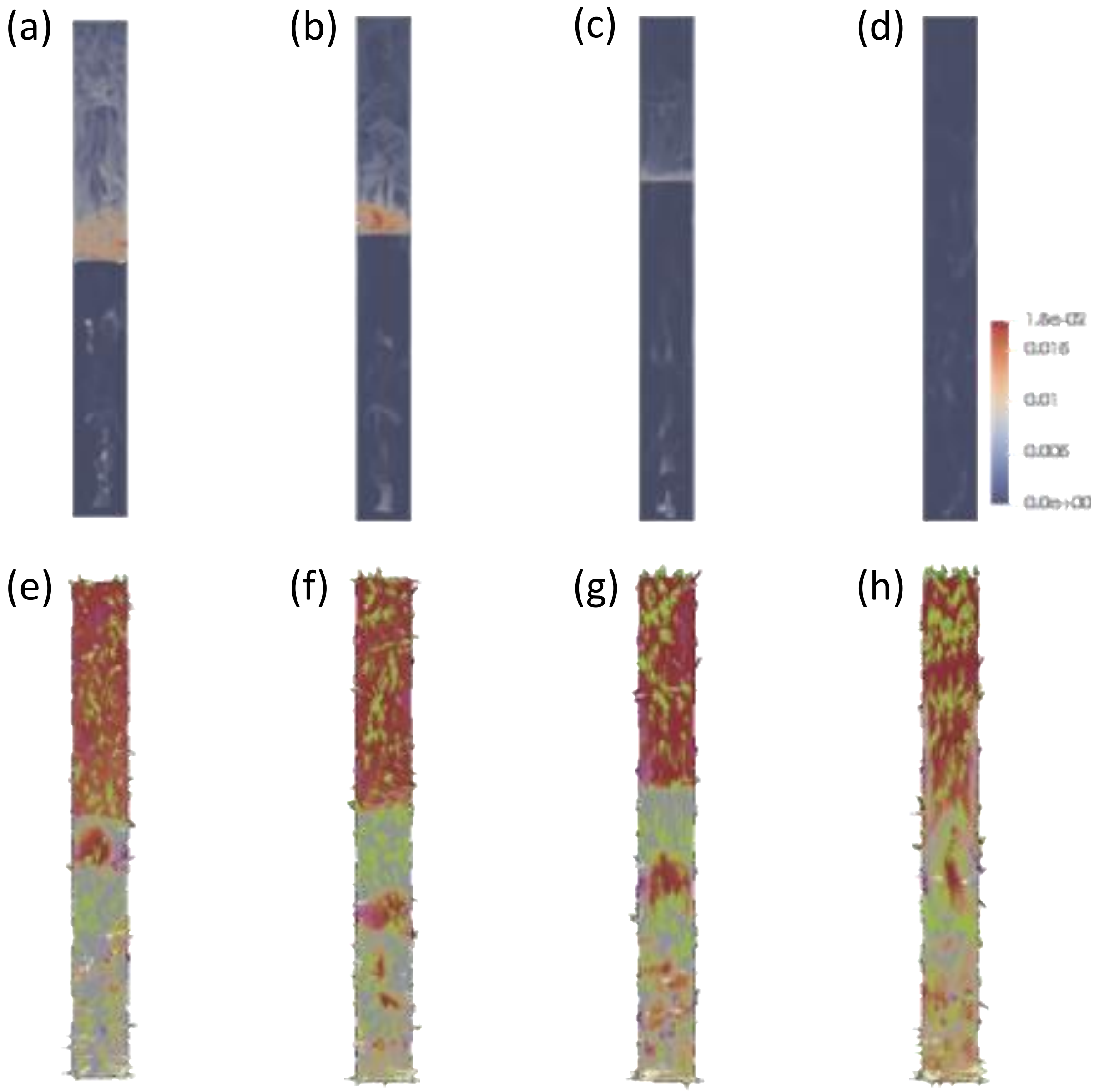

Fig. 2-8 (a) – (d) Axial cross section showing char concentration at bubbling (1.8 *U/U$_{mf}$*), bubbling to slugging (2.5 *U/U$_{mf}$*), fully developed slugging (3.8 *U/U$_{mf}$*), and turbulent fluidization (7.5 *U/U$_{mf}$*). (e) – (h) Axial cross section showing char trajectory vectors upward (pink) and downward (green) at bubbling (1.8 *U/U$_{mf}$*), bubbling to slugging (2.5 *U/U$_{mf}$*), fully developed slugging (3.8 *U/U$_{mf}$*), and turbulent fluidization (7.5 *U/U$_{mf}$*).

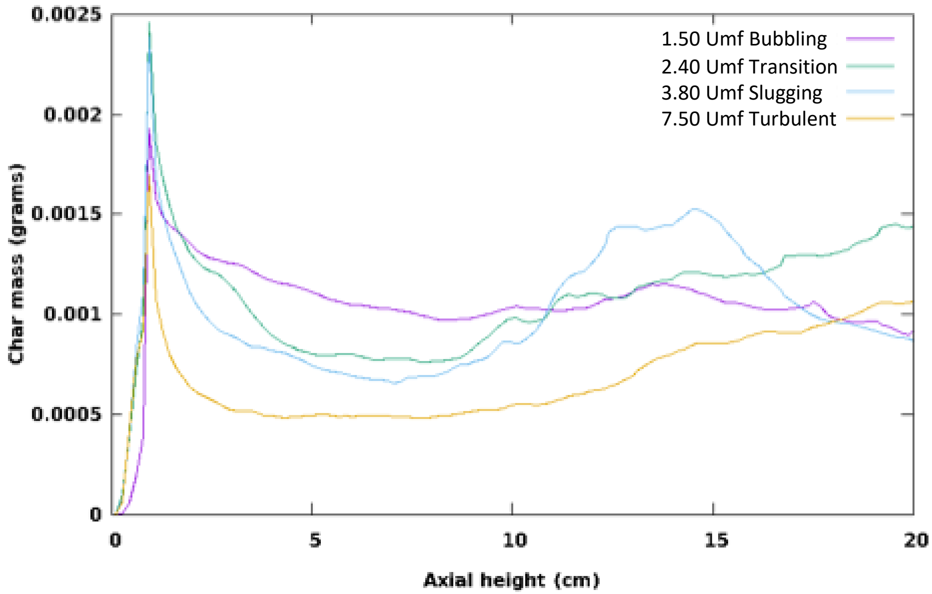

Fig. 2-9 Char particle axial profile for 278 *μm* particles at various superficial velocities, *U/U_{mf}*.

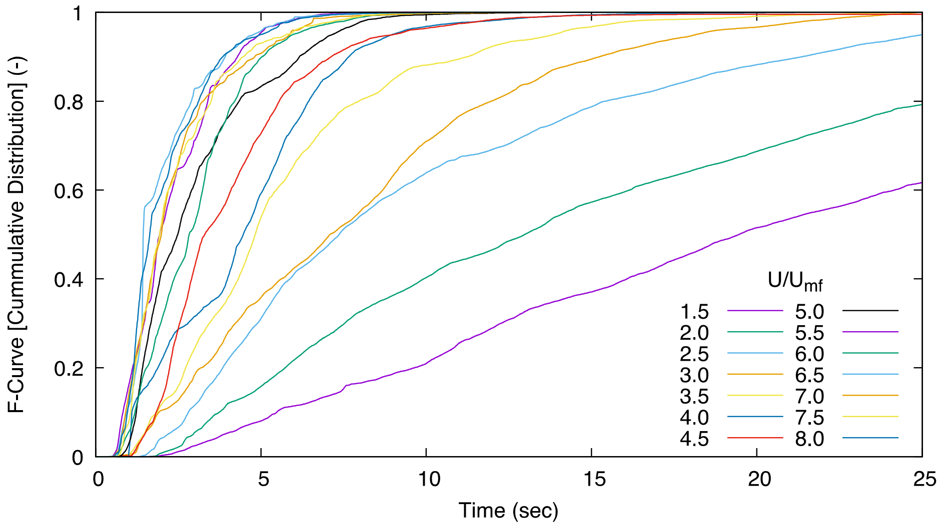

Fig. 2-10 Char particle residence time distribution (RTD) at various superficial velocities, U/U_{mf}.

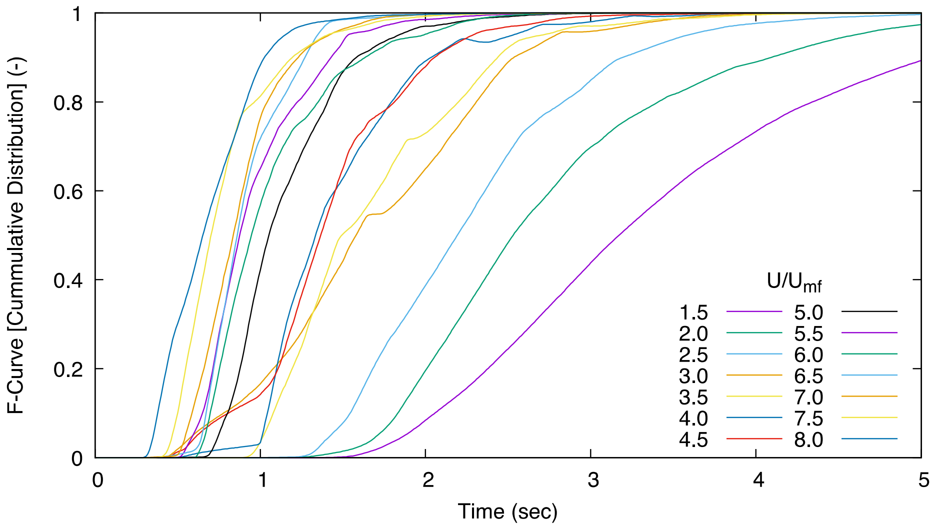

Fig. 2-11 Tar vapor residence time distribution (RTD) at various superficial velocities, *U/U_mf*.

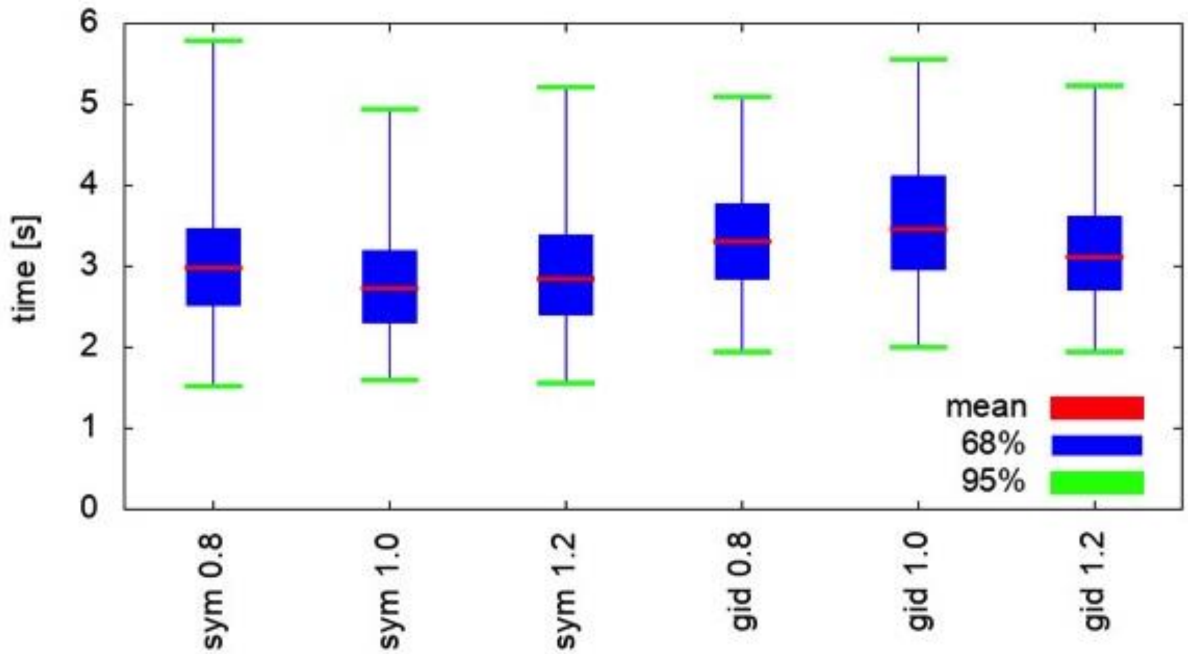

Fig. 2-12 Drag and mesh effects on biomass particle residence time distribution. [sym=Syamlal-O'Brien drag, gid=Gidaspow drag].

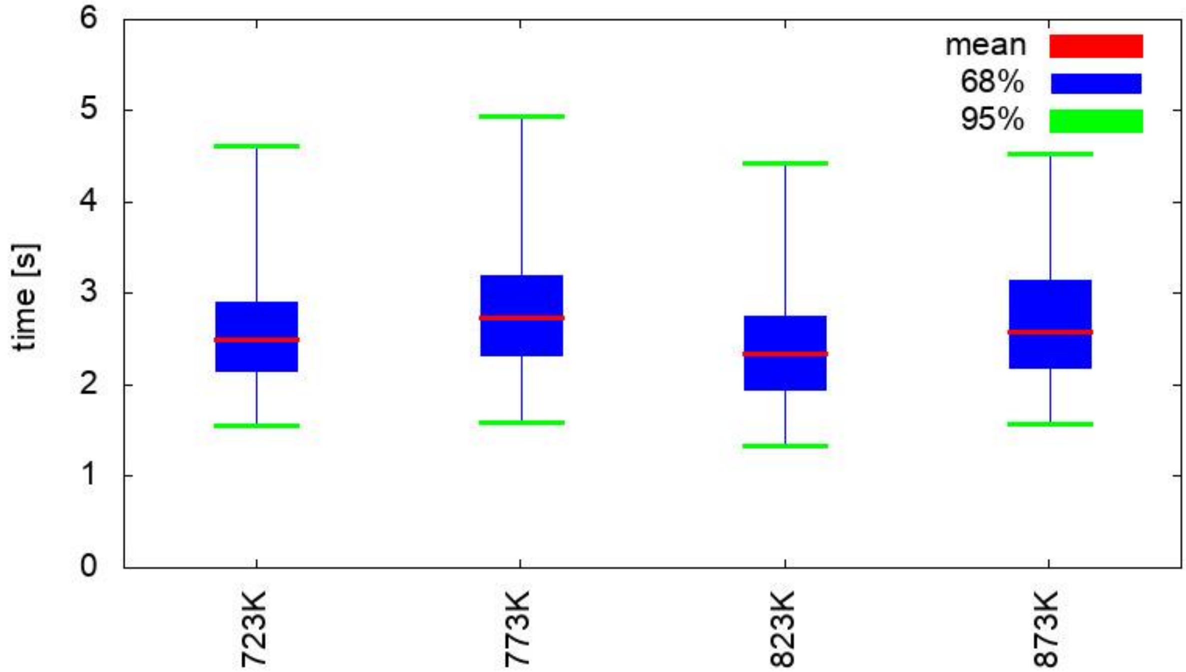

Fig. 2-13 Temperature effect on residence time of biomass particles.

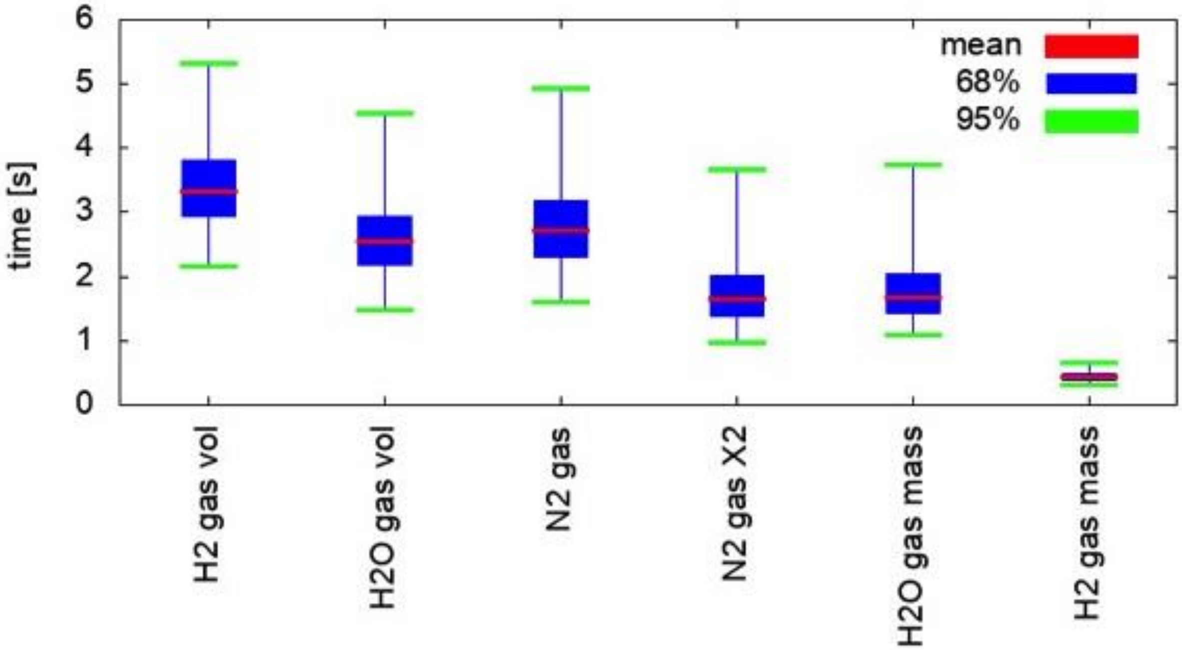

Fig. 2-14 Effect of different gas types on biomass particle RTD.

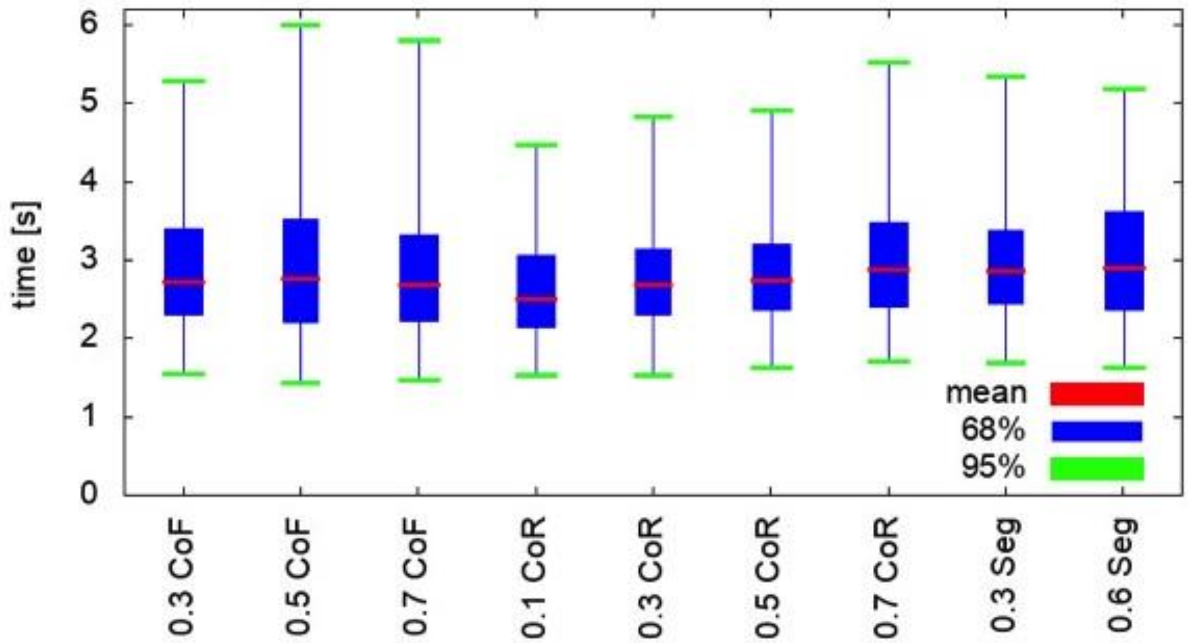

Fig. 2-15 Biomass particle collision and mixing properties effect on RTD.

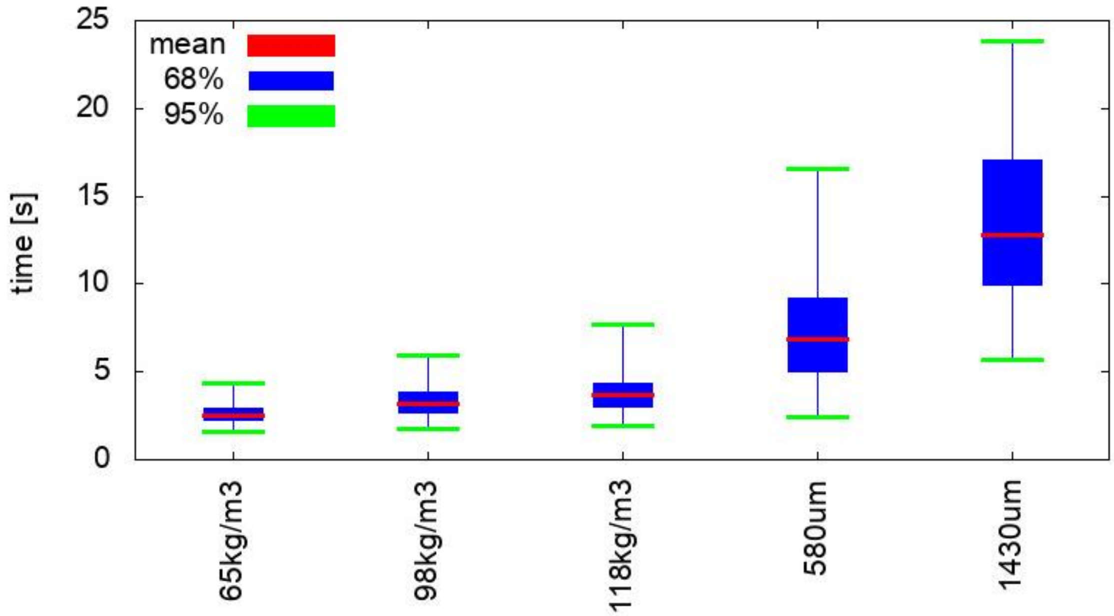

Fig. 2-16 Biomass particle density and size effect on RTD.

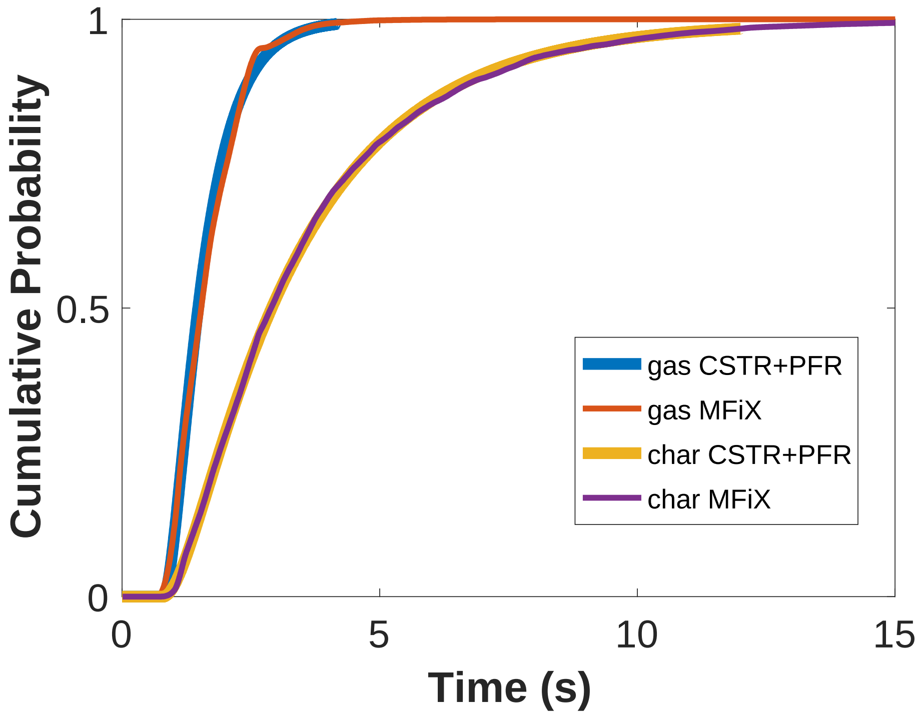

Fig. 2-17 Three CSTR in series can be used to match with MFiX char and tar RTD data.

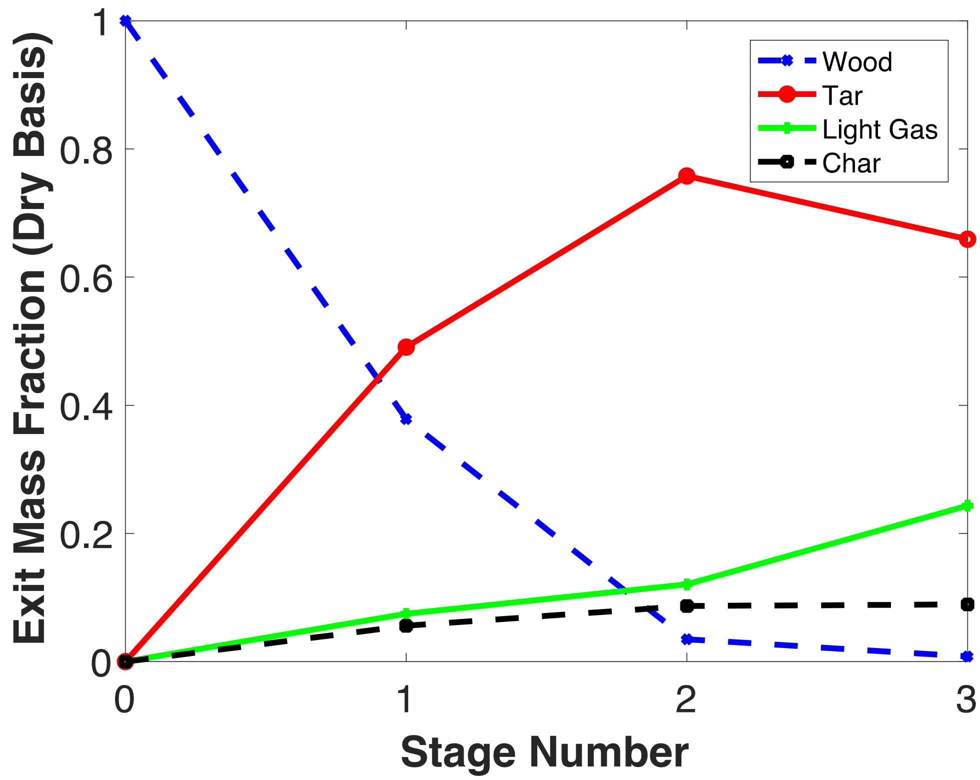

Fig. 2-18 Pyrolysis yield (Liden) from the three stages represent different regions in the reactor for the 10 cm static bed height at 4 U/U_{mf}.

Table 2-1 Experimental and modeling parameters.

Property	Units	Experiment	Model
Particle Sauter mean diameter (sand)	m	500×10^{-6}	500×10^{-6}
Particle density (sand)	kg/m^3	2500	2500
Particle Sauter mean diameter (biomass char)	m	278×10^{-6}	278×10^{-6}
Particle density (biomass char)	kg/m^3	—	80
Temperature	K	773	773
Pressure (inlet)	kPa	133	133
Fluidizing N_2 velocity (range)	m/s	0.249	0.07 – 0.45
Minimum fluidization	m/s	0.0565	0.0565
Coefficient of restitution	—	—	0.9
Angle of repose	°	—	55
Friction coefficient	—	—	0.1

Table 2-2 Nominal parameters and parameter matrix

Simulation matrix													
Case	**Mesh** [d_p]	**Biomass density** [$g \cdot cm^{-3}$]	**Biomass diameter** [cm]	**Gas molecular weight** [$g \cdot mol^{-1}$]	**Gas superficial velocity** [$cm \cdot s^{-1}$]	**Segregation slope coefficient** [–]	**Coefficient of restitution** [–]	**Coefficient of friction** [–]	**Reactor temperature** [K]	**Minimum Fluidization Velocity, U_{mf}** [cm/s]	**Superficial to minimum Fluidization Velocity, U/U_{mf}** [–]	**Fluidizing gas viscosity** [g/cm-s]	**Drag type**
1	5.4	0.082	0.0278	28	24.9	0	0.9	0.3	773	5.66	4	3.5×10^{-4}	Syamlal-O'Brien
2	5.4	0.082	0.0278	28	24.9	0	0.9	0.5	773	5.66	4	3.5×10^{-4}	Syamlal-O'Brien
3	5.4	0.082	0.0278	28	24.9	0	0.9	0.7	773	5.66	4	3.5×10^{-4}	Syamlal-O'Brien
4	5.4	0.082	0.0278	28	24.9	0	0.1	0.1	773	5.66	4	3.5×10^{-4}	Syamlal-O'Brien
5	5.4	0.082	0.0278	28	24.9	0	0.3	0.1	773	5.66	4	3.5×10^{-4}	Syamlal-O'Brien
6	5.4	0.082	0.0278	28	24.9	0	0.5	0.1	773	5.66	4	3.5×10^{-4}	Syamlal-O'Brien
7	5.4	0.082	0.0278	28	24.9	0	0.7	0.1	773	5.66	4	3.5×10^{-4}	Syamlal-O'Brien
8	5.4	0.0656	0.0278	28	24.9	0	0.9	0.1	773	5.66	4	3.5×10^{-4}	Syamlal-O'Brien
9	5.4	0.0984	0.0278	28	24.9	0	0.9	0.1	773	5.66	4	3.5×10^{-4}	Syamlal-O'Brien
10	5.4	0.1181	0.0278	28	24.9	0	0.9	0.1	773	5.66	4	3.5×10^{-4}	Syamlal-O'Brien
11	5.4	0.082	0.0580	28	24.9	0	0.9	0.1	773	5.66	4	3.5×10^{-4}	Syamlal-O'Brien
12	5.4	0.082	0.1430	28	24.9	0	0.9	0.1	773	5.66	4	3.5×10^{-4}	Syamlal-O'Brien
13	5.4	0.082	0.0278	28	33.9	0	0.9	0.1	773	5.66	6.0	3.5×10^{-4}	Syamlal-O'Brien
14	5.4	0.082	0.0278	2	24.9	0	0.9	0.1	773	79.21	0.29	1.8×10^{-4}	Syamlal-O'Brien
15	5.4	0.082	0.0278	18	24.9	0	0.9	0.1	773	8.79	2.83	2.6×10^{-4}	Syamlal-O'Brien
16	5.4	0.082	0.0278	2	24.9	0	0.9	0.1	773	79.21	4	1.8×10^{-4}	Syamlal-O'Brien
17	5.4	0.082	0.0278	18	24.9	0	0.9	0.1	773	8.80	4	2.6×10^{-4}	Syamlal-O'Brien
18	5.4	0.082	0.0278	28	24.9	0	0.9	0.1	773	5.66	4	3.5×10^{-4}	Syamlal-O'Brien
19	5.4	0.082	0.0278	28	24.9	0.3	0.9	0.1	773	5.66	4	3.5×10^{-4}	Syamlal-O'Brien
20	5.4	0.082	0.0278	28	24.9	0.6	0.9	0.1	773	5.66	4	3.5×10^{-4}	Syamlal-O'Brien
21	5.4	0.082	0.0278	28	24.9	0	0.9	0.1	723	5.66	4	3.5×10^{-4}	Syamlal-O'Brien
22	5.4	0.082	0.0278	28	24.9	0	0.9	0.1	823	5.66	4	3.5×10^{-4}	Syamlal-O'Brien
23	5.4	0.082	0.0278	28	24.9	0	0.9	0.1	873	5.66	4	3.5×10^{-4}	Syamlal-O'Brien
24	6.6	0.082	0.0278	28	24.9	0	0.9	0.1	773	5.66	4	3.5×10^{-4}	Syamlal-O'Brien
25	5.4	0.082	0.0278	28	24.9	0	0.9	0.1	773	5.66	4	3.5×10^{-4}	Syamlal-O'Brien
26	5	0.082	0.0278	28	24.9	0	0.9	0.1	773	5.66	4	3.5×10^{-4}	Syamlal-O'Brien
27	6.6	0.082	0.0278	28	24.9	0	0.9	0.1	773	5.66	4	3.5×10^{-4}	Gidaspow
28	5.4	0.082	0.0278	28	24.9	0	0.9	0.1	773	5.66	4	3.5×10^{-4}	Gidaspow
29	5	0.082	0.0278	28	24.9	0	0.9	0.1	773	5.66	4	3.5×10^{-4}	Gidaspow

CHAPTER 3 : DESIGN CONSIDERATIONS FOR A LABORATORY-SCALE FLUIDIZED BED BIOMASS FAST PYROLYSIS REACTOR

A version of this chapter will be originally published by Emilio Ramirez et al.:

Ramirez, E., Finney, C.E.A., Daw, C. S. (In Preparation). "Computational study on biomass fast pyrolysis: Design considerations for a laboratory-scale fluidized bed." To be submitted.

The work in this chapter was analyzed and written by Emilio Ramirez. Stuart Daw gave guidance and discussions on the approach. Charles provided guidance on the time irreversibility approach. James E Parks II and Thomas D. Foust provided support to visit and interact with biomass fast pyrolysis experimental groups at the National Renewable Energy Laboratory. Emilio will be submitting the paper and will ensure all journal requirements are fulfilled.

The CFD simulations from the previous chapter are utilized in this chapter to further evaluate effects of hydrodynamics on biomass fast pyrolysis. These simulations were also modified to investigate the effect of biomass particle size and biomass mass flow and sand bed height. A short discussion on reactor diameter and particle size distribution is given, and their effects can be extrapolated from previous work and the results shown in this work. The guiding hypothesis for this work was that high-speed pressure signals at the upper part of the bed can be used to detect shifts toward or away from maximum biomass fast-pyrolysis yield conditions. Results from this work show the guiding hypothesis is true and relates biomass char particle flow with yield. This work also provides guidance on how to expand the MFiX/MATLAB chemistry model to include ash/char catalytic effects, water effects, and particle heat up effects in future work.

Abstract

Fast pyrolysis is a leading candidate process for converting biomass to liquid fuels. During fast pyrolysis in bubbling-bed or circulating-bed reactors, biomass particles are rapidly heated through contacting with hot gases and solids, and their constituent components decompose into volatiles, ash, and char. The product vapor/gas composition, which determines the yield of fuel-compatible molecules, is highly dependent on the bubbling intensity, which promotes mixing and heat and mass transfer within the biomass particles and at the particle surfaces as they transit through the reactor. Fluidized-bed hydrodynamic characterization at smaller scales is a vital first step in reactor scale-up.

In this study, we simulate a 3D bubbling fluidized-bed biomass fast-pyrolysis reactor from a prior study [151]. This study explores operating effects on hydrodynamics and biomass conversion as the gas flow is increased through the bubbling-to-slugging transition and turbulent regime, with all the other operating variables held constant. We employ MFiX, an open-source software package supported by the U.S. Department of Energy (DOE), which utilizes a continuum (two-fluid) approach for modeling the reactor hydrodynamics. Bubbling intensity and dynamic characteristics were evaluated utilizing pressure-based measurements [123]. A novel approach based on time irreversibility is introduced to evaluate hydrodynamics.

Mixing, hydrodynamics, and pyrolysis yields are compared which show the effect of fluidizing gas and fluidization regime on biomass fast pyrolysis in bubbling–bed reactors of Geldart Group B particles. This work highlights the importance of initial reactor design for optimizing yield. We will discuss implications on future numerical simulations and experiments based on our observations.

Introduction and Background

Biomass fast pyrolysis complex multi-scale processes

Optimizing yields from fast-pyrolysis bubbling-bed reactors is a complex process that requires knowledge of fluidization and chemistry at multiple scales [152]. However, to focus our effort and simplify modeling challenges we lump these effects at particle and reactor scales. Fluidized-bed reactor behavior is complex due to the ergodic hydrodynamic behavior [54]; thus, effects on biomass particles are difficult to understand. At the particle scale the complex geometry [153] used to transport fluids and minerals in the plants also pose challenges for heat and mass transfer. The biomass morphology and properties depend on species and even within the same species, composition is largely heterogeneous. Furthermore, feed handling and preprocessing also affect particle morphology and chemistry which affects how biomass particles will interact in the bubbling bed. Internal biomass particle effects include thermal heating, mass transfer, and conversion kinetics [139]. Various kinetic schemes [9, 125, 131, 154-156] are available in literature that lump heating, mass transfer, and chemical yield in first-order Arrhenius rate equations. To help understand particle heat and mass transfer and conversion kinetics much work has been performed on bench-scale fixed beds [157]. However, scalable fluidized-bed bench experiments are necessary for industrial scaleup [15, 158].

At the reactor scale, the complex hydrodynamics affect thermal heating [130] in the bed and freeboard, particle and gas/vapor mixing [141], segregation, elutriation, attrition, fragmentation [159], and residence time [132]. Biomass particle attrition and fragmentation result in smaller particles with shorter residence time distribution (RTD). However, capturing the complex size/geometry changes are difficult to predict in a model due to the complex mechanical agitation/interactions inside the fluidized bed [160]. A method used to measure particle and gas/vapor mixing, segregation, and elutriation is by measuring residence time distribution of particles and gas/vapors [132]. However, at the bubbling-to-slugging transition and fully developed slugging, RTD curves may look different due to gas bypassing [161, 162] through intermittent large gas bubbles and recirculation. At the higher fluidization velocity, biomass char particles reach a RTD limit that must be considered when establishing operating conditions [151, 163]. Biomass particle mixing is also affected by superficial gas velocity and fluidization regime [140, 141, 164]. Fluidized-bed regime transition depends on sand particle properties, sand particle size distribution [165], bed height, and reactor operating conditions (temperature, pressure, gas type) [122]. Fundamental particle fluidization concepts must be applied to acquire an understanding how a biomass pyrolysis bubbling-bed reactor will behave.

Hydrodynamic effects on pyrolysis yields/quality

Within the bubbling bed of sand, biomass is de-volatized into char, ash, tar (oil), and non-condensable gases [124]. Due to the high heat-transfer characteristic of bubbling beds, biomass particles, ~0.0005 m, are quickly de-volatized in < 2 seconds [150]. However, tar vapor released from biomass particles in the lowest part of the bed during devolatization has a longer residence time, and the tar concentration is cracked through secondary reactions to non-condensable gases [125, 131, 133, 152, 166]. Secondary cracking of tar occurs in the bed and the hot freeboard region, where high temperatures provide an environment for these secondary cracking reactions.

Fluidization dynamics in the bubbling-bed reactor must be such that the particle RTD is long enough to maximize conversion of biomass but minimize tar RTD to maximize tar/oil yield quantity. However, the fluidization regime also affects oil quality (composition) [31]. The required tar vapor (oil) chemical composition for synthesizing fuels will likely be different from that required for developing chemical products [126]. Bubbling-bed reactor operating conditions must be chosen to maximize quality and composition [72, 167]. The kinetics used in this study uses a lumped approach to determine quantity of tar, gas, and char and does not distinguish composition. More complex kinetics [125, 155] can be used to extract compositional effects at various fluidization regimes.

Hydrodynamic effects on biomass fast pyrolysis have been noted in experimental studies [31, 168], but most studies focus on tar vapor yield. Lee et al. [31] showed biomass fast-pyrolysis in a bubbling bed at various U/U_{mf} affected oil yield quantity and composition. Their study also investigated effects of bed height on biomass fast-pyrolysis yield. Kim [168] showed fluidizing gas affects biomass fast-pyrolysis yield. In a review of biomass fast pyrolysis, Butler et al. [15] noted vapor residence time and biomass feed rate affect yield. They also found space velocity affects the range of gasoline product yield directly. Furthermore, biomass particles and concentration affect fluidization in beds [141, 164]. Zhang et al. [169, 170] found biomass concentration and particle size affect the transition from bubbling to turbulent fluidization. Larger biomass particles promoted the collapse of bubbles to smaller size. Higher concentration resulted in decreased transition velocity. It is vital to design the bubbling-bed reactor specifically for biomass fast-pyrolysis processing at specific operating conditions.

Focus of this work

The focus of this work is to utilize a validated and verified [151] MFiX computational model to determine optimal reactor operation and fluidization conditions needed to maximize oil yield. A second focus is to show that a reasonable high-speed pressure diagnostic approach can be used in real time that is non-intrusive to determine maximum yield. Finally, this work will provide guidance on how to use computational fluid dynamics and pressure diagnostics to set up optimal reactor operation for typical experiments of this type. Based on previous work [123], high-speed pressure diagnostics located near the top of the fluidized bed can be used to detect bubble speed and coalescence events. Thus, pressure diagnostics may be used as an indicator toward or away from optimal biomass fast pyrolysis yield conditions.

Technical Approach

Fluidized bed simulation conditions

This work utilized the geometry of an experimental laboratory-scale reactor used for biomass processing research at the National Renewable Energy Laboratory (NREL). A schematic of the reactor is shown in Chapter 2. The inner diameter D_r and height H_r of the reactor are 0.0508 and 0.4335 m, respectively. Operating conditions were chosen to match baseline experiments at NREL and are listed in Chapter 2, Table 1 [128, 134]. Initially, quartz sand particles with diameter d_s of 5.0×10^{-4} m and density ρ_s of 2500 kg/m^3 were set at an expanded bed height H_o of 0.1475 m, with an initial void fraction of 0.59. The sand particle–particle properties were defined with a coefficient of restitution of 0.9 [40, 135-137] and angle of repose at 55°[138].The particle–wall collision specularity coefficient was set to 0.6; however when normalized slip velocity goes to zero, it is calculated internally using a relation developed by Li et al. [78, 81]. Reacting pine biomass particles, with char-like properties, of Sauter mean diameter d_{sm} of 2.78×10^{-4} m and density ρ_s of 80 kg/m^3 were uniformly inserted through a point source, 0.01016 m high from the bottom, at 0.0001181 kg/s. The reactor outlet is open to pressure at 133 kPa. Each simulation was initiated by uniformly adding pre-heated nitrogen gas at 773 K through the reactor bottom with a mass-flow inlet based on superficial gas velocity, U, as a multiple of the minimum fluidization gas velocity, U_{mf}. The minimum fluidization velocity was measured at 0.0263 m/s at STP and corrected to 0.056 m/s to account for 'hot' reactor operating conditions, and the Syamlal-O'Brien drag-model [82] parameters were assigned based on the corrected U_{mf}.

Simulations were first tested in [151]. The same simulations are used in this work and further analyzed to determine methods and effects on maximum yields. This work also investigates effects of bed depth and biomass flow using the same simulation.

Relationship between hydrodynamics and residence times in FB reactors

Bed height

The static bed height, the height of the inert particle medium in the reactor prior to fluidization, is lifted upward by the gas pumping force and particle−particle interaction, causing the bed to expand and contract. Within the bed there are pockets of gas, bubbles delineated by a particle cloud, rising upward. Bubble sizes vary and depend on the static bed height, superficial velocity, particle properties, and fluidizing gas. If the static bed height to bed diameter ratio is large enough, slugging bubbles (bubbles that span the diameter of the reactor) will develop [48]. This work explores the effect of bed height on biomass fast-pyrolysis yield.

Bed diameter, previous work

The reactor diameter in bench-scale reactors has the potential to have wall effects on fluidized-bed hydrodynamics, such as at slugging conditions. Bench-scale beds operated at slugging conditions with diameters smaller than 30 cm have higher through flow and less well mixed particle behavior than larger diameter beds (>30 cm) [29]. However, most biomass pyrolysis bench scale units are smaller than 30 cm. When biomass pyrolysis bench-scale reactors are scaled up, hydrodynamic effects must be considered such that biomass and tar mixing and residence time are similar.

Biomass particle size, previous work

Biomass particle size distribution was also shown to also play an important role in optimizing biomass fast pyrolysis processes. The authors in [139, 163] showed each bin of different particle sizes resulted in a different residence time distribution. The biomass particle size distribution is an operating parameter that can be varied to acquire a different quantity of pyrolysis product yield. For these reasons biomass particle size distribution must be an integral part of the reactor design and operation plan.

Biomass flow effects

Biomass flow effects must take into account particle properties but also focus on the quantity of mass flow. As larger amount of biomass mass flow is placed in the reactor, more pyrolysis yield is expected, however bubbling-bed hydrodynamics must be considered. In literature there are correlations for particle terminal velocity [144, 171] which provide guidance for conditions such that particles will elutriate. These correlations can be applied to multiple bin sizes in a biomass particle size distribution to guide conditions necessary such that all particles elutriate out of the reactor. However, these correlations do not account for the maximum biomass quantity that can be continuously removed from inside the reactor. Fluidizing-gas superficial velocity determines how much biomass/char will accumulate in the reactor. Biomass mass flow into the reactor must equal mass flow out of the reactor. The maximum mass flow for a specific biomass feedstock particle size distribution can be determined experimentally or utilizing simulations, as will be shown. The particle size distribution used in this work is based on [139]. The particle sizes investigated were 40, 58, 100, 278, 344, 426, 543 μm at various feed-rate factors of 0.1, 0.5, 1.0, 1.5, 2.0, relative to the nominal feed rate of 0.118 g/s.

CFD simulations

Major assumptions and constraints

Computational fluid dynamics (CFD) [83] is employed to simulate the biomass fast-pyrolysis process in the bubbling-bed reactor described above over a range of fluidization velocities. Numerous fluidized-bed researchers have found CFD to be a useful complement to experimental measurements [78, 79, 84, 85]. One benefit of CFD is that it provides spatiotemporal details about pressures, velocities, flows, and concentrations that are either impossible or extremely difficult to obtain experimentally. CFD has also been employed in numerous studies of gas–solid fluidized beds [84, 86], but very limited number of biomass fast-pyrolysis CFD studies have addressed hydrodynamic effects [15, 31].

The specific CFD implementation used in this study employed the Eulerian–Eulerian computational Two-Fluid Model (TFM) [89, 90], which approximates the flowing phases(i.e. gas and solids) as interpenetrating continua. The TFM is in contrast to numerical simulations that resolve discrete particles or molecules [88, 91-93]. While the TFM approach does not resolve individual particles, it has been demonstrated to reproduce major hydrodynamic features, including bubbles [40, 77, 79], residence time [145], and mixing [146, 147]. Detailed information on the TFM and reaction formulation can be found in Gidaspow [89] and [97].

To carry out our simulations, we utilized MFiX (Multiphase Flow with Interphase eXchange), which is an open-source CFD software developed primarily at the National Energy

Technology Laboratory [94]. The multi-species gas phase was simulated as compressible, and stress tensors for the gas and solid phases were related to shear stress using Newton's law. To model solids transport properties, such as solids pressure and viscosity, the kinetic theory of granular flow [94] together with the Schaeffer frictional stress tensor formulation [95] and the sigmoidal blending stress function [77, 86, 96] were employed to relate the computed solids temperature with solids transport properties. Furthermore, the gas–solid momentum transfer used the Syamlal-O'Brien correlation [82] for the drag model. The discretization scheme utilized a finite-volume approach with a staggered 3D grid [97]. Scalar values, pressure and void fraction, were stored in the cell center, while velocities were computed on the cell surfaces. Additionally, second-order discretization was utilized using the SMART approach together with the chi-scheme which improved convergence and accuracy of the simulation [148]. A modified SIMPLE approach [97] is also used and improves speed and stability through variable time stepping, solid volume-fraction correction, and solids-pressure evaluation. The no-slip condition was applied to the gas and solid phase on the side walls while the Jackson and Johnson partial-slip wall boundary condition [98] was applied to the solid phase.

To characterize the spatiotemporal dynamics generated by MFiX, we tracked detailed variations in pressure and gas and solid species mass as time series at each computational grid point. As explained below, these raw time series were then further processed to produce simulated (virtual) measurements of the local pressure fluctuations, pyrolysis yield, and residence time distribution for the gas/tar and biomass. We then analyzed and compared the pressure time series at upper axial location in the bed to determine the bubbling and slugging states [123]. The pyrolysis yield at the outlet was measured to determine conversion of gas, tar, and char coming out of the reactor. The gas and biomass tracer mass time series were then analyzed to acquire residence time distribution at the various fluidization states.

Simulation results assumed biomass devolatization time is ~1 second [9] and char-like properties were used for the biomass to capture flow statistics, residence time, and mixing. Furthermore, our simulation does not account for attrition or fragmentation, and a single size was used for the sand phase and a different single size was used for the biomass/char/ash phase based on data from NREL [139]. The molecular weights were chosen based on the types of species in each phase. However, there is uncertainty in the molecular weights based on the heterogeneity of the biomass material, the material type, and how it was harvested.

Mesh and stationary issues

A general concern for multiphase flow CFD simulations is establishing a computational grid size that is sufficiently refined so spatiotemporal dynamics no longer depend on grid resolution (i.e., grid independence). Based on prior mesh resolution studies [123], the cylindrical mesh was chosen with 15 cells in the radial direction and 256 cells in the axial direction, and with 6 azimuthal cells.

Methods of analysis applied to simulation results

Pressure statistics were measured and analyzed as stated in [123]. The upper section of the static bed height, $0.75 < H/H_o < 0.95$, was used for pressure measurements. The pressure time series from 20–45 seconds of simulation time was used for analysis. Standard deviation was used to determine the turbulent regime [172, 173] and fully developed slugging [54]. Kurtosis was investigated in relation to the bubbling-to-slugging transition [123]. Mean pressure can be used to find the minimum fluidization velocity U/U_{mf}=1. In this case we only simulated 1.3 – 8.0 U/U_{mf}.

Based on prior work, the maximum time and location of irreversibility in the pressure time series at various flows was also analyzed and is based on the work of Cox et al. [174]. Time irreversibility is a measure of the entropy in the fluidized-bed hydrodynamics caused by the interaction of the gases and particles, similar to thermodynamic irreversibility. The pressure data were applied to the irreversibility metric, T_3, where *N* is the index of the time-series values and *h* is the lag (or delay). The absolute maximum location and time was acquired from the T_3 metric.

$$T3 = \frac{\sqrt{N-h}\ \sum_{s=1}^{N}(y_{s+h}-y_{s-h})^3}{\left(\sum_{s=1}^{N}(y_{s+h}-y_{s-h})^2\right)^{\frac{3}{2}}}$$

Biomass particle mixing was also investigated at the various fluidization conditions. There are many mixing metrics that could be investigated, but for this work the Kramer's mixing index[141, 175] was chosen. Biomass char fraction data were collected within the static bed height, 20 cm, and was time averaged at each computational cell, in 10620 locations. These data were then applied to the Kramer mixing index, *M*:

$$M = \frac{\sigma_0^2 - \sigma^2}{\sigma_0^2 - \sigma_r^2}$$

$$\sigma = \sqrt{\frac{1}{n-1}\sum_{i=1}^{n}(X_i - \bar{X})^2}$$

Here σ_0^2 is the char mass fraction standard deviation when sand and char are completely segregated, and σ_r^2 is the char mass fraction standard deviation when sand and char are completely mixed. The completely mixed and segregated cases were created from char and sand data extracted when the bed was fluidized, and the following assumptions were made: For the completely mixed case, the emulsion and bubbles in the bed had the same char fraction, making $\sigma_r^2 = 0$. For the completely segregated case, the 0.2 cm tall char layer above the bed had no sand, with a void fraction of 0.51, and bubbles and emulsion in the char layer had the same char fraction, making $\sigma_0^2 = 0.3129$.

Results and Discussion

Hydrodynamic and pressure for fluidization

Fig. 3-1 shows pressure statistics, standard deviation, skewness, kurtosis at 1.3 – 8.0 U/U_{mf}. The standard deviation has a peak when the turbulent regime begins [172, 173] at 6 – 7 U/U_{mf}. These superficial gas inlet velocities for the system are in general agreement with correlations for the onset of the turbulent regime [56, 173]. The standard deviation also had an inflection point at ~3.5 U/U_{mf}, indicating fully developed slugging [54, 123].

Skewness and kurtosis were also investigated to determine the bubbling-to-slugging transition. At ~1.8 – 2.2 U/U_{mf}, kurtosis reached a minimum and skewness transitioned from negative to positive, indicating a change in the pressure dynamics. These results were compared with axial cross-section visualizations [151] and represent the bubbling-to-slugging transition. However, these pressure trends were inconsistent with pressure statistics investigated in a bubbling bed of sand [123]. As noted in [151] the same simulation setup was used as in [123], however biomass char was continually inserted into the bubbling bed. It is possible that biomass concentration may have affected pressure measurements, as noted in experiments of sand and biomass mixtures [165, 170]. Although skewness and kurtosis results were not what was expected, other pressure dynamics were investigated.

Pressure time irreversibility was measured based on time-series trends from this work and previous work [123]. A description of the maximum time and location of irreversibility can be found in the Method of analysis. Fig. 3-2(a) shows maximum time irreversibility for pressure measurements at various U/U_{mf}. At 1.8 U/U_{mf} the maximum time of irreversibility increases sharply, indicating a sudden change in pressure dynamics. The change in maximum time irreversibility is caused by bubble/particle interactions and oscillations between large and small bubble [176] eruptions near the surface of the bed.

The location of the maximum time of irreversibility was also acquired at a range of U/U_{mf}, Fig. 3-2(b). In the bubbling regime, 1.3 – 1.7 U/U_{mf}, the location between irreversible events increases, more bubbles and bubble eruptions. However, there is a sudden decrease between events at 1.8 U/U_{mf}, indicating entropy generation by bubbles occurs less often. As U/U_{mf} increases, the events between maximum time irreversibility continue to increase, likely due to the more periodic ogive slugging bubbles.

Fig. 3-3 shows biomass fast pyrolysis yield at 1.3 – 8.0 U/U_{mf}. In the bubbling-to-slugging transition, 1.8 – 3.5 U/U_{mf}, tar vapor yield remains at ~0.49 and then continues to increase. As the slugging bed transitions to turbulent fluidization, tar vapor yield continues to increase, reaching 0.71 tar vapor yield at 8.0 U/U_{mf}. Although biomass particle residence time distribution converges to a limit as fluidizing mass flow increases, the tar vapor residence time distribution continues to decrease, resulting in less secondary tar cracking and increasing overall tar vapor yield at the reactor exit. Interestingly, the char yield does not change much through the flow regimes, which agree with Lee et al. [31]. Furthermore, the amount of unconverted wood yield also increases at higher flows, because of shorter residence time for conversion of wood during fast pyrolysis.

RTD confidence intervals were also calculated using the mean RTD curve as described in Chapter 2 methods of analysis applied to CFD simulations. The confidence interval RTD data was processed with the mean RTD using the CSTR/PFR model and applied to the hybrid low-order Liden kinetics and are shown in Fig. 3-3 as lines above and below the mean yield.

Mixing related to hydrodynamics

Hydrodynamic information on char mixing was also acquired using Kramer's mixing metric at various gas flows, Fig. 3-4. Char mixing increased in the bubbling regime, 1.3 – 1.8 U/U_{mf}, and in a portion of the bubbling-to-slugging transition, 1.8 – 2.0 U/U_{mf}. As larger ogive slugging bubbles become dominant in the bubbling-to-slugging transition, 2.0 – 3.4 U/U_{mf}, particle and gas recirculation and mixing oscillate about a point. At fully developed slugging, 3.4 U/U_{mf}, mixing decreases and then increases, ~4 – 5 U/U_{mf}, as the bed transitions to turbulent fluidization. The fluidized bed is decently well mixed throughout all regimes based on Kramer's metric, but the best mixing occurs at turbulent fluidization, which also requires more pumping energy for the higher gas mass flow and results in higher wear and attrition. Note that the jitter in Kramer's metric between U/U_{mf} flows is probably from finite-sample effects. Furthermore, the larger oxygen concentration at higher flows relative to biomass vapors may have adverse effects on vapor quality and composition, which are not addressed in this study.

Impact of parametric sensitivities

Bed height

Fig. 3-5 shows biomass RTD for biomass char tracer particles at various sand bed heights H/H_o, where H_o is the nominal case with a 10 cm bed at bubbling conditions, 4 U/U_{mf}. As the sand bed height increased beyond 0.6 H_o, the bubbling bed began to transition to fully developed slugging. Sand bed height did not appear to have an effect on char mean residence time, however, the RTD curve was shifted. This might be explained by the particles in the freeboard at this nominal fluidizing gas mass flow rate travel at about the same rate as in the fluidized bed of sand. At higher superficial velocities residence time effects may be greater.

Fig. 3-6 shows RTD for tar vapors at various H/H_o, where H_o is the nominal case with a 10 cm bed at bubbling conditions, 4 U/U_{mf}. As H/H_o increased, a shorter time was required to completely remove the tar vapor tracer. The bed void fraction causes gases/vapors to speed up through the bed until reaching the freeboard section where they slow down. However, the RTD trends with increasing H/H_o are inconsistent due to complex mixing and recirculation events caused by large ogive slugging bubbles.

Biomass flow

Fig. 3-7 shows maximum reactor char outflow at various size cuts from a biomass feed particle size distribution, [139]. As the particle size cut increases, the maximum char that can be removed decreases, indicating biomass feed above this flow will accumulate in the reactor. Particle cut sizes 40 – 278 µm did not reach a limit at the maximum feed flow range of 0.47 g/s. Results from this computational study also agreed with terminal velocity calculations for particle elutriation [144, 171]. Biomass feed particle size distribution must be carefully selected for the designed biomass mass flow and fluidization gas mass flow. Otherwise, char will accumulate in the reactor which can adversely affect tar vapor yield due to catalytic reactions with ash in the char.

Fig. 3-8 shows RTD for the particle size distribution at 0.118 g/s biomass inflow. As biomass particles become larger, they take longer to be removed from the reactor, Fig. 3-7, because gravitational force is greater than the drag force exerted on the particle. Particle sizes 344, 426, and 543 µm accumulate in the reactor and have the longest residence time. Furthermore, the 543 µm particle size has a discontinuity at ~24 seconds which needs to be investigated further. Particle sizes in the particle size distribution must not exceed the maximum amount that can exit, based on reactor design.

Fig. 3-9 (a) shows char concentration along the axial height of the reactor for the 100 µm particle at various flows, relative to 0.118 g/s. The 100 µm char particle concentration at the various biomass feed flow rates is constant throughout the reactor, including in the bed section. An increase particle size to 278 µm diameter in Fig. 3-9(b), results in char concentration increasing at the higher biomass flow rates. Although the 278 µm particles do not fill the reactor freeboard, there is a large concentration above the bubbling bed and freeboard at the higher biomass feed rate flows. As tar vapors exit the reactor, they must traverse any layers of char in the freeboard to exit the reactor. These layers of char can contain reacting species or catalyzing ash which can have adverse effects on pyrolysis vapor yield. Hydrodynamics not only affect residence time and mixing, but also vapor contacting with any solids in the bed and freeboard.

Conclusions and Recommendations

Predicted impact of reactor operation to pyrolysis yield

This study utilized a 3D CFD bubbling bed reactor model to study hydrodynamic effects, and RTD data were extracted. A series of CSTRs were used to represent the RTD curves from the CFD model. The CSTR stages were then applied to the Liden pyrolysis kinetics [133] in a

MATLAB code. The hydrodynamics and reactions were separated in the hybrid model to efficiently determine effects of reactor operation on biomass pyrolysis yield.

Hydrodynamic regime transitions (minimum fluidization, fully developed slugging, and turbulent) were determined using pressure statistics. We also showed a novel approach for measuring time irreversibility in pressure time series to detect the bubbling-to-slugging transition. These metrics were utilized to investigate effects of fluidization on pyrolysis yield, mixing, and char holdup in bed and freeboard (axial profile).

In its current state, the hybrid model predicted a local tar vapor maximum yield in the bubbling-to-slugging transition. However, the global maximum yield occurred in the turbulent regime, partly due to the shorter residence times as fluidizing gas mass flow increased. This model lumped species and did not account for catalyzing effects of char accumulation in the bed or freeboard. The model included particle heating rate and water content effects but were disabled for this work and can be investigated in future studies.

Typical bubbling-bed reactors are designed for combustion and drying, which require longer residence times than those required for pyrolysis processes. To maximize drying and combustion, reactor bed and freeboard is tall enough to maximize energy extraction and minimize sand elutriation. Pyrolysis bubbling bed reactors must be designed to extract optimal yield and composition. The bubbling bed should be deep enough to maximize biomass devolatization, with the freeboard section short enough to prevent sand elutriation. This will minimize secondary tar cracking and vapors can be quickly removed from the reactor to minimize residence time in the freeboard. For scale-up, the bench scale reactor bed diameter must be wide enough to minimize wall effects [162].

Some options to reduce the residence time include:

1. Shallow bed of sand
2. Short freeboard section
3. Bed H/D ratio such that high velocities can be achieved without slugging
4. Temperature reduction in the freeboard region
5. Increasing the Weight Hourly Space Velocity (WHSV) in the freeboard by adding secondary air above the bed splash zone

Verified and validated CFD hydrodynamic models provide useful insight of the reactor physics which cannot be probed in experimental reactors. The hybrid approach used here can be efficiently used to conduct optimization studies on high-performance computers that require a fraction of the time (3 days) compared to solving reaction chemistry within the CFD simulation (2–3 weeks).

Testing key hypotheses

In the introduction some hypotheses were presented. These hypotheses guided the work herein, and findings are listed below.

1. The top of the bed, below the static bed height is the optimal location for pressure measurements. Typically, pressure measurements are made near the distributor to measure the minimum fluidization (mean) and turbulent fluidization (standard deviation). However, in this work, pressure measurements from CFD simulations at the upper part of the bed detected these transitions, as well as, the bubbling-to-slugging transition (kurtosis and time series temporal asymmetry).

2. Pressure fluctuations in the upper part of the bed, Chapter 1 and 2, appear to reflect bubble speed and coalescence events. These bubble events are an indicator of reactor conditions, such as mixing, heat transfer, segregation, residence time, etc. and can be associated with metrics of interest, Chapter 2 and 3.
3. In these simulations, the pressure signals appear fast enough to detect shifts toward or away from optimal yield conditions. It appeared that optimal yield in bubbling beds with beds deep enough to reach slugging conditions maximum tar yield at turbulent fluidization, where gases and tar vapors are quickly removed from the reactor. At such high fluidizing gas mass flow pyrolysis vapor quality and composition may be different than at lower fluidizing gas flow.

Recommendations for future experiments, measurements, computer simulations needed beyond current MFiX studies/capabilities

The work presented, shows how fluidization regime and fluidizing gas mass flow [31, 168, 177] affect biomass fast-pyrolysis yield in a fluidized bed. Biomass feed rate and particle sizes also appeared to have detrimental effects in terms of char/ash holdup in the bed and freeboard. To our knowledge there has not been such a comprehensive fluidization regime study on biomass fast-pyrolysis reactors that do and do not exhibit slugging conditions.

Using the axial profile of char concentration this hybrid model can be expanded to include char/ash effects on the pyrolysis yields from the reactor. Feedstocks have varying amounts of char and ash concentrations which must be investigated with a robust approach that can capture the hydrodynamics and chemistry efficiently.

Future work for this model should include experimental validation from a biomass fast-pyrolysis reactor at a range of fluidizing-gas mass flows. Measurements should include: high-speed pressure measurements near H_o of the bubbling bed; chemistry yield; sand, biomass, and char particle size distribution measurements [178]; fluidizing-gas properties and flows; biomass and sand properties characterization [178]; biomass mass flow; and reactor geometry. Using these data, modelers, and experimentalists can ensure hydrodynamic consistency between experiments and simulations.

Other future work includes comparing the model with different biomass tracers such as the work of Daw and Halow [140] or Kohler et al. [164]. This would expand the current work and ensure the modeling parameters chosen are relevant at a range of flows at different fluidization regimes.

Appendix: Figures

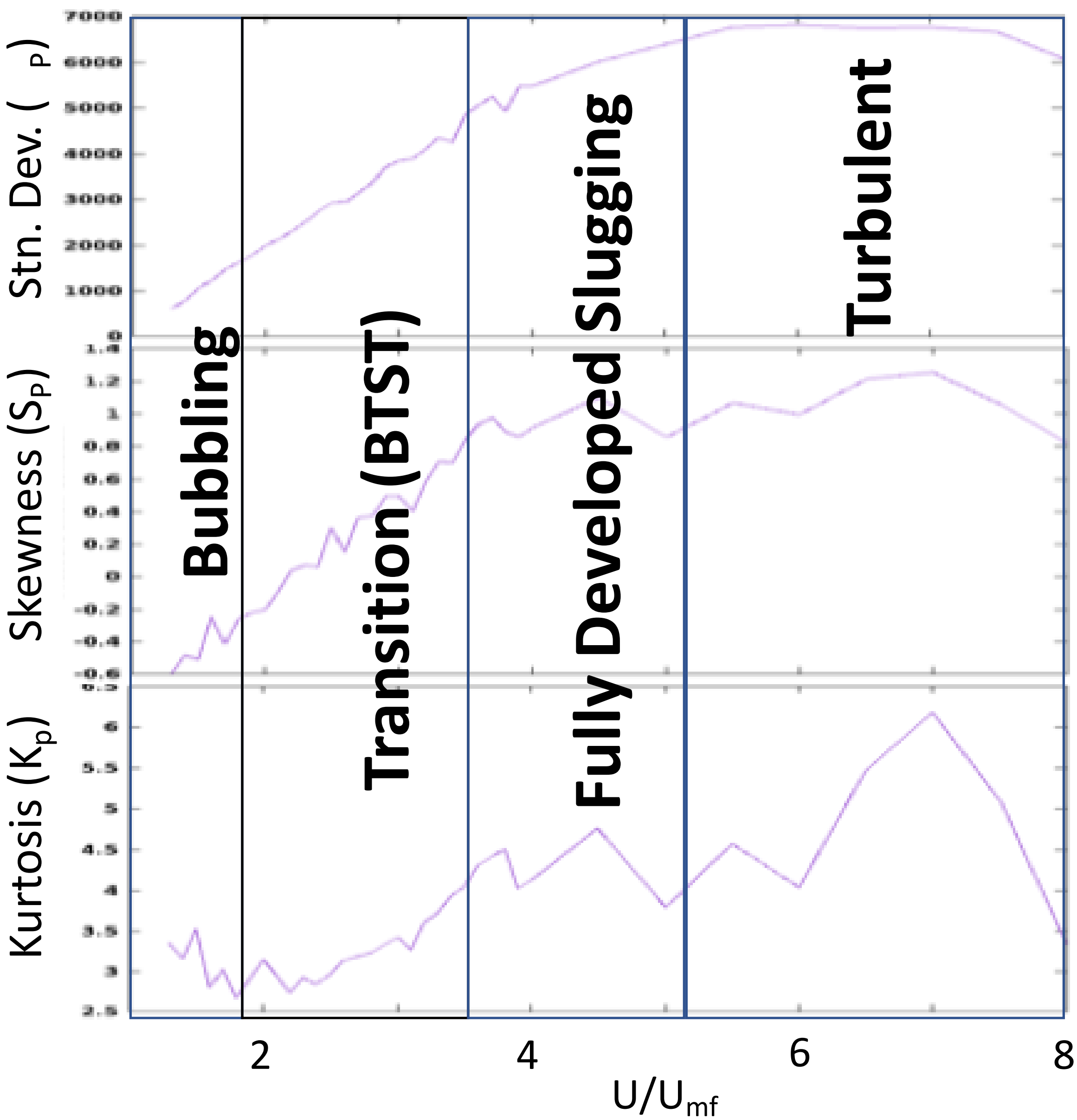

Fig. 3-1 Pressure statistics, (a) standard deviation, (b) skewness, and (c) kurtosis, at various superficial velocities, *U/U_{mf}*.

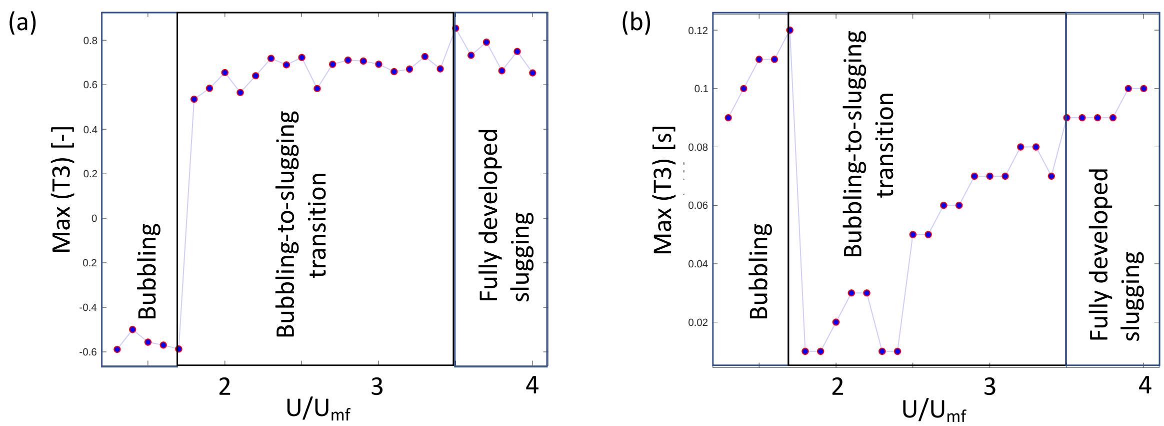

Fig. 3-2 Pressure time irreversibility metric at various superficial velocities, *U/U_{mf}*. (a) maximum time of irreversibility. (b) location of maximum irreversibility.

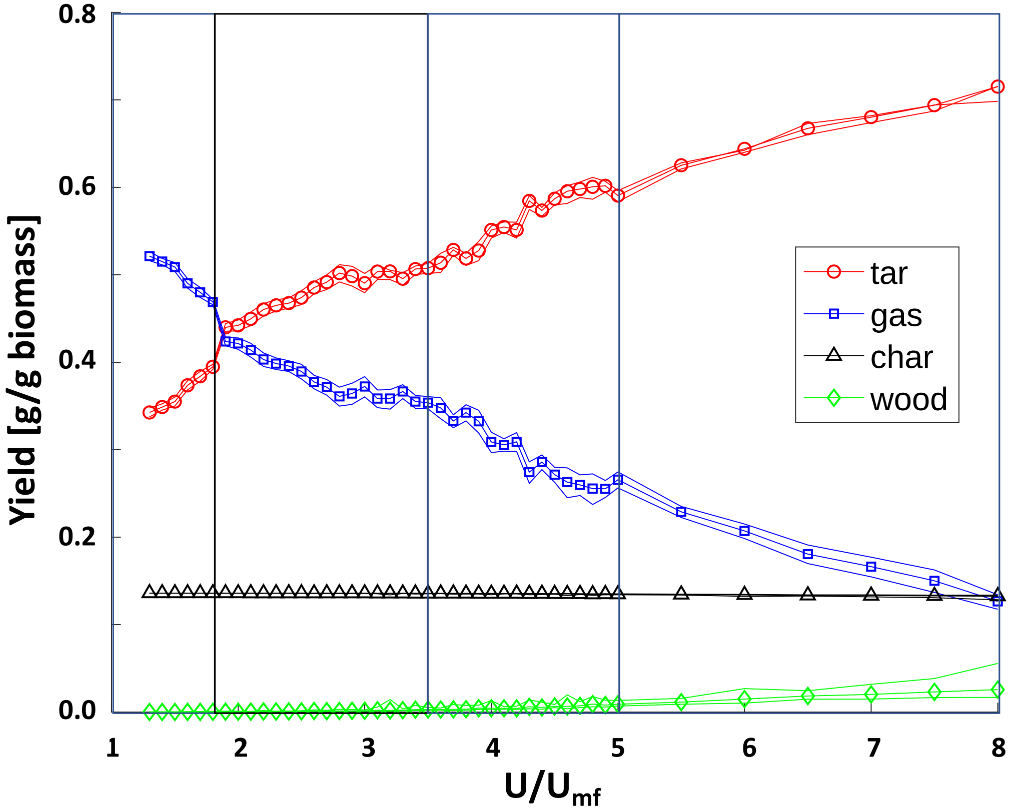

Fig. 3-3 Hybrid model biomass fast pyrolysis yield using Liden kinetics at superficial velocities, U/U_{mf}. Line bands represent ±1σ confidence intervals.

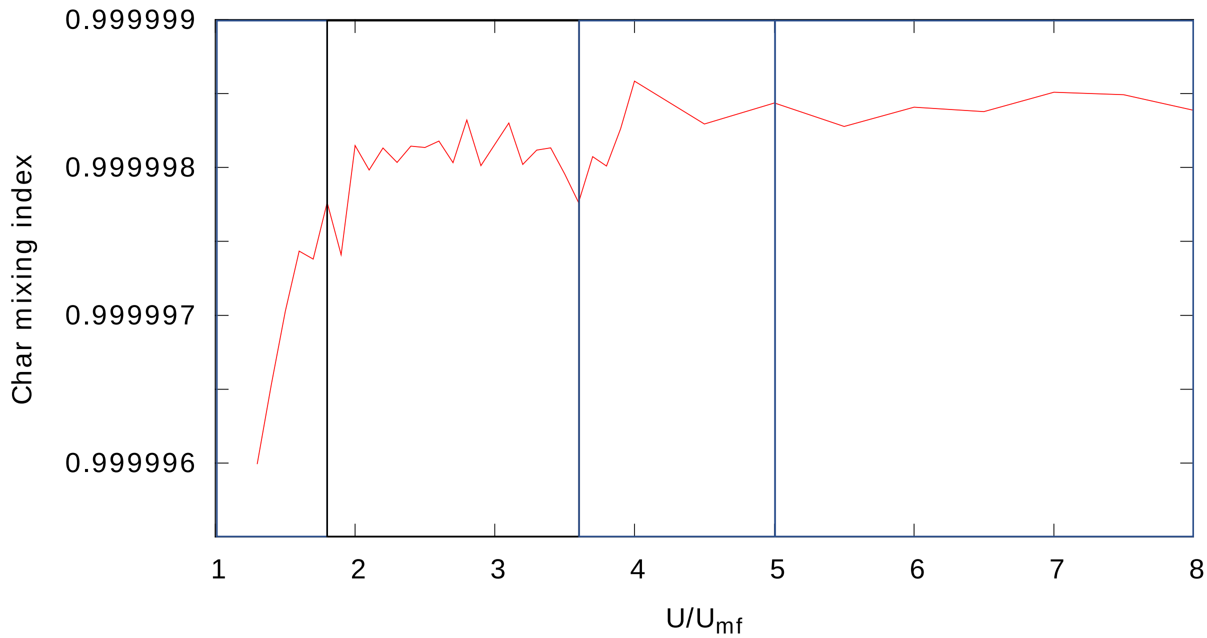

Fig. 3-4 Kramer's mixing metric [175] at various superficial velocities, *U/U_{mf}*.

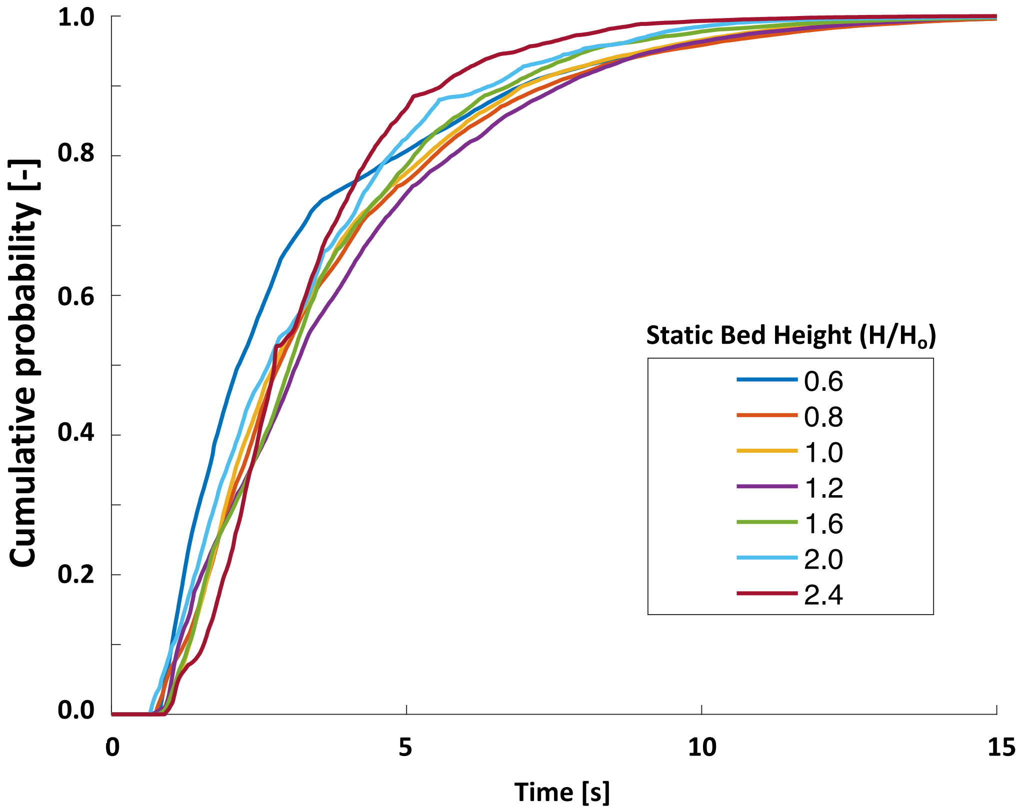

Fig. 3-5 Char particle residence time distribution (RTD) with respect to sand bed height 0.6 < H/H_o < 2.4 at 4 U/U_{mf} and H_o=10 cm.

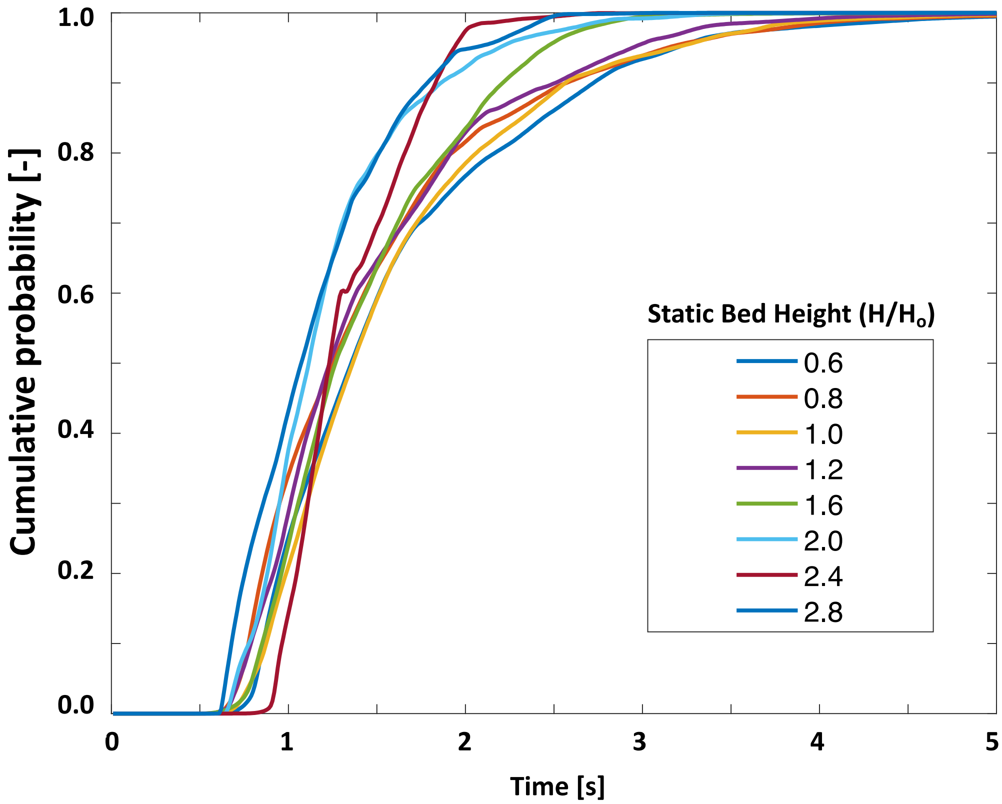

Fig. 3-6 Tar vapor residence time distribution (RTD) with respect to static bed height 0.6 < *H/H_o* < 2.4 at 4 *U/U_{mf}* and *H_o*=10 cm.

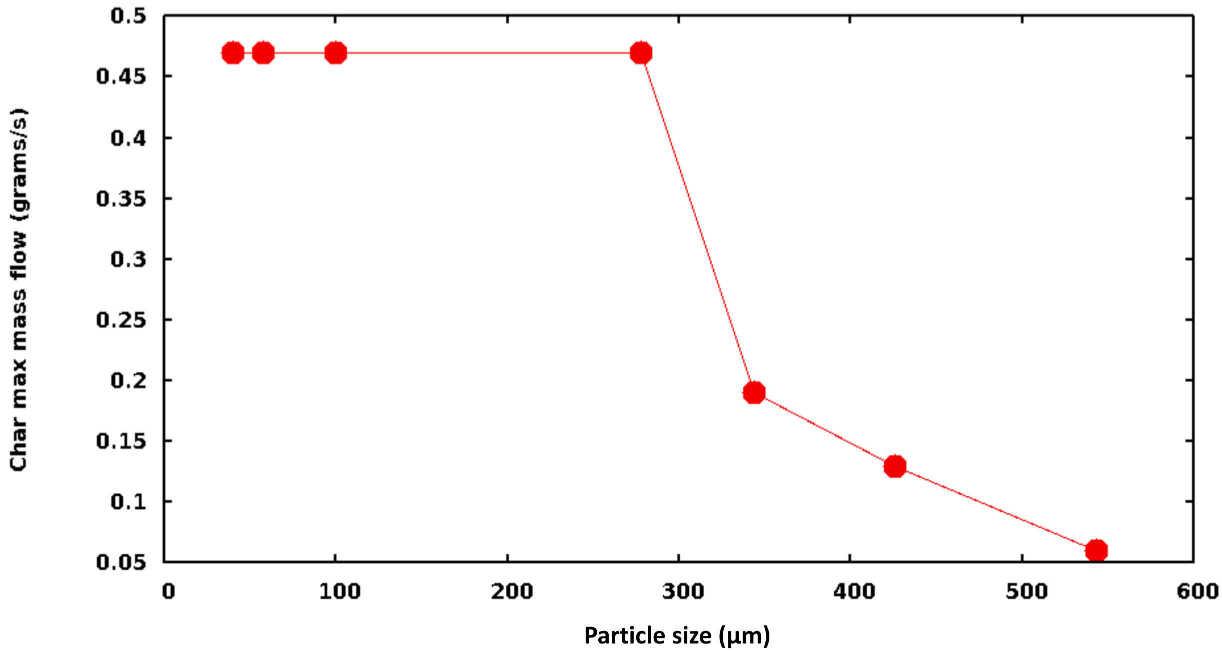

Fig. 3-7 Char particle maximum mass flow for a particle size distribution 40 µm < d_p < 543 µm.

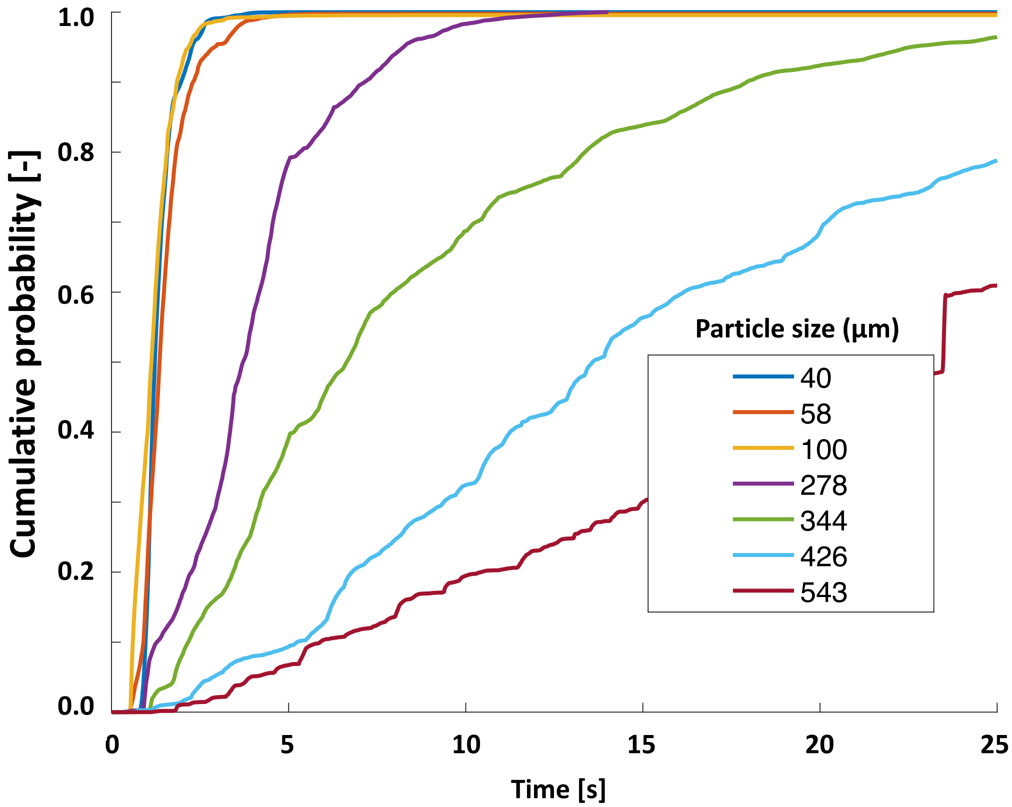

Fig. 3-8 Char particle exit RTD at 4 U/U_{mf} for non-reacting biomass feed particles sized between 40 and 543 microns.

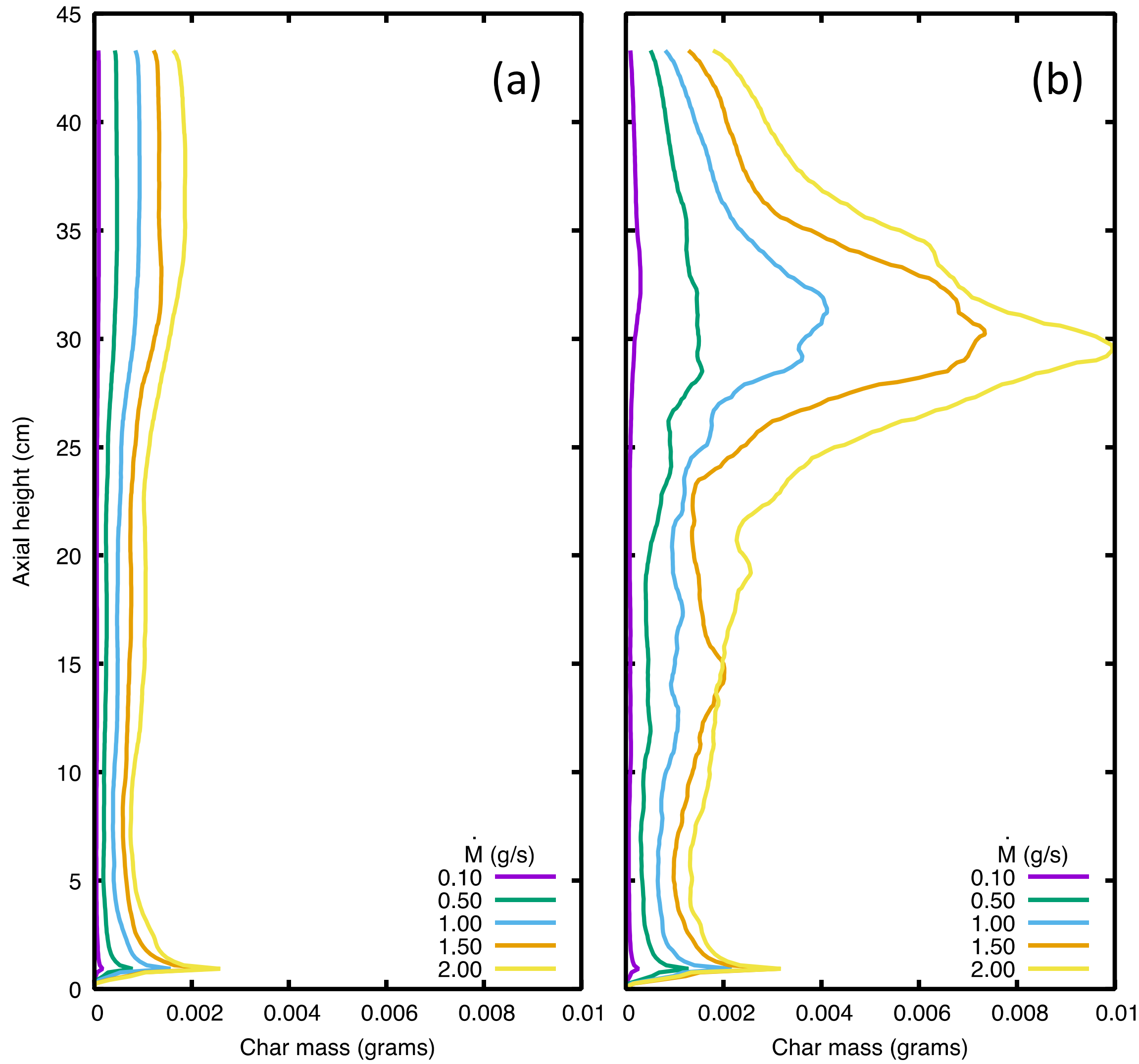

Fig. 3-9 (a) Simulated time-average axial profile for 100 micron char particles in the simulated reactor at a range of biomass feed rates relative to 0.118 g/s. (b) Simulated time-average axial profile for 278 micron char particles in the simulated reactor at a range of feed rates relative to 0.118 g/s. Note profile differences between 3.9 (a) and (b).

CHAPTER 4 : CONCLUSIONS

Summary

Computational fluid dynamics simulations of biomass fast–pyrolysis bubbling–bed reactors are a feasible approach for designing reactor conditions and understanding the underlying physics governing hydrodynamics at a range of fluidizing conditions. This dissertation work has revealed the following points regarding biomass fast-pyrolysis bubbling-bed reactors:

- Computational fluid dynamics simulations appear to provide a mechanism for quantifying the combined effects of hydrodynamics and chemistry that can be useful for understanding dominant processes involved in biomass fast pyrolysis.
- Biomass particle properties, bed particle properties, fluidizing gas composition, and fluidizing gas flow are factors that have major effects on gas and particle residence times and have major impacts on bio-oil yield when Liden kinetics are assumed.
- Two-fluid codes like MFiX can provide useful details about pyrolysis reactor hydrodynamics and gas and solid RTDs.
- MFiX simulations provide valuable information and visualization of the complex hydrodynamics which are difficult to obtain experimentally.
- Combining MFiX hydrodynamics with low-order chemistry models offers potential benefits in simulation speed and flexibility.
- Fluidized bed hydrodynamics, which include mixing, elutriation, and residence time, is complex and difficult.
- Large biomass particles and high biomass flow can potentially result in undesirable reactor hydrodynamics.

- Direct comparisons between computational simulations and high-speed experimental void fraction and pressure measurements are needed to validate and improve existing CFD models.
- Computational simulations of the bubbling-to-slugging transition with other CFD approaches such as the Eulerian–Lagrangian Discrete Element Method (DEM) are needed to resolve questions about the best approach for capturing the fundamental physics.
- More experimental and simulation studies of the detailed relationship between bubble and pressure dynamics are needed to allow pressure signals to be a useful indicator of bubble patterns.
- Computational simulations and corresponding experimental measurements are needed to determine how significant biomass concentration is to regime transitions, such as the bubbling-to-slugging transition, and the effects on altering chemical conversion and the efficiency of heat and mass transfer.

Chapter Summary

Chapter 0 gave an overview of biomass fast pyrolysis, fluidized beds, and quantitative approaches to evaluating hydrodynamics. A problem statement was outlined regarding a disconnect between hydrodynamics and biomass fast-pyrolysis yield. A fundamental understanding of hydrodynamic effects on biomass fast-pyrolysis yield is necessary for future scale-up activities. An outline and structure for the dissertation was also provided.

Chapter 1 is a version of the originally published work by Emilio Ramirez *et al.* in *Chemical Engineering Journal* titled “Computational Study of the Bubbling-to-Slugging Transition in a Laboratory-Scale Fluidized Bed.” The objective of Chapter 1 was to acquire an improved understanding of the physics of slugging in fluidized beds of Geldart Group B particles. This worked utilized a computational fluid dynamics model to quantify and investigate the hydrodynamic regime transitions. Pressure and bubble statistics were evaluated at bubbling-to-slugging fluidization regimes. Auto-correlation and cross-correlation techniques were also investigated. Pressure statistic data at various fluidization conditions agreed with bubble statistic data. The bubbling-to-slugging transition was also detected using pressure statistics. Furthermore, published work on bubble/pressure dynamics appeared to support bubble and pressure data acquired from the computational fluid dynamics simulations. In conclusion, an understanding of the bubbling-to-slugging hydrodynamics was acquired that could be applied to future simulation and experimental work.

Chapter 2 used the computational fluid dynamics model from Chapter 1, but sub–models enabled included kinetics and multiple species: biomass, char, char tracer, gas, tar, and tar tracer. The objective of Chapter 2 was to relate slugging to bio-oil yield for biomass fast pyrolysis in bubbling beds. Initially hydrodynamics of the non-reacting model was validated with a biomass mixing study, and an elutriation study that used tracer particles with properties similar to char. The reacting model was then validated with an experimental setup at NREL. A hybrid MFiX/MATLAB model was developed that also agreed with the pyrolysis experimental data. The hybrid model showed how hydrodynamics, sand/biomass mixing, at various fluidization conditions, bubbling, bubbling-to-slugging transition, fully developed slugging, and turbulent fluidization affected biomass fast-pyrolysis yield. This work also included a parametric study on the residence time distribution which can be used with an experimental hydrodynamic study to set up the simulation of interest. In conclusion, the hybrid MFiX/MATLAB model showed how mixing, elutriation, segregation, and chemistry were affected as the fluidized bed transitioned through bubbling, bubbling-to-slugging, fully developed slugging, and turbulent fluidization.

Chapter 3 work utilized the simulations from Chapter 2 and focused on optimizing and controlling biomass fast-pyrolysis yield. The objective of Chapter 3 was to identify how to use pressure fluctuations to monitor and control bio-oil yield from bubbling–bed biomass pyrolysis reactors. Time irreversibility and statistics from pressure measurements were able to detect the bubbling-to-slugging transition. This work also showed how pressure statistics are used to measure the other regime transitions, from bubbling to turbulent regimes. Mixing and segregation effects were also evaluated at the various fluidization regimes. Effects of bed height and biomass flow on residence time and yield were also shown. Guidance on using computational fluid dynamics was also given for future biomass fast-pyrolysis reactor designs. Optimal conditions for biomass fast pyrolysis must decrease the residence time in the reactor by designing the bed and freeboard sections short enough to allow enough time for biomass devolatization and reduce secondary tar cracking. In conclusion, pressure measurements in the upper part of the bed can be used to monitor and control hydrodynamics which affect mixing, segregation, elutriation, and chemistry.

Impact Potential

The work presented here has the potential to guide optimization of bubbling-bed reactors for different applications. Legacy coal and biomass energy–generation facilities currently operate bubbling-bed reactors below capacity due to a lack of fluidization technology knowledge, losing significant amounts of revenue and increasing capital expenses. These legacy facilities also operate outside of optimal reactor design conditions and emit significantly more CO_2 per MW_e produced.

The work presented here provides fluidization visualizations that are easy to understand and are quantifiable. In its current state, the work provides guidance for designing conditions in a bench-scale biomass fast-pyrolysis reactor, but any suitable kinetic model can be applied to the already available residence time distribution data contained herein.

Another major impact of this work is the ability to change the way experimental groups design bubbling–bed reactor operating conditions. Published work on biomass fast-pyrolysis reactor experiments do not make justifications for choosing specific reactor geometry or operating conditions. Furthermore, vital reactor operating information is not included in published work to ensure consistency with models and other experimental reactors. This work provides an understanding of important reactor hydrodynamic parameters which must be considered at the design stage to ensure optimal yield.

Future Work

Given the caveats of interdependence this novel approach using hydrodynamic data from a CFD model with a separate chemistry model can be used to quickly screen multiple cases to do parametric screening. This allows testing many conditions and finding effects on chemistry. Although this work used CFD data to acquire chemistry from a separate MATLAB model, this approach can be reversed. Optimal tar vapor and char particle residence time distribution can be acquired from a low-order chemistry model such as the MATLAB model used here with a regression analysis. The optimal char and tar-vapor residence time distributions can then be matched by the bubbling-bed reactor using parametric sweeps with open-source software such as DAKOTA.

The current work was validated by a single reactor operating condition with multiple replicates. We were unable to acquire more experimental data at other operating conditions to do further validation. This study can be expanded by providing experimental data at different points of the fluidizing regimes for validation of the model.

The MFiX model and the hybrid model included moisture and heat-transfer effects which were not enabled for the current simulations. These effects have the potential to negatively affect residence time and yield, which should be investigated at the reactor and particle scale.

More complex modeling approaches are available through the MFiX suite, such as the variable density model and the quadrature method of moments. These approaches are more complex, but capture some complex phenomenon using the Two-Fluid Model. The DEM model can also be utilized but requires more computational resources.

LIST OF REFERENCES

[1] M.S. Mettler, D.G. Vlachos, P.J. Dauenhauer, Top Ten Fundamental Challenges of Biomass Pyrolysis for Biofuels, Energy & Environmental Science 5 (2012) 7797-7809.
[2] R. French, S. Czernik, Catalytic pyrolysis of biomass for biofuels production, Fuel Processing Technology 91 (2010) 25-32.
[3] D. Meier, B. van de Beld, A.V. Bridgwater, D.C. Elliott, A. Oasmaa, F. Preto, State-of-the-art of fast pyrolysis in IEA bioenergy member countries, Renewable and Sustainable Energy Reviews 20 (2013) 619-641.
[4] T. Werpy, G. Petersen, A. Aden, J. Bozell, J. Holladay, J. White, A. Manheim, D. Eliot, L. Lasure, S. Jones, Top value added chemicals from biomass. Volume 1-Results of screening for potential candidates from sugars and synthesis gas, DTIC Document, 2004.
[5] E. de Jong, A. Higson, P. Walsh, M. Wellisch, Bio-based chemicals value added products from biorefineries, IEA Bioenergy, Task42 Biorefinery (2012).
[6] H. Lu, E. Ip, J. Scott, P. Foster, M. Vickers, L.L. Baxter, Effects of particle shape and size on devolatilization of biomass particle, Fuel 89 (2010) 1156-1168.
[7] L. Chen, C. Dupont, S. Salvador, M. Grateau, G. Boissonnet, D. Schweich, Experimental study on fast pyrolysis of free-falling millimetric biomass particles between 800 degrees C and 1000 degrees C, Fuel 106 (2013) 61-66.
[8] C.E. Greenhalf, D.J. Nowakowski, A.B. Harms, J.O. Titiloye, A.V. Bridgwater, A comparative study of straw, perennial grasses and hardwoods in terms of fast pyrolysis products, Fuel 108 (2013) 216-230.
[9] C. Di Blasi, Modeling chemical and physical processes of wood and biomass pyrolysis, Progress in Energy and Combustion Science 34 (2008) 47-90.
[10] R.S. Miller, J. Bellan, Numerical Simulation of Vortex Pyrolysis Reactors for Condensable Tar Production from Biomass, Energy & Fuels 12 (1998) 25-40.
[11] E. Ranzi, A. Cuoci, T. Faravelli, A. Frassoldati, G. Migliavacca, S. Pierucci, S. Sommariva, Chemical Kinetics of Biomass Pyrolysis, Energy & Fuels 22 (2008) 4292-4300.
[12] M.W. Jarvis, T.J. Haas, B.S. Donohoe, J.W. Daily, K.R. Gaston, W.J. Frederick, M.R. Nimlos, Elucidation of Biomass Pyrolysis Products Using a Laminar Entrained Flow Reactor and Char Particle Imaging, Energy & Fuels 25 (2011) 324-336.
[13] P. Ranganathan, S. Gu, Computational fluid dynamics modelling of biomass fast pyrolysis in fluidised bed reactors, focusing different kinetic schemes, Bioresource Technology 213 (2016) 333-341.
[14] R.C.H.J. Brown, National program 207: bioenergy and energy alternatives, Distributed biomass to diesel workshop Richland, WA, USA, 2006.
[15] E. Butler, G. Devlin, D. Meier, K. McDonnell, A review of recent laboratory research and commercial developments in fast pyrolysis and upgrading, Renewable and Sustainable Energy Reviews 15 (2011) 4171-4186.
[16] D. Kunii, O. Levenspiel, Chapter 1 - Introduction, Fluidization Engineering (Second Edition), Butterworth-Heinemann, Boston, 1991, pp. 1-13.
[17] D. Kunii, O. Levenspiel, Chapter 15 - Circulation Systems, Fluidization Engineering (Second Edition), Butterworth-Heinemann, Boston, 1991, pp. 359-395.
[18] J.R. Grace, H. Bi, Introduction to Circulating Fluidized Beds, in: J.R. Grace, A.A. Avidan, T.M. Knowlton (Eds.) Circulating Fluidized Beds, Springer Netherlands, Dordrecht, 1997, pp. 1-20.
[19] S. Shaul, E. Rabinovich, H. Kalman, Generalized flow regime diagram of fluidized beds based on the height to bed diameter ratio, Powder Technology 228 (2012) 264-271.
[20] D. Geldart, Types of gas fluidization, Powder Technology 7 (1973) 285-292.
[21] D. Geldart, The effect of particle size and size distribution on the behaviour of gas-fluidised beds, Powder Technology 6 (1972) 201-215.
[22] R. Beetstra, J. Nijenhuis, N. Ellis, J.R. van Ommen, The influence of the particle size distribution on fluidized bed hydrodynamics using high-throughput experimentation, AIChE Journal 55 (2009) 2013-2023.
[23] G.C. Brouwer, E.C. Wagner, J.R. van Ommen, R.F. Mudde, Effects of pressure and fines content on bubble diameter in a fluidized bed studied using fast X-ray tomography, Chemical Engineering Journal 207–208 (2012) 711-717.
[24] J.R. van Ommen, J. Nijenhuis, C.M. van den Bleek, M.-O. Coppens, Four Ways To Introduce Structure in Fluidized Bed Reactors, Industrial & Engineering Chemistry Research 46 (2007) 4236-4244.
[25] J.S. Halow, G.E. Fasching, P. Nicoletti, J.L. Spenik, Observations of a fluidized bed using capacitance imaging, Chemical Engineering Science 48 (1993) 643-659.

[26] P.N. Rowe, B.A. Partridge, E. Lyall, Cloud formation around bubbles in gas fluidized beds, Chemical Engineering Science 19 (1964) 973-985.
[27] L.T. Fan, T.C. Ho, W.P. Walawender, Measurements of the rise velocities of bubbles, slugs and pressure waves in a gas-solid fluidized-bed using pressure fluctuation signals, Aiche Journal 29 (1983) 33-39.
[28] M. Rüdisüli, Characterization of rising gas bubbles in fluidized beds by means of statistical tools, ETH Zurich, 2012.
[29] A. Bakshi, C. Altantzis, L.R. Glicksman, A.F. Ghoniem, Gas-flow distribution in bubbling fluidized beds: CFD-based analysis and impact of operating conditions, Powder Technology 316 (2017) 500-511.
[30] G. Sun, J.R. Grace, Experimental determination of particle dispersion in voids in a fluidized bed, Powder Technology 80 (1994) 29-34.
[31] S.-H. Lee, M.-S. Eom, K.-S. Yoo, N.-C. Kim, J.-K. Jeon, Y.-K. Park, B.-H. Song, S.-H. Lee, The yields and composition of bio-oil produced from Quercus Acutissima in a bubbling fluidized bed pyrolyzer, Journal of Analytical and Applied Pyrolysis 83 (2008) 110-114.
[32] Q. Xiong, F. Xu, E. Ramirez, S. Pannala, C.S. Daw, Modeling the impact of bubbling bed hydrodynamics on tar yield and its fluctuations during biomass fast pyrolysis, Fuel 164 (2016) 11-17.
[33] A. Trendewicz, R. Braun, A. Dutta, J. Ziegler, One dimensional steady-state circulating fluidized-bed reactor model for biomass fast pyrolysis, Fuel 133 (2014) 253-262.
[34] Y. Li, M. Kwauk, The Dynamics of Fast Fluidization, in: J.R. Grace, J.M. Matsen (Eds.) Fluidization, Springer US, Boston, MA, 1980, pp. 537-544.
[35] M. Aghbashlo, R. Sotudeh-Gharebagh, R. Zarghami, A.S. Mujumdar, N. Mostoufi, Measurement Techniques to Monitor and Control Fluidization Quality in Fluidized Bed Dryers: A Review, Drying Technology 32 (2014) 1005-1051.
[36] E. Rasanen, J. Rantanen, J.P. Mannermaa, J. Yliruusi, The characterization of fluidization behavior using a novel multichamber microscale fluid bed, Journal of Pharmaceutical Sciences 93 (2004) 780-791.
[37] M. Xu, P.W.S. Heng, C.V. Liew, Evaluation of coat uniformity and taste-masking efficiency of irregular-shaped drug particles coated in a modified tangential spray fluidized bed processor, Expert Opinion on Drug Delivery 12 (2015) 1597-1606.
[38] R.C. Zijerveld, F. Johnsson, A. Marzocchella, J.C. Schouten, C.M. van den Bleek, Fluidization regimes and transitions from fixed bed to dilute transport flow, Powder Technology 95 (1998) 185-204.
[39] D. Kunii, O. Levenspiel, Chapter 3 - Fluidization and Mapping of Regimes, Fluidization Engineering (Second Edition), Butterworth-Heinemann, Boston, 1991, pp. 61-94.
[40] N. Reuge, L. Cadoret, C. Coufort-Saudejaud, S. Pannala, M. Syamlal, B. Caussat, Multifluid Eulerian modeling of dense gas-solids fluidized bed hydrodynamics: Influence of the dissipation parameters, Chemical Engineering Science 63 (2008) 5540-5551.
[41] M. Abbasi, J.R. Grace, R. Sotude-Gharebagh, R. Zarghami, N. Mostoufi, Numerical comparison of gas-liquid bubble columns and gas-solid fluidized beds, Canadian Journal of Chemical Engineering 93 (2015) 1838-1848.
[42] H.T. Bi, J.R. Grace, Regime transitions: Analogy between gas-liquid co-current upward flow and gas-solids upward transport, International Journal of Multiphase Flow 22, Supplement (1996) 1-19.
[43] S. Nedeltchev, New methods for flow regime identification in bubble columns and fluidized beds, Chemical Engineering Science 137 (2015) 436-446.
[44] J.P. Constantineau, J.R. Grace, C.J. Lim, G.G. Richards, Generalized bubbling–slugging fluidized bed reactor model, Chemical Engineering Science 62 (2007) 70-81.
[45] P. Lettieri, G. Saccone, L. Cammarata, Predicting the Transition from Bubbling to Slugging Fluidization Using Computational Fluid Dynamics, Chemical Engineering Research and Design 82 (2004) 939-944.
[46] J. Baeyens, D. Geldart, An investigation into slugging fluidized beds, Chemical Engineering Science 29 (1974) 255-265.
[47] T.E. Broadhurst, H.A. Becker, Onset of fluidization and slugging in beds of uniform particles, AIChE Journal 21 (1975) 238-247.
[48] P.S.B. Stewart, J.F. Davidson, Slug flow in fluidised beds, Powder Technology 1 (1967) 61-80.
[49] M. Deza, F. Battaglia, A CFD Study of Pressure Fluctuations to Determine Fluidization Regimes in Gas-Solid Beds, Journal of Fluids Engineering-Transactions of the Asme 135 (2013).
[50] D.T. Argyriou, H.L. List, R. Shinnar, Bubble growth by coalescence in gas fluidized beds, AIChE Journal 17 (1971) 122-130.

[51] T.C. Ho, N. Yutani, L.T. Fan, W.P. Walawender, The onset of slugging in gas solid fluidized–beds with large particles, Powder Technology 35 (1983) 249-257.
[52] W.J. Thiel, O.E. Potter, Slugging in Fluidized Beds, Industrial & Engineering Chemistry Fundamentals 16 (1977) 242-247.
[53] W.J. Thiel, O.E. Potter, Mixing of solids in slugging gas-fluidized beds, Aiche Journal 24 (1978) 561-569.
[54] C.S. Daw, C.E.A. Finney, M. Vasudevan, N.A. van Goor, K. Nguyen, D.D. Bruns, E.J. Kostelich, C. Grebogi, E. Ott, J.A. Yorke, Self-Organization and Chaos in a Fluidized Bed, Physical Review Letters 75 (1995) 2308-2311.
[55] C. Finney, S. Daw, J. Halow, Measuring Slugging Bed Dynamics with Acoustic Sensors, KONA Powder and Particle Journal 16 (1998) 125-135.
[56] G.S. Lee, S.D. KIM, Pressure fluctuations in turbulent fluidized beds, Journal of Chemical Engineering of Japan 21 (1988) 515-521.
[57] S.H. Lee, S.D. Kim, S.H. Park, Statistical and deterministic chaos analysis of pressure fluctuations in a fluidized bed of polymer powders, Korean Journal of Chemical Engineering 19 (2002) 1020-1025.
[58] M. Rüdisüli, T.J. Schildhauer, S.M.A. Biollaz, J. Ruud van Ommen, Bubble characterization in a fluidized bed by means of optical probes, International Journal of Multiphase Flow 41 (2012) 56-67.
[59] S. Satija, L.-S. Fan, Characteristics of slugging regime and transition to turbulent regime for fluidized beds of large coarse particles, AIChE Journal 31 (1985) 1554-1562.
[60] S.C. Saxena, N.S. Rao, Fluidization characteristics of gas-fluidized beds: Air and glass beads system, Energy 14 (1989) 811-826.
[61] J. van der Schaaf, J.C. Schouten, F. Johnsson, C.M. van den Bleek, Non-intrusive determination of bubble and slug length scales in fluidized beds by decomposition of the power spectral density of pressure time series, International Journal of Multiphase Flow 28 (2002) 865-880.
[62] J.M. Weber, J.S. Mei, Bubbling fluidized bed characterization using Electrical Capacitance Volume Tomography (ECVT), Powder Technology 242 (2013) 40-50.
[63] S.C. Saxena, N.S. Rao, Pressure fluctuations in a gas fluidized bed and fluidization quality, Energy 15 (1990) 489-497.
[64] B. Du, W. Warsito, L.-S. Fan, Imaging the choking transition in gas-solid risers using electrical capacitance tomography, Industrial & Engineering Chemistry Research 45 (2006) 5384-5395.
[65] B. Du, W. Warsito, L.S. Fan, ECT studies of gas-solid fluidized beds of different diameters, Industrial & Engineering Chemistry Research 44 (2005) 5020-5030.
[66] J.S. Halow, P. Nicoletti, Observations of fluidized bed coalescence using capacitance imaging, Powder Technology 69 (1992) 255-277.
[67] Y.T. Makkawi, P.C. Wright, Fluidization regimes in a conventional fluidized bed characterized by means of electrical capacitance tomography, Chemical Engineering Science 57 (2002) 2411-2437.
[68] K. Ichiki, H. Hayakawa, Dynamical simulation of fluidized–beds – hydrodynamically interacting granular particles, Physical Review E 52 (1995) 658-670.
[69] C.C. Pain, S. Mansoorzadeh, C.R.E. de Oliveira, A study of bubbling and slugging fluidised beds using the two-fluid granular temperature model, International Journal of Multiphase Flow 27 (2001) 527-551.
[70] C.C. Pain, S. Mansoorzadeh, C.R.E. de Oliveira, A.J.H. Goddard, Numerical modelling of gas-solid fluidized beds using the two-fluid approach, International Journal for Numerical Methods in Fluids 36 (2001) 91-124.
[71] S.J. Zhang, A.B. Yu, Computational investigation of slugging behaviour in gas-fluidised beds, Powder Technology 123 (2002) 147-165.
[72] N. Reuge, L. Cadoret, B. Caussat, Multifluid Eulerian modelling of a silicon Fluidized Bed Chemical Vapor Deposition process: Analysis of various kinetic models, Chemical Engineering Journal 148 (2009) 506-516.
[73] M.J.V. Goldschmidt, J.A.M. Kuipers, W.P.M. van Swaaij, Hydrodynamic modelling of dense gas-fluidised beds using the kinetic theory of granular flow: effect of coefficient of restitution on bed dynamics, Chemical Engineering Science 56 (2001) 571-578.
[74] C. Loha, H. Chattopadhyay, P.K. Chatterjee, Euler-Euler CFD modeling of fluidized bed: Influence of specularity coefficient on hydrodynamic behavior, Particuology 11 (2013) 673-680.
[75] C. Loha, H. Chattopadhyay, P.K. Chatterjee, Effect of coefficient of restitution in Euler–Euler CFD simulation of fluidized-bed hydrodynamics, Particuology 15 (2014) 170-177.

[76] P. Fede, O. Simonin, A. Ingram, 3D numerical simulation of a lab-scale pressurized dense fluidized bed focussing on the effect of the particle-particle restitution coefficient and particle–wall boundary conditions, Chemical Engineering Science 142 (2016) 215-235.
[77] N. Xie, F. Battaglia, S. Pannala, Effects of using two- versus three-dimensional computational modeling of fluidized beds: Part II, budget analysis, Powder Technology 182 (2008) 14-24.
[78] T. Li, Y. Zhang, J.R. Grace, X. Bi, Numerical Investigation of Gas Mixing in Gas-Solid Fluidized Beds, Aiche Journal 56 (2010) 2280-2296.
[79] A. Bakshi, C. Altantzis, R.B. Bates, A.F. Ghoniem, Eulerian–Eulerian simulation of dense solid–gas cylindrical fluidized beds: Impact of wall boundary condition and drag model on fluidization, Powder Technology 277 (2015) 47-62.
[80] A. Bakshi, C. Altantzis, R.B. Bates, A.F. Ghoniem, Study of the effect of reactor scale on fluidization hydrodynamics using fine-grid CFD simulations based on the two-fluid model, Powder Technology 299 (2016) 185-198.
[81] T. Li, S. Benyahia, Evaluation of wall boundary condition parameters for gas–solids fluidized bed simulations, AIChE Journal 59 (2013) 3624-3632.
[82] M. Syamlal, T. O'brien, A Generalized Drag Correlation for Multiparticle Systems, Unpublished Report U.S. Department of Energy. Office of Fossil Energy, 1987.
[83] S. Patankar, Numerical heat transfer and fluid flow, CRC Press, 1980.
[84] A. Acosta-Iborra, C. Sobrino, F. Hernández-Jiménez, M. de Vega, Experimental and computational study on the bubble behavior in a 3-D fluidized bed, Chemical Engineering Science 66 (2011) 3499-3512.
[85] S. Pannala, S. Madhava, T.J. O'Brien, Computational Gas-Solids Flows and Reacting Systems: Theory, Methods and Practice, IGI Global, Hershey, PA, USA, 2011, pp. 1-500.
[86] N. Xie, F. Battaglia, S. Pannala, Effects of using two- versus three-dimensional computational modeling of fluidized beds - Part I, hydrodynamics, Powder Technology 182 (2008) 1-13.
[87] S.H. Hosseini, W. Zhong, M.N. Esfahany, L. Pourjafar, S. Azizi, CFD Simulation of the Bubbling and Slugging Gas-Solid Fluidized Beds, Journal of Fluids Engineering-Transactions of the ASME 132 (2010).
[88] G. Wu, J. Ouyang, B. Yang, Q. Li, F. Wang, Lagrangian-Eulerian simulation of slugging fluidized bed, Particuology 10 (2012) 72-78.
[89] D. Gidaspow, Multiphase flow and fluidization: continuum and kinetic theory descriptions, Academic Press 1994.
[90] M. Ishii, K. Mishima, Two-fluid model and hydrodynamic constitutive relations, Nuclear Engineering and Design 82 (1984) 107-126.
[91] J. Bruchmuller, B.G.M. van Wachem, S. Gu, K.H. Luo, R.C. Brown, Modeling the thermochemical degradation of biomass inside a fast pyrolysis fluidized bed reactor, AIChE Journal 58 (2012) 3030-3042.
[92] N.G. Deen, M. Van Sint Annaland, M.A. Van der Hoef, J.A.M. Kuipers, Review of discrete particle modeling of fluidized beds, Chemical Engineering Science 62 (2007) 28-44.
[93] N.A. Shoushtari, S.A. Hosseini, R. Soleimani, Investigation of segregation of large particles in a pressurized fluidized bed with a high velocity gas: A discrete particle simulation, Powder Technology 246 (2013) 398-412.
[94] M. Syamlal, W. Rogers, T.J. O'Brien, MFIX documentation: Theory guide, National Energy Technology Laboratory, Department of Energy, Technical Note DOE/METC-95/1013 and NTIS/DE95000031 (1993).
[95] D.G. Schaeffer, Instability in the evolution equations describing incompressible granular flow, Journal of Differential Equations 66 (1987) 19-50.
[96] S. Pannala, C.S. Daw, C.E.A. Finney, S. Benyahia, M. Syamlal, T.J. O'Brien, Modeling the Collisional-Plastic Stress Transition for Bin Discharge of Granular Material, AIP Conference Proceedings 1145 (2009) 657-660.
[97] M. Syamlal, MFiX documentation: Numerical technique, National Energy Technology Laboratory, Department of Energy, Technical Note No. DOE/MC31346-5824 (1998).
[98] P.C. Johnson, R. Jackson, Frictional–collisional constitutive relations for granular materials, with application to plane shearing, Journal of Fluid Mechanics 176 (1987) 67-93.
[99] R.J. van Ommen, S. Sasic, J. van der Schaaf, S. Gheorghiu, F. Johnsson, M.-O. Coppens, Time-series analysis of pressure fluctuations in gas–solid fluidized beds – A review, International Journal of Multiphase Flow 37 (2011) 403-428.
[100] R.J. van Ommen, J. van der Schaaf, J.C. Schouten, B.G.M. van Wachem, M.-O. Coppens, C.M. van den Bleek, Optimal placement of probes for dynamic pressure measurements in large-scale fluidized beds, Powder Technology 139 (2004) 264-276.

[101] C.M. Boyce, J.F. Davidson, D.J. Holland, S.A. Scott, J.S. Dennis, The origin of pressure oscillations in slugging fluidized beds: Comparison of experimental results from magnetic resonance imaging with a discrete element model, Chemical Engineering Science 116 (2014) 611-622.
[102] A. Bakshi, C. Altantzis, R.B. Bates, A.F. Ghoniem, Multiphase-flow Statistics using 3D Detection and Tracking Algorithm (MS3DATA): Methodology and application to large-scale fluidized beds, Chemical Engineering Journal 293 (2016) 355-364.
[103] H.T. Bi, A critical review of the complex pressure fluctuation phenomenon in gas–solids fluidized beds, Chemical Engineering Science 62 (2007) 3473-3493.
[104] P. Blomgren, A. Palacios, B. Zhu, S. Daw, C. Finney, J. Halow, S. Pannala, Bifurcation analysis of bubble dynamics in fluidized beds, Chaos 17 (2007) 013120.
[105] G.J. Castilho, M.A. Cremasco, L. de Martin, J.M. Aragon, Experimental Fluid Dynamics Study in a Fluidized Bed by Deterministic Chaos Analysis, Particulate Science and Technology 29 (2011) 179-196.
[106] F. Johnsson, R.C. Zijerveld, J.C. Schouten, C.M. van den Bleek, B. Leckner, Characterization of fluidization regimes by time-series analysis of pressure fluctuations, International Journal of Multiphase Flow 26 (2000) 663-715.
[107] K. Nguyen, C.S. Daw, P. Chakka, M. Cheng, D.D. Bruns, C.E.A. Finney, M.B. Kennell, Spatio-temporal dynamics in a train of rising bubbles, The Chemical Engineering Journal 64 (1996) 191-197.
[108] A. Tufaile, J.C. Sartorelli, Chaotic behavior in bubble formation dynamics, Physica A: Statistical Mechanics and its Applications 275 (2000) 336-346.
[109] J. van der Schaaf, J.R. van Ommen, F. Takens, J.C. Schouten, C.M. van den Bleek, Similarity between chaos analysis and frequency analysis of pressure fluctuations in fluidized beds, Chemical Engineering Science 59 (2004) 1829-1840.
[110] R.B. Randall, Frequency analysis, Brül & Kjor1987.
[111] D.W. Scott, On optimal and data-based histograms, Biometrika 66 (1979) 605-610.
[112] U. Ayachit, The ParaView Guide: A Parallel Visualization Application, (2015).
[113] D. Kunii, O. Levenspiel, Chapter 5 - Bubbles in Dense Beds, Fluidization Engineering (Second Edition), Butterworth-Heinemann, Boston, 1991, pp. 115-135.
[114] C. Rautenbach, R.F. Mudde, X. Yang, M.C. Melaaen, B.M. Halvorsen, A comparative study between electrical capacitance tomography and time-resolved X-ray tomography, Flow Measurement and Instrumentation 30 (2013) 34-44.
[115] P.N. Rowe, B.A. Partridge, An x-ray study of bubbles in fluidised beds, Chemical Engineering Research and Design 75, Supplement (1997) S116-S134.
[116] J.-H. Lim, K. Bae, J.-H. Shin, J.-H. Kim, D.-H. Lee, J.-H. Han, D.H. Lee, Effect of particle–particle interaction on the bed pressure drop and bubble flow by computational particle-fluid dynamics simulation of bubbling fluidized beds with shroud nozzle, Powder Technology 288 (2016) 315-323.
[117] N. de Nevers, J.-L. Wu, Bubble coalescence in viscous fluids, AIChE Journal 17 (1971) 182-186.
[118] A.A. Mouza, G.K. Dalakoglou, S.V. Paras, Effect of liquid properties on the performance of bubble column reactors with fine pore spargers, Chemical Engineering Science 60 (2005) 1465-1475.
[119] F. Wang, L.-S. Fan, Gas-Solid Fluidization in Mini- and Micro-channels, Industrial & Engineering Chemistry Research 50 (2011) 4741-4751.
[120] H.T. Bi, J.R. Grace, J. Zhu, Propagation of pressure waves and forced oscillations in gas-solid fluidized beds and their influence on diagnostics of local hydrodynamics, Powder Technology 82 (1995) 239-253.
[121] S.-H. Lee, Personal email correspondence regarding static bed height in "Statistical and Deterministic Chaos Analysis of Pressure Fluctuations in a Fluidized Bed of Polymer Powders", Unpublished Results.
[122] S. Shaul, E. Rabinovich, H. Kalman, Typical Fluidization Characteristics for Geldart's Classification Groups, Particulate Science and Technology 32 (2014) 197-205.
[123] E. Ramirez, C.E.A. Finney, S. Pannala, C.S. Daw, J. Halow, Q. Xiong, Computational study of the bubbling-to-slugging transition in a laboratory-scale fluidized bed, Chemical Engineering Journal 308 (2017) 544-556.
[124] A.V. Bridgwater, Review of fast pyrolysis of biomass and product upgrading, Biomass and Bioenergy 38 (2012) 68-94.
[125] E. Ranzi, P.E.A. Debiagi, A. Frassoldati, Mathematical Modeling of Fast Biomass Pyrolysis and Bio-Oil Formation. Note II: Secondary Gas-Phase Reactions and Bio-Oil Formation, ACS Sustainable Chemistry & Engineering 5 (2017) 2882-2896.

[126] A.J. Ragauskas, C.K. Williams, B.H. Davison, G. Britovsek, J. Cairney, C.A. Eckert, W.J. Frederick, J.P. Hallett, D.J. Leak, C.L. Liotta, J.R. Mielenz, R. Murphy, R. Templer, T. Tschaplinski, The Path Forward for Biofuels and Biomaterials, Science 311 (2006) 484.
[127] R.C. Brown, T.R. Brown, Biorenewable Resources: Engineering New Products from Agriculture, Second edition. ed., John Wiley & Sons, Ames, Iowa, 2013.
[128] K. Iisa, R.J. French, K.A. Orton, A. Dutta, J.A. Schaidle, Production of low-oxygen bio-oil via ex situ catalytic fast pyrolysis and hydrotreating, Fuel 207 (2017) 413-422.
[129] H. Cui, J.R. Grace, Fluidization of biomass particles: A review of experimental multiphase flow aspects, Chemical Engineering Science 62 (2007) 45-55.
[130] X.Q. Wang, S.R.A. Kersten, W. Prins, W.P.M. van Swaaij, Biomass pyrolysis in a fluidized bed reactor. Part 2: Experimental validation of model results, Industrial & Engineering Chemistry Research 44 (2005) 8786-8795.
[131] D. Lathouwers, J. Bellan, Modeling of dense gas–solid reactive mixtures applied to biomass pyrolysis in a fluidized bed, International Journal of Multiphase Flow 27 (2001) 2155-2187.
[132] F. Berruti, A.G. Liden, D.S. Scott, Measuring and modelling residence time distribution of low density solids in a fluidized bed reactor of sand particles, Chemical Engineering Science 43 (1988) 739-748.
[133] A.G. Liden, F. Berruti, D.S. Scott, A kinetic model for the production of liquids from the flash pyrolysis of biomass, Chemical Engineering Communications 65 (1988) 207-221.
[134] K. Iisa, R.J. French, K.A. Orton, M.M. Yung, D.K. Johnson, J. ten Dam, M.J. Watson, M.R. Nimlos, In Situ and ex Situ Catalytic Pyrolysis of Pine in a Bench-Scale Fluidized Bed Reactor System, Energy & Fuels 30 (2016) 2144-2157.
[135] J. Horabik, M. Molenda, Parameters and contact models for DEM simulations of agricultural granular materials: A review, Biosystems Engineering 147 (2016) 206-225.
[136] C. González-Montellano, Á. Ramírez-Gómez, J. Fuentes, E. Gallego, F. Ayuga, Determination of the mechanical properties of biomass briquettes for use in DEM simulations, SPC-07: SILOS AND GRANULAR MATERIALS (SIGMA) 100 (2012).
[137] X. Zhao, Q. Eri, Q. Wang, An Investigation of the Restitution Coefficient Impact on Simulating Sand-Char Mixing in a Bubbling Fluidized Bed, Energies 10 (2017) 617.
[138] F. Alonso-Marroquín, Á. Ramírez-Gómez, C. González-Montellano, N. Balaam, D.A.H. Hanaor, E.A. Flores-Johnson, Y. Gan, S. Chen, L. Shen, Experimental and numerical determination of mechanical properties of polygonal wood particles and their flow analysis in silos, Granular Matter 15 (2013) 811-826.
[139] M.B. Pecha, E. Ramirez, G.M. Wiggins, D. Carpenter, B. Kappes, S. Daw, P.N. Ciesielski, Integrated Particle- and Reactor-Scale Simulation of Pine Pyrolysis in a Fluidized Bed, Energy & Fuels 32 (2018) 10683-10694.
[140] C.S. Daw, J. Halow, Statistical Analysis of Axial Flotsam Particle Mixing in Bubbling Fluidized Beds, Industrial & Engineering Chemistry Research 57 (2018) 361-370.
[141] H.C. Park, H.S. Choi, The segregation characteristics of char in a fluidized bed with varying column shapes, Powder Technology 246 (2013) 561-571.
[142] M. Asachi, E. Nourafkan, A. Hassanpour, A review of current techniques for the evaluation of powder mixing, Advanced Powder Technology 29 (2018) 1525-1549.
[143] H.S. Fogler, Essentials of Chemical Reaction Engineering, Pearson Education 2010.
[144] D. Kunii, O. Levenspiel, Fluidization Engineering, Elsevier 2013.
[145] L. Wei, Y. Lu, J. Wei, Hydrogen production by supercritical water gasification of biomass: Particle and residence time distribution in fluidized bed reactor, International Journal of Hydrogen Energy 38 (2013) 13117-13124.
[146] A. Sharma, S. Wang, V. Pareek, H. Yang, D. Zhang, CFD modeling of mixing/segregation behavior of biomass and biochar particles in a bubbling fluidized bed, Chemical Engineering Science 106 (2014) 264-274.
[147] W. Bai, N.K.G. Keller, T.J. Heindel, R.O. Fox, Numerical study of mixing and segregation in a biomass fluidized bed, Powder Technology 237 (2013) 355-366.
[148] M. Darwish, F. Moukalled, The χ-schemes: a new consistent high-resolution formulation based on the normalized variable methodology, Computer Methods in Applied Mechanics and Engineering 192 (2003) 1711-1730.
[149] R.D. Larsen, Box-and-Whisker Plots, Journal of Chemical Education 62 (1985) 302-305.
[150] C. Di Blasi, C. Branca, Temperatures of wood particles in a hot sand bed fluidized by nitrogen, Energy & Fuels 17 (2003) 247-254.
[151] E. Ramirez, T. Li, M. Shahnam, C.S. Daw, Computational study on biomass fast pyrolysis: Hydrodynamic effects on the performance of a laboratory-scale fluidized bed reactor, Chemical Engineering Journal (In Preparation).

[152] M. Sharifzadeh, M. Sadeqzadeh, M. Guo, T.N. Borhani, N.V.S.N. Murthy Konda, M.C. Garcia, L. Wang, J. Hallett, N. Shah, The multi-scale challenges of biomass fast pyrolysis and bio-oil upgrading: Review of the state of art and future research directions, Progress in Energy and Combustion Science 71 (2019) 1-80.
[153] P.N. Ciesielski, M. Crowley, M. Nimlos, A. Sanders, G. Wiggins, D. Robichaud, B. Donohoe, T. Foust, Biomass Particle Models with Realistic Morphology and Resolved Microstructure for Simulations of Intraparticle Transport Phenomena, Energy & Fuels 29 (2014) 242-254.
[154] P. Debiagi, G. Gentile, A. Cuoci, A. Frassoldati, E. Ranzi, T. Faravelli, A predictive model of biochar formation and characterization, Journal of Analytical and Applied Pyrolysis 134 (2018) 326-335.
[155] E. Ranzi, P.E.A. Debiagi, A. Frassoldati, Mathematical Modeling of Fast Biomass Pyrolysis and Bio-Oil Formation. Note I: Kinetic Mechanism of Biomass Pyrolysis, ACS Sustainable Chemistry & Engineering 5 (2017) 2867-2881.
[156] C. Branca, C. Di Blasi, R. Elefante, Devolatilization and heterogeneous combustion of wood fast pyrolysis oils, Industrial & Engineering Chemistry Research 44 (2005) 799-810.
[157] R.E. Guedes, A.S. Luna, A.R. Torres, Operating parameters for bio-oil production in biomass pyrolysis: A review, Journal of Analytical and Applied Pyrolysis 129 (2018) 134-149.
[158] J.A. Garcia-Nunez, M.R. Pelaez-Samaniego, M.E. Garcia-Perez, I. Fonts, J. Abrego, R.J.M. Westerhof, M. Garcia-Perez, Historical Developments of Pyrolysis Reactors: A Review, Energy & Fuels 31 (2017) 5751-5775.
[159] A. Kokkoris, R. Turton, A phenomenological model predicting the attrition and the reduction of attrition due to the addition of solid lubricants in slugging beds, Powder Technology 84 (1995) 39-47.
[160] R. Cocco, Y. Arrington, R. Hays, J. Findlay, S.B.R. Karri, T.M. Knowlton, Jet cup attrition testing, Powder Technology 200 (2010) 224-233.
[161] E. Ramirez, A. Bakshi, T. Li, M. Shahnam, C.S. Daw, C.E.A. Finney, Computational study on biomass fast pyrolysis: bubble effects in a laboratory-scale fluidized bed, TC Biomass 2017: The international conference on thermochemical conversion science Chicago, Illinois, 2017.
[162] A. Bakshi, A.F. Ghoniem, C. Altantzis, Mixing dynamics in bubbling fluidized beds, AIChE Journal 63 (2017) 4316-4328.
[163] E. Ramirez, T. Li, M. Shahnam, C.S. Daw, Computational Study on Biomass Fast Pyrolysis: Hydrodynamic Effects in a Laboratory-Scale Fluidized Bed, World Congress on Particle TechnologyOrlando, Florida, 2018.
[164] A. Köhler, A. Rasch, D. Pallarès, F. Johnsson, Experimental characterization of axial fuel mixing in fluidized beds by magnetic particle tracking, Powder Technology 316 (2017) 492-499.
[165] G. Sun, J.R. Grace, Effect of particle size distribution in different fluidization regimes, AIChE Journal 38 (1992) 716-722.
[166] R.S. Miller, J. Bellan, A Generalized Biomass Pyrolysis Model Based on Superimposed Cellulose, Hemicelluloseand Liqnin Kinetics, Combustion Science and Technology 126 (1997) 97-137.
[167] J.R.H. Grace, D., Design of fluidised beds with internal baffles, Chemical and Process Engineering. 51 (1970) 127.
[168] S.W. Kim, Pyrolysis conditions of biomass in fluidized beds for production of bio-oil compatible with petroleum refinery, Journal of Analytical and Applied Pyrolysis 117 (2016) 220-227.
[169] Y. Zhang, B. Jin, W. Zhong, B. Ren, R. Xiao, Characterization of Fluidization and Segregation of Biomass Particles by Combining Image Processing and Pressure Fluctuations Analysis, International Journal of Chemical Reactor Engineering 7 (2009).
[170] Y. Zhang, B.S. Jin, W.Q. Zhong, Fluidization, Mixing and Segregation of a Biomass-Sand Mixture in a Fluidized Bed, International Journal of Chemical Reactor Engineering 6 (2008) 30.
[171] M.L. de Souza-Santos, Solid fuels combustion and gasification: modeling, simulation, CRC Press 2010.
[172] H.T. Bi, N. Ellis, I.A. Abba, J.R. Grace, A state-of-the-art review of gas-solid turbulent fluidization, Chemical Engineering Science 55 (2000) 4789-4825.
[173] H.T. Bi, J.R. Grace, Flow regime diagrams for gas–solid fluidization and upward transport, International Journal of Multiphase Flow 21 (1995) 1229-1236.
[174] D.R. Cox, G. Gudmundsson, G. Lindgren, L. Bondesson, E. Harsaae, P. Laake, K. Juselius, S.L. Lauritzen, Statistical Analysis of Time Series: Some Recent Developments [with Discussion and Reply], Scandinavian Journal of Statistics 8 (1981) 93-115.
[175] J. Gyenis, Assessment of mixing mechanism on the basis of concentration pattern, Chemical Engineering and Processing: Process Intensification 38 (1999) 665-674.

[176] C. Sobrino, J.A. Almendros-Ibáñez, D. Santana, C. Vázquez, M. De Vega, Maximum entropy estimation of the bubble size distribution in fluidized beds, Chemical Engineering Science 64 (2009) 2307-2319.
[177] A.-N. Huang, C.-P. Hsu, B.-R. Hou, H.-P. Kuo, Production and separation of rice husk pyrolysis bio-oils from a fractional distillation column connected fluidized bed reactor, Powder Technology 323 (2018) 588-593.
[178] J.R. Tucker, L.J. Shadle, S. Benyahia, J. Mei, C. Guenther, M.E. Koepke, Improvement in Precision, Accuracy, and Efficiency in Standardizing the Characterization of Granular Materials, (2013).

APPENDIX

This appendix contains the website link to the location of the MFiX and MATLAB files used in this dissertation.

https://github.com/eramire2/

Questions: ramirez.emilio1@gmail.com

VITA

Introduction

Emilio Ramirez completed his PhD in Energy Science and Engineering at the Bredesen Center, a joint program between the University of Tennessee, Knoxville and Oak Ridge National Lab. Prior to joining the Bredesen Center he operated and maintained an industrial fluidized bed facility, where he created empirical models to optimize and increase reliability.

During his PhD studies he worked with experimentalists at the National Renewable Energy Laboratory and the National Energy Technology Laboratory on fluidized bed simulations. His dissertation work focused on a project for the Chemistry and Computational Physics Consortium, a multi-laboratory, multi-scale, computational modeling collaboration to improve bio-oil quality, upgrading catalyst, process integration, and scale-up.

Current Research

His PhD research focused on understanding the multiphase hydrodynamic effects of fluidized beds on biomass fast pyrolysis chemistry. Since reactor measurements are difficult or (in some case) impossible, he employed simulations to gain an understanding of reactor effects. To establish meaningful data for reactor operators, he utilized useful data processing approaches which can be readily applied on real world reactors. The topics of his current research can be broadly categorized into two groups.

The first group, bubbling bed hydrodynamics, mixing, flow, elutriation, and effects of gas and particle properties. Understanding and quantifying these effects are critical for efficient reactor design and operation. Although fluidized beds are widely utilized for power and chemical processing, reactors are still designed and operated empirically. With the development of new, efficient computing resources and detailed physics of fluidization, fluidized beds can be better understood through validated and verified complex models.

The second group, heat transfer, chemistry, and chemical species residence time are aspects that are important during reactive conditions. However, in thermochemical reactors these effects are typically coupled to hydrodynamic effects. Thus, having a solid hydrodynamic understanding of the problem is important to quantifying those effects on reactive conditions. The final chapters of his dissertation quantify the hydrodynamic effects on chemistry in a fluidized bed reactor. His current work shows how hydrodynamic effects and reactor design can be utilized to have greater control on chemical yield and quality.

Future Work

At this point, his primary interest is in fluidized bed reactor simulations. Coming from industry he pursued this interest using robust open source software for simulating the reactor and data analysis. However, as briefly discussed above he previously worked on industrial scale fluidized beds where he acquired skills which can be readily applied to experimental reactors. In the immediate future, he would like to apply his modeling efforts on resolving the challenge with industrial scale up effects. In the long term, he sees himself working on expanding his expertise through simulations and experimental work.